5-13-2022

A Drift-Flux Model for Upward Two-Phase in Pipes with High Velocity Flows

Woochan Lee
Louisiana State University and Agricultural and Mechanical College

A DRIFT-FLUX MODEL FOR UPWARD TWO-PHASE IN PIPES WITH HIGH VELOCITY FLOWS

A Dissertation

Submitted to the Graduate Faculty of the
Louisiana State University and
Agricultural and Mechanical College
in partial fulfillment of the
requirements for the degree of
Doctor of Philosophy

in

The Craft & Hawkins Department of Petroleum Engineering

by
Woochan Lee
B.A., University of Texas at Austin, 2010
M.S., Louisiana State University, 2015
August 2022

ACKNOWLEDGEMENTS

I want to express great respect and appreciation to Dr. Paulo Waltrich. During the long years of my full-time and part-time Ph.D. study, he did not give up on me and continued offline and online communication. He provided me many insights and advice for my study. Without him, I could not make this achievement. I also appreciate my committee members, for their endurance and advises on my study.

I am sincerely grateful to my beloved wife who has been supporting me during the long years of my Master and Ph.D. studies. Whenever I faced unwilling situations and my hopes turned into despair, she encouraged me not to lose hopes and my optimistic and charming characters. She supported my studies by well-taking care of our son and family without my existence during my study and works. I am also thankful to my family who always have strong faith in me fully supported me so that I could complete the study. I also appreciate the support of my colleagues from Korea National Oil Corporation and Abu Dhabi National Oil Company.

I would like to end the acknowledgements with the quote by Johann Christoph Friedrich von Schiller, “Keep true to the dreams of thy youth.” Whenever I come to see the quote, it reminds me of all my pasts and current and makes me dream of the future.

TABLE OF CONTENTS

LIST OF TABLES

LIST OF FIGURES

SYMBOLS

u_{sg}: superficial gas velocity

u_{sg}: superficial liquid velocity

D: pipe diameter

∂: interface tension

α: void fraction

H: Liquid holdup

ρ: fluid density

μ: fluid viscosity

g: gravity

θ: pipe angle deviation from vertical

P: pressure

dP/dZ: pressure gradient

f: friction factor

Re: Reynolds number

q: flow rate

V: volume

A: area

p_{wf}: well flowing pressure

p_{wh}: well head pressure

p_e: reservoir pressure

p_b: bubble point pressure

k: permeability

h: formation thickness

B_o: oil formation volume factor

r_e: reservoir radius

r_w: well radius

N_{lv}: liquid velocity number

N_{gv}: gas velocity number

N_d: diameter number

N_l: Liquid viscosity number

C_o: drift-fluxcoefficient

u_d: drift-fluxvelocity

v_∞: bubble rise velocity

v_{BS}: bubble swarm velocity

v_{TB}: Taylor bubble velocity

$\overline{v_\infty}$: Average bubble rise velocity

N_{nd}: Non-dimensional parameter

$N_{\mu f}$: Fluid viscous number

Subscript l (or L) : liquid

Subscript g (or G) : gas

Subscript m (or M) or TP : mixture

ABSTRACT

This study proposes the evaluation and development of a drift-flux model for upward two-phase high-velocity flow in large diameter pipes. A case where the proposed model is applicable is WCD (Worst-Case-Discharge) calculations for offshore wells. WCD assumes relatively larger pipe diameters and higher flow rates than the flow experiments at laboratory conditions utilized to validate and develop most of the flow models available in the literature.

Most of the two-phase flow models describe flow regime transitions as discrete processes by assigning the required void fraction or velocity for each flow regime transition. Therefore, for each flow regime, flow-regime-dependent correlations or fixed drift-flux parameters are applied, which lead to a wide variety of flow regime maps and complications of flow models.

Unlike others, the model proposed does not have sudden pressure surge or reduction along with flow regime transitions from bubbly to non-bubbly flow regimes. Also, it doesn't have fixed drift-flux coefficients for each flow regime. Further, rather than assigning a fixed void fraction or velocity for bubbly/churn flow transition, it applies the minimum pressure gradient estimated by the bubbly flow model to determine bubbly/non-bubbly flow transition.

The proposed drift-flux model is validated for a wide range of experimental and field data and compared with pressure loss models in commercial software. Among all the models, the proposed model gives the lowest average absolute pressure error (2%) and standard deviation (4.5%) for the tested 279 field data points.

1. INTRODUCTION

After the Deepwater Horizon (Macondo) incident of 2010, one of the worst incidents in the oil and gas industry, U.S. federal regulators have mandated operators to report WCD scenario for proposed wells. According to the U.S. Bureau of Ocean Energy Management (BOEM), WCD is the maximum daily liquid hydrocarbon flow rate during blowout events. Either the top of the wellhead without a blowout preventer (BOP) or a BOP without internal restriction is considered a discharge point of liquid flow. SPE technical report for Calculation of Worst-Case Discharge (2015) stated hydrocarbon fluid flow in larger diameter (greater than 4 in) pipes of long vertical (greater than1000 ft) wells at higher liquid flow rates (greater than 10,000 stb/d) are typically considered as WCD.

Well-known flow models such as Duns and Ros (1963), Beggs and Brill (1973), Hagedorn and Brown (1964), Poetmann and Carpenter (1952), and Fancher and Brown (1964) were built with smaller diameter pipes and lower flow rates than the described WCD conditions. Therefore, some questions arose, which motivated the author to commence this study:

- Are existing two-phase flow models reliable for WCD calculations?
- If not, what is the main reason for the unreliability?
- How can a model be improved for large diameter pipes?

Takacs (2001) reviewed pressure drop models for oil wells and concluded that it is difficult to choose a model that fits a wide range of conditions. Further, a model is more reliable when test data are similar to the model development condition. Ali (2009) compared pressure prediction models for her experiment using 10-in pipe for high flow rates up to 31,000 bbl/d. The result was that Hagedorn and Brown (1964), Duns and Ros (1963), Beggs and Brill (1973), and OLGA steady

state model show large deviations, as high as 50%. In addition, the SPE technical report for Calculation of Worst-Case Discharge (2015) stated, “most flow correlations were developed for small diameter pipe, so their applicability to larger-diameter pipe and open hole is uncertain”. Therefore, it is doubtful that pressure drop models built with smaller diameter pipes are suitable for large diameter pipes that are commonly found in the field.

Ali (2009) summarized the flow regimes observed during vertical flow experiments of earlier scholars. Among the 24 studies for pipe diameter larger than 5-in, the slug flow commonly observed in smaller diameter pipes is not observed. Instead, churn flow is found in these studies. Hence, it is logical to assume that flow behavior is different in small and large diameter pipes and the difference makes flow models built with small diameters less credible for large diameter pipes (Ali, 2009).

Therefore, if a model can accurately present churn flow behavior in large diameter pipes, the model’s pressure and flow rate predictions will be more reliable.

1.1. Objectives of This Research

For more accurate WCD calculation, the objectives of this research are as follows:

- Develop an improved pressure drop prediction method for multiphase flow in large-diameter pipes using drift-flux model.
- Evaluate pressure drop estimations with laboratory and field data for large-diameter pipes using flow models in PIPESIM and the proposed model.

The proposed model has been validated for a wide range of flowing conditions and pipe diameters. The experimental data of air-water mixture flow in 4, 8, and 12-in diameter vertical pipes at the Petroleum Engineering Research and Technology Transfer Laboratory (PERTT Lab) at Louisiana

State University are employed for the evaluation. Field data at a wide range of liquid (10 -27,000 bbl/d) and gas rates (30 – 34,000 Mscf/d), pressure (10 – 7,000 psig), and diameter (2 – 6.2 in) that have not been studied well before are tested.

1.2. Dissertation Outline

The contents of each chapter in the dissertation are summarized below: In chapter 1, the motivation and objectives of this study are described. In chapter 2, Worst-Case-Discharge Calculation, flow regime map, friction factor, and two-phase flow models for small and large diameter pipes are explained. In chapter 3, a new drift-flux pressure drop model for two-phase up-flow in large-diameter pipes is proposed and described. In chapter 4, the proposed model is compared with existing models in commercial software for bottom hole pressure estimations. In chapter 5, a WCD scenario is built to demonstrate how to apply the proposed model for WCD calculation. Chapter 6 furnishes the conclusion of this study and recommendations for future research.

2. LITERATURE REVIEW

2.1. Worst Case Discharge

During and after the Deepwater Horizon (Macondo) incident in 2010, many attempts were made to estimate the quantity of oil spill. McNutt et al. (2011) estimated liquid flow rate through 9.875 in casing without BOP to be between 35,000 and 106,000 stb/d. The wide range of such estimates is due to many uncertainties in the key parameters, such as well opening length to the reservoir, reservoir permeability, fluid transfer path, BOP pressure, and bottom-hole. The sensitivity study by McNutt et al. (2011) indicates that among Bottom-Hole Pressure (BHP), BOP, Gas Oil Ratio (GOR), and pipe roughness, BHP has the greatest impact on flow rate estimation, as shown in Figure 1 For instance, 35 % change in BHP from 8,500 to 11,500 psi varies the estimated flow rates from 40,000 to 88,000 bbl/d. The vertical dark bar represents the predicted mean flow rate of 75,000 stb/d

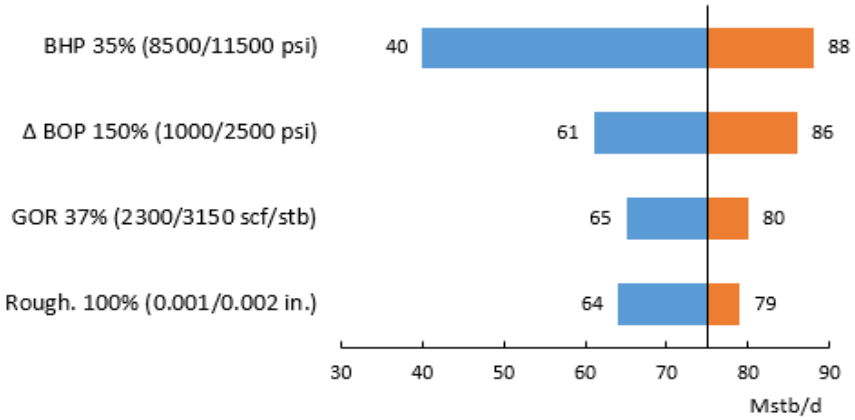

Figure 1. A tornado diagram showing the two ends of flow rate estimations for varying parameters (McNutt et al., 2011).

This indicates that BHP is one of the main parameters affecting flow rate estimation significantly. The generic wellbore flow model equations (Eq. 1 – Eq. 3) include fluid properties such as mixture density (ρ_{TP}), friction factor (f), and mixture velocity (u_m). Each flow model would calculate those

parameters differently, which leads to different pressure gradient values per model. Therefore, the strong dependence of WCD calculation on flow model selection is highly evident.

$$\frac{dp}{dL} = \rho_{TP} g sin\theta + 2f\rho_{TP} {u_m}^2 / D \quad (1)$$

$$p_{wf} = p_{wh} + \int_0^L \frac{dp}{dL} dL \quad (2)$$

$$q \propto \frac{kh(p_e - p_{wf})}{B_o \mu \, ln\left(\frac{r_e}{r_w}\right)} \; for \; p_{wf} > p_b \quad (3)$$

There are a few studies which validated their models at conditions comparable to WCD calculation (Oudeman, 2010; Yuan et al., 2014; Liu et al., 2015; Waltrich, 2017). Oudeman (2010) developed a model for WCD calculations with North Netherland gas field data with gas flows annulus between 3.5 in drill pipe and 7 in casing. However, as per BOEM guideline, WCD calculation must be for a full bore without drill pipe or any constraint. Yuan et al. (2014) and Liu (2015) reviewed the literature on the WCD models and field data Oudeman (2016) used. Waltrich et al. (2017) tested several models against experimental pressure gradient in large diameter pipes and found that most models had pressure gradient errors larger than 50 %. Since multiphase flow behavior in large-diameter pipes can be considerably different from flow dynamics in small-diameter pipes (Ali, 2009; Omebere-Iyari et al., 2007; Kataoka & Ishii, 1981; Waltrich et al., 2017), study on wellbore models for high flow rate in large-diameter pipes is still needed.

The workflow and the details of consideration of WCD calculation is explained in SPE Technical report (SPE Committee, 2015) and are summarized in Figure 2. Among all the steps listed in Figure 2, 'Select outflow correlation (TPR)' is the main interest of this study. Hence, an outflow correlation is proposed and compared with other outflow correlations in this study.

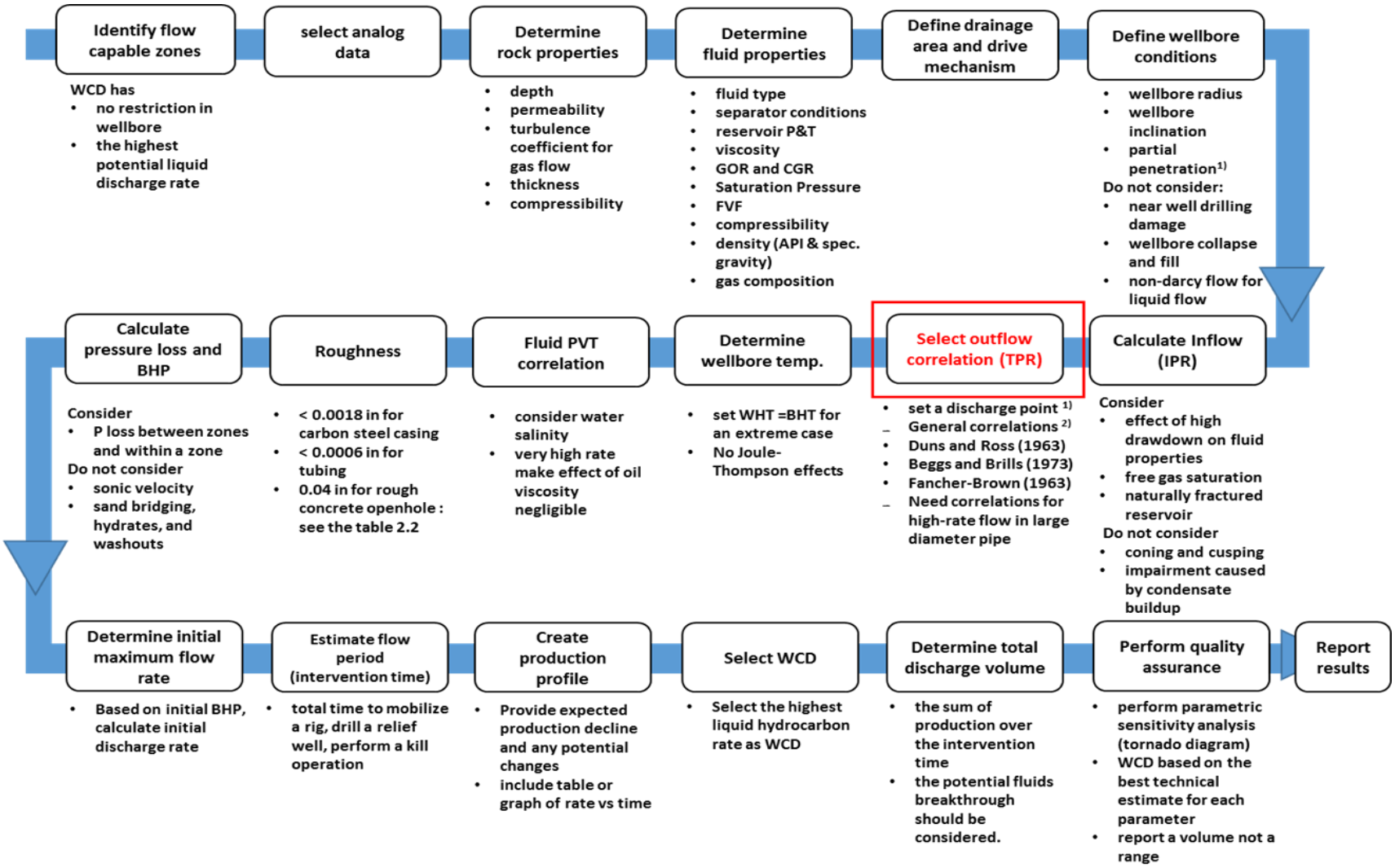

1) Top of wellhead without BOP or BOP without internal restriction
2) - Use Duns and Ross modified (1963) as an upper limit on pressure drop in oil wells.
- Use Beggs and Brills (1973) if Duns and Ross modified is not available.
- Use Fancher-Brown (1963) as a lower limit on wellbore pressure drop because of no slippage consideration. Any flow correlation resulting in lower FBHP than Fancher-Brown (1963) can be exclude as not reasonable.

Figure 2. Workflow presenting basic steps and information for WCD calculation (after SPE Committee, 2015)

2.2. Two-Phase Flow Patterns in Upward Vertical Pipes

Two-phase flow in pipe is characterized by fluid phases distribution in a pipe section. It is important to define a corresponding flow regime for appropriate flow analysis (Shoham, 2006). A classic classification of two-phase flow patterns in vertical pipes is shown in Figure 3. As gas rate increases for a fixed liquid rate, flow regime changes from bubble to slug, churn, and annular flow. The flow regimes presented in Figure 3 can be briefly described as follows (Taitel et al., 1980):

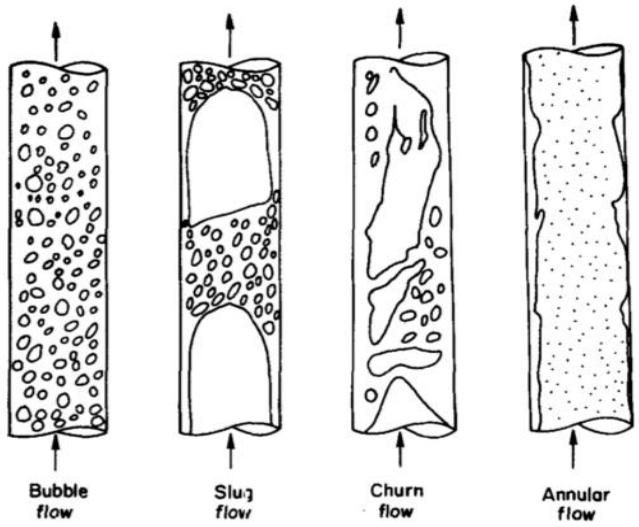

Figure 3. Air-water distribution in vertical flow pipes (Taitel et al., 1980)

1) Bubbly flow*:* The gas phase in the form of discrete bubbles is approximately uniformly distributed in a continuous liquid column.
2) Slug flow*:* Most of the gas is located in large bullet-shaped bubbles often called "Taylor bubbles", which move uniformly upward, with their diameter closed to the pipe diameter. Liquid slugs between Taylor bubbles contain small gas bubbles. A downward liquid flow in a thin film between Taylor bubbles and the pipe wall is also observed.
3) Churn flow*:* Churn flow is much more disorganized and chaotic than slug flow. Liquid slugs are destroyed by the high-velocity gas phase, which makes the liquid phase to

fall and accumulate in a point upstream. The accumulated liquid creates a bridge and it is lifted by the drag effect of the gas phase. This mechanism of falling liquid and drag by the gas phase results in an oscillatory or alternating motion of the liquid.

4) Annular flow*:* The continuous gas column drags the liquid phase upwards as thin liquid film. The gas core also carries entrained liquid droplets.

Different studies define and classify flow regimes in different manners. This disagreement is mainly caused by 1) subjective flow regime identification by visual observation, 2) gradual occurrence of flow regime transition, and 3) pipe diameter, pipe inclination, operating pressure and temperature, and flowing fluid properties-dependent flow regimes (Shoham, 2006). As it will be described in the following sections, in large pipe diameters, churn flow, instead of slug flow was observed by many scholars (Ali, 2009). For this reason, representation of churn flow behavior is key to predicting pressure drop and rates for flow in large pipe diameters. Therefore, developing a flow model that can predict flow regime and describe flow behavior in large pipe diameters adequately are the main focuses of this study.

2.3. Friction Factor

Since total pressure loss is the sum of frictional and gravitational pressure loss, friction factor is also one of the important considerations to develop the model in this study. Moody diagram is a well-known reference for friction factor calculation for pipe flow. Relations among friction factor, Reynolds number, and relative roughness are graphically shown on Moody diagram. The diagram consists of 4 zones: laminar flow, critical zone, transition zone, and complete turbulence zone. Friction factor for laminar flow (R_e< 3000) can be estimated as:

$$f_{moody} = \frac{64\mu}{\rho v d} = \frac{64\mu}{R_e} \tag{4}$$

where f_{moody} is a moody friction factor that is 4 times the fanning friction factor. Moody (1944) applied Colebrook correlation (Colebrook, 1939) for the transition zone between smooth and rough pipes. Colebrook's equation has two parts for smooth and rough pipe flow. The friction factor for flow in smooth pipes is expressed as:

$$\frac{1}{\sqrt{f_{moody}}} = 1.74 - 2log\frac{18.6}{R_e\sqrt{f_{moody}}} \tag{5}$$

for flow in rough pipes is adapted from Nikuradse's (1933) sand-grain experiments for fully rough wall pipes. The friction factor for fully rough wall pipes are independent of Reynolds number:

$$\frac{1}{\sqrt{f_{moody}}} = 1.74 - 2log\frac{2\varepsilon}{d} \tag{6}$$

Therefore, a universal function of friction for flow in smooth and rough pipes is:

$$\frac{1}{\sqrt{f_{moody}}} = 1.74 - 2\log\left(\frac{18.6}{R_e\sqrt{f_{moody}}} - \frac{2\varepsilon}{d}\right) \tag{7}$$

Colebrook equation is applicable for Reynolds number between 4000 and 10^8. Due to implicit form of Colebrook equation, numerous explicit approximations have been developed. Zigrang and Sylvester (1985) is considered one of the most accurate and simple approximation (Brill and Mukherjee, 1999). In addition, Fang et al. (2011) evaluated approximations of Colebrook equation (Romeo et al, 2002; Buzzelli, 2008; Serghides, 1984; Zigrang and Sylvester, 1982; Vatankhah and Kouchakzadeh, 2009; Chen, 1979; Barr, 1981; Serghides, 1984) and Zigrang and Sylvester (1982) had lower relative errors to Colebrook equation. Zigrang and Sylvester (1982) is expressed as:

$$\frac{1}{\sqrt{f_{moody}}} = -2log\left[\frac{2\varepsilon/d}{3.7} - \frac{5.02}{R_e}\log\left(\frac{2\varepsilon/d}{3.7} + \frac{13}{R_e}\right)\right] \tag{8}$$

For smooth pipe, Blasius (1908) is commonly used for transition and complete turbulence zone on Moody diagram:

$$f_{moody} = 0.184{R_e}^{-0.2} \text{ for } 10^5 < R_e < 2\text{x}10^6 \quad (9)$$

$$f_{moody} = 0.316{R_e}^{-0.25} \text{ for } 3000 < R_e \leq 10^5 \quad (10)$$

Noriyuki and Terao (2017) presented friction factor correlation using an experimental study conducted at Hi-Reff (High Reynolds number actual flow facility) at National Metrology Institute of Japan. The facility has approximately 200 m (656 ft) long pipe with water tank located at 30 m (98.4 ft) height. Noriyuki and Terao (2017) used pressure drop in 0.1 m (3.94 in) and 0.387m (15.2 in) diameter smooth pipes (roughness = 10-7 and 2x10-7 m) which covered Reynolds number between 1.2x104 and 107. They presented the best fitting for the wide range of Reynolds number:

$$\frac{1}{\sqrt{f_{moody}}} = -2.064\log\left(R_e\sqrt{f_{moody}}\right) - 1.025 - 15614{R_e}^{-1.231} \quad (11)$$

Fang et al (2010) evaluated several single-phase friction factor (Chen, 1979; Zigrang and Sylvester, 1982; and Churchill, 1977) along with different ranges of relative roughness and developed friction factor for smooth and rough pipe.

$$f_{moody} = 1.613\left[\ln(0.234R_r^{1.1007} - \frac{60.525}{R_e^{1.11.05}} + \frac{56.291}{R_e^{1.0712}}\right]^{-2} \quad (12)$$

For the WCD scenario to be explained in Chapter 5, the predicted Reynolds number is between 4 x106 and 6 x106, which is in the rang e of Colebrook friction factor correlation.

2.4. Definition of Large Diameter Pipes.

Throughout this study, the terms, “large diameter” and “small diameter” occur often. Therefore, before proceeding further, “large diameter” shall be defined first.

As explained in the above section, with increasing gas rate at a fixed liquid rate, flow regime in small pipe diameters changes from bubble to slug, churn, and annular flow. However, slug flow is not observed during experimental studies on two-phase flow with pipe diameter larger than 4 in

(Kataoka & Ishii, 1987; Omebere-Iyari et al., 2007; Prasser et al., 2007; Ali, 2009, and Waltrich et al., 2017). According to Ali (2009), among 24 experimental studies on two-phase flow with vertical pipe greater than 5 in ID, churn flow was observed in all studies, instead of slug flow. Kataoka and Ishii (1987) experimentally proved that when the pipe diameter is greater than stable slug bubble limit, slug bubbles are collapsed and broken up into smaller bubbles. This behavior is the main difference in flow between small and large diameter pipes. Kataoka and Ishii defined critical pipe diameter where slug flow does not exist as Eq. (13).

$$D^* = D\sqrt{\frac{g(\rho_l - \rho_g)}{\sigma}} \geq 40 \tag{13}$$

Here D, σ, subscript g, and subscript $l$represent inner pipe diameter, surface tension, gas phase, and liquid phase respectively. For air/water mixture experiments in vertical pipes at near atmospheric pressure, the diameter which meets $D^* = 40$ is about 4 in. Many studies (Bharathan & Wallis, 1983; Kataoka & Ishii, 1987; Shen et al., 2014, Hibiki & Ishii, 2003; Ali, 2009; Waltrich et al., 2017) applied the critical diameter D^* of Kataoka and Ishii (1987) to differentiate large diameter pipes ($D^* \geq$40) from those with small diameter ($D^* \leq$18.5).

When critical diameter is applied to air/water system and oil/gas (30° API oil, 96.5% methane gas) system above atmospheric pressure, different behaviors are seen in the two systems (Figure 4). For air/water system, diameter satisfying D^*= 40 increases slightly from 4 in to 5 in with pressure increasing from atmospheric pressure to 3,000 psia. However, for the oil/gas system, diameter meeting $D^* = 40$ decreases with higher pressure and approaches 1.5 in near 3,000 psia and 60 °F. The difference in behavior is caused by surface tension between oil and gas. Surface tension between air and water at 60 °F is about 72 N/m and stays almost constant with pressure increment.

However, surface tension between oil and gas decreases with higher pressure from 28.8 N/m at 14.7 psia to 3.7 N/m at 3,000 psia. For water and steam (Shen et al., 2010), the trend is almost like the oil/gas system. As stated above, many scholars did not observe slug flow in diameter larger than 5 in in their air/water experiments. Therefore, employing flow models predicting slug flow may not be adequate for oil/gas flow in diameter larger than D^*= 40 and it may be less than 2 in in field conditions. Unless specified, pipes with diameter larger than 4 in are considered large diameter pipes throughout this study.

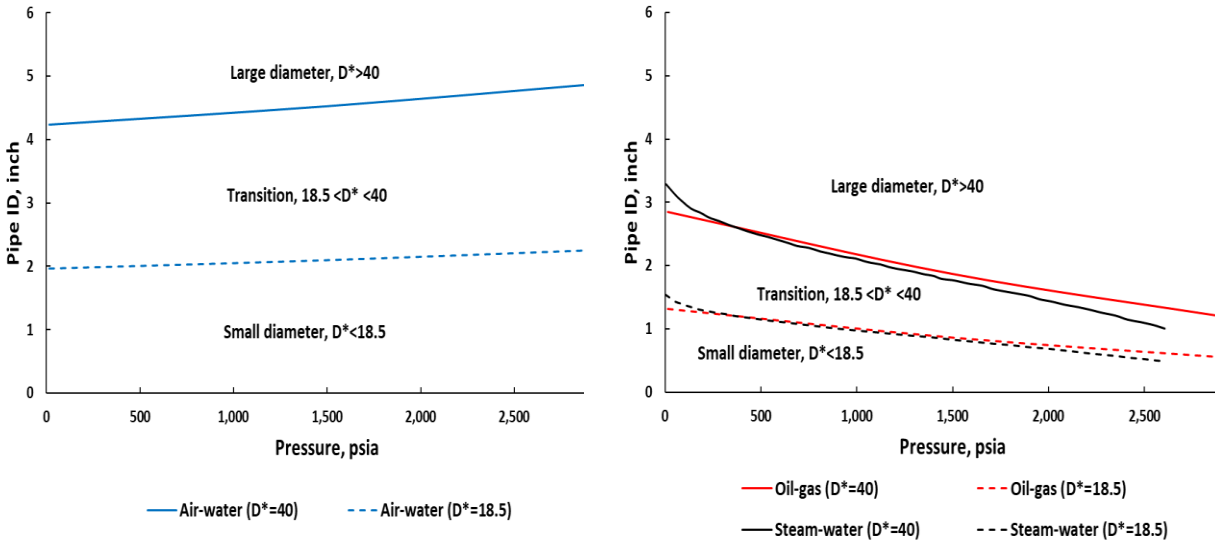

Figure 4. Large and small diameter estimation with increasing pressure:
(Left) air - water, (Right) oil - gas and water - steam

2.5. Two-Phase Flow Models

Two-phase flow models can be categorized as empirical correlations, mechanistic models, and other flow models (drift-flux model and computational fluid dynamics- CFD). Empirical correlations and mechanistic models are commonly employed in petroleum engineering. Development conditions and flow regimes of the flow models in each category are briefly described in this chapter.

2.5.1. Empirical Correlations

An empirical correlation represents a curve fit to laboratory or field data and is therefore relatively simpler than mechanistic models; but its validity is generally limited within the range of model's development conditions (Shi et al., 2005). The experimental or field condition of empirical correlations are presented in the following.

1) Poettmann and Carpenter (1952)

Poettmann and Carpenter (1952) developed pressure gradient correlations in vertical multiphase flow pipes. They used field data from 34 flowing oil wells and 15 gas lift wells completed with 2, 2 ½, and 3in nominal diameter tubing. The gas lift wells had gas liquid ratio (GLR), oil rate, and depth between 1.1 and 41 Mscf/bbl, 5 and 80 bbl/d, and 1,050 ft and 3,700 ft respectively. The flowing oil wells had GLR, oil rate, and depth between 0.19 to 5.1 Mscf/bbl, 60 to 1,400 bbl/day, and 3,000 ft to 11,000 ft respectively. Produced oil gravity varied from 30° to 54° API. Surface temperature was assumed to be 80 °F. They assumed no-slip conditions and a constant friction coefficient over the well length.

2) Baxendell and Thomas (1961)

The Baxendell and Thomas (1961) correlation is an extension of the findings of Poettmann and Carpenter (1952) for higher flow rates. It was developed with 25 data points from a 6,250 ft (1905 m) deep well producing oil at 12,000 bbl/d. The well was completed with 2 7/8 in outer diameter (OD) tubing and 7 in ID casing, with 3 1/2 OD in tubing and 7 in ID casing. For the annular flow experiments, the liquid rates between 200 and 5,100 bbl/d (mostly above 2,000 bbl/d) were tested. The oil gravity, viscosity, and GOR were 34° API, 2.58 cP at 160 °F, and 120 to 160 gas volume/oil volume respectively. The average flow temperature was 180 °F.

3) Duns and Ros (1963)

The Duns and Ros (1963) correlation was developed with 4,000 experimental data of liquid and gas mixture flow in 1.26, 3.16, and 5.6 in ID and 33 ft long vertical pipes. The liquid viscosity varied from 1 to 300 cP. Their flow regime map (Figure 5) is divided into three regions: Region I, where continuous liquid exists, as do bubble, plug, and part of froth flow regime; Region II, where liquid and gas phase alternates. Slug flow and the rest of froth flow regime are in Region II. Continuous gas phase exists in Region III, as also mist flow. Transition is the area between Region II and Region III.

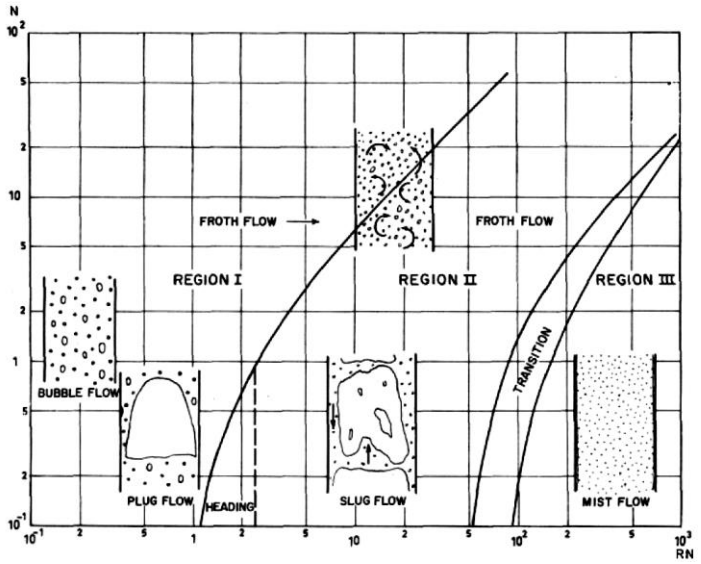

Figure 5. Two-phase flow regime map developed with upward flow in 1.26 to 5.6-in diameter pipes (Duns and Ros, 1963)

Duns and Ros (1963) proposed four dimensionless numbers: liquid velocity (N_{lv}), gas velocity (N_{gv}), pipe diameter (N_d), and liquid viscosity (N_l). These parameters are used to determine slip velocity, liquid holdup, friction factor, flow regime, and eventually pressure gradient. As can be seen from Eq. 14 to 17, these dimensionless numbers are functions of fluid velocity ($u_{sl}$and u_{sg}), liquid density (ρ_l), gravity (g), surface tension (σ), and pipe diameter (d).

$$N_{lv} = u_{sl}\sqrt[4]{\frac{\rho_l}{g\sigma}} \tag{14}$$

$$N_{gv} = u_{sg}\sqrt[4]{\frac{\rho_l}{g\sigma}} \tag{15}$$

$$N_d = d\sqrt{\frac{\rho_l g}{\sigma}} \tag{16}$$

$$N_l = \mu_l\sqrt[4]{\frac{g}{\rho_l \sigma^3}} \tag{17}$$

4) Fancher and Brown (1963)

Fancher and Brown (1963) used data from a 8,000 ft well completed with 2 3/8 in OD tubing. The testing liquid flow rate and GLR varied from 75 to 936 bbl/d and from 0.10 to 9.4 Mscf/bbl. Oil gravity and viscosity were 34 °API at 60 °F and 0.46 cP at 3,375 psig. Gas specific gravity was 0.57. They extended the Poettman and Carpenter (1952) correlation to lower-density fluids and included GLR as an additional parameter. Fancher and Brown (1963) did not consider flow regimes in their flow correlation.

5) Hagedorn and Brown (1964)

The Hagedorn and Brown (1964) correlation was developed with a 1,500 ft vertical experimental well completed with 1, 1 1/4, and 1 1/2 in tubing using air, water, and oil at 80°F. Liquid viscosity was 1, 10, 30, 35, and 110 cP and oil API gravity was between 26 °API and 34° API. As many as 2,905 pressure points were obtained from 475 tests in test well and 106 tests from Fancher and Brown (1963). Unlike other tested correlations, Hagedorn and Brown did not measure actual liquid hold-up, nor employ flow regime for pressure estimation. Rather, they developed correlations to estimate pseudo liquid hold-up to match their measured pressure gradient. For liquid hold-up

correlation, they applied the four dimensionless parameters (Eq. 5 – 8) proposed by Duns and Ros (1963). Liquid hold-up correlation plot is presented in Figure 6.

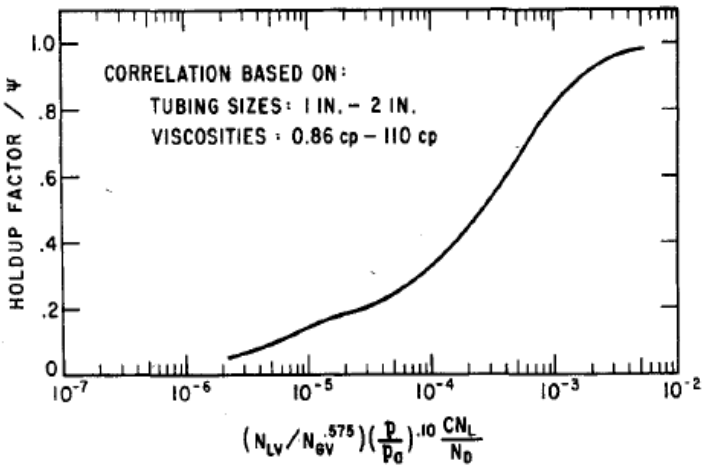

Figure 6. Liquid holdup correlation of Hagedorn and Brown (1964)

6) Dukler (1964)-Flanigan (1958)

The Dukler et al. (1964) correlation was used to calculate the liquid hold-up and the frictional pressure drop for two phase flow in a horizontal pipe. The Flanigan (1958) liquid hold-up correlation was developed from the data in a 16 in ID gas dominated uphill pipeline. To determine gravitational pressure losses in uphill flow and downhill flow, these two flow models are combined into one correlation.

7) Beggs and Brill (1973)

The Beggs and Brill (1973) correlation was derived from 584 two-phase (air and water) flow tests with 1 and 1 1/2 in ID and two 45 ft long acrylic pipes in various inclination angles from horizontal to ± 90°. It determined flow regimes in horizontal pipe as segregated, intermittent, and distributed flow and then calculated flow-regime-specific void fraction and pressure gradient. For inclined pipe, the void fraction in horizontal pipe was corrected and used for further calculation. Therefore, their flow regime map does not represent an actual flow regime for non-horizontal pipes (Figure

8). For flow pattern transition and liquid hold-up calculation, empirical coefficients are used for each flow regime category. Under three flow regime categories (segregated, intermittent, and distributed flow), sub-flow regimes were included as shown in Figure 7. In the revised flow regime map (Brill and Beggs, 1991), flow regime boundaries were modified to add transition flow regime.

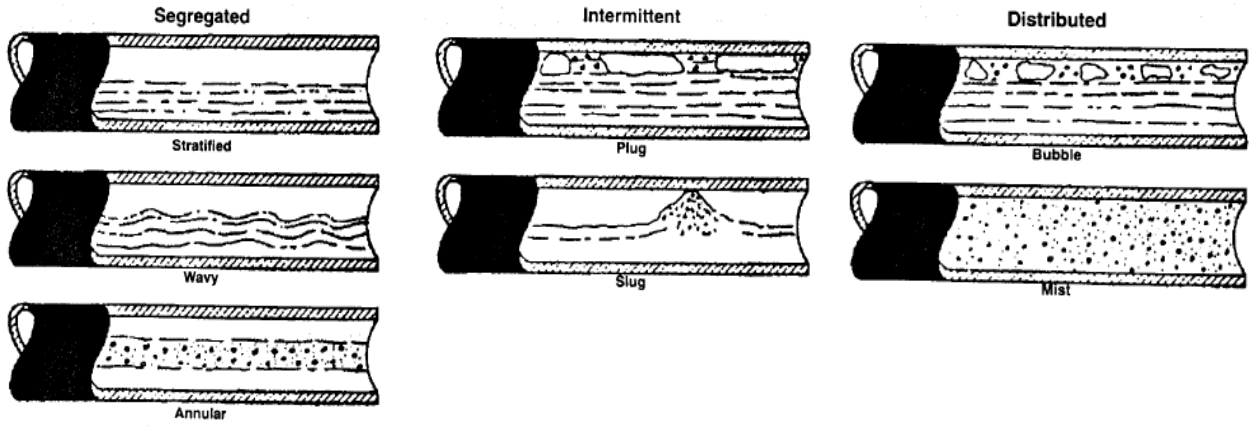

Figure 7. Flow patterns observed in 1 and 1 1/2 in horizontal pipes (Beggs and Brill, 1973)

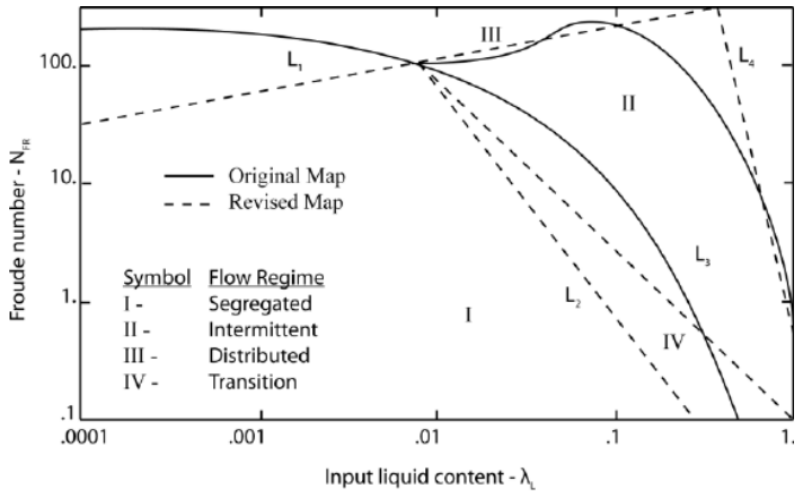

Figure 8. Original and revised flow regime maps (Brill and Beggs, 1991)

8) Gray (1974)

The Gray (1974) correlation was specifically designed for gas and condensate vertical wells. It assumed that friction factor was affected by relative roughness, but not by Reynolds number. The

correlation was validated with 108 sets of well data. The data ranges include flow velocity below 50 ft/s, tube diameter smaller than 3 1/2 in., condensate gas ratio (CGR) less than 50 bbl/MMscf, and WGR smaller than 5 bbl/MMscf.

9) Teles (2020)

Teles (2010) studied a data-driven model for multiphase flow in pipes. Teles built automated flow loops using 1.049 in ID and 7.8 ft and 45 ft long pipes and obtained dimensionless numbers, pressure gradient, and drift-flux parameters using the flow loops experiments. Then, Teles built a model determining liquid holdup and pressure gradient in two methods. The first method is to estimate the pressure gradient and liquid holdup from the experimental data, which have similar dimensionless numbers. The second method is to calculate liquid holdup and pressure gradient using the obtained drift-flux parameters. Teles recommended to adopt machine learning algorithms to directly predict pressure gradient using more data.

As described above, many empirical correlations are flow regime dependent and validated with air-water two phases flow in small diameter pipes. This may lead improper application of empirical correlation for oil-gas flow in large diameter pipes.

2.5.2. Mechanistic Models

A mechanistic correlation is built from general physical laws and observations and is as such relatively more complex than empirical models. The experimental or field conditions of mechanistic correlations are briefly described below.

1) Orkiszewski (1967)

Orkiszewski (1967) combined pre-existing correlations with his slug flow model for the pressure gradient of two-phase flow in production wells. The studies used for Orkiszewski's flow regime

were Griffith and Wallis (1961) for bubble and slug flow; Duns and Ros (1963) for annular mist flow and for the slug to mist flow transition. The model was verified with 148 measured pressure data from Hagedorn and Brown (1964), Poettmann and Carpenter (1952), Fancher and Brown (1963), Baxendell and Thomas (1961), and heavy oil wells (10 ° to 20 °API).

2) Aziz et al. (1972)

Aziz et al. (1972) presented liquid hold-up and pressure drop calculations for wells producing oil and gas. Aziz et al. (1972) applied the flow regime map of Govier and Aziz (1972) which consists of bubble, slug, froth, and annular flow (Figure 9). The authors tested their model against 48 field data from earlier publications including 38 data points from Espanol et al. (1969), 1 point from Poettmann and Carpenter (1952), 1 point from Orkiszewski (1967), and 8 points from Energy Resources Conservation Board. Well depth ranged from 4,300 to 12,500 ft and most of the wells were more than 8,000 ft deep. Tubing ID was 2.376 in and oil rates between 100 and 1,300 bbl/d, while the majority of flow rates were less than 200 bbl/d. GOR were below 10 Mscf/bbl, most of them between 0.15 and 1.60 Mscf/bbl. Oil API gravity and WOR were 36 °- 47 ° (mostly 44°) API and 1.38 bbl/bbl respectively.

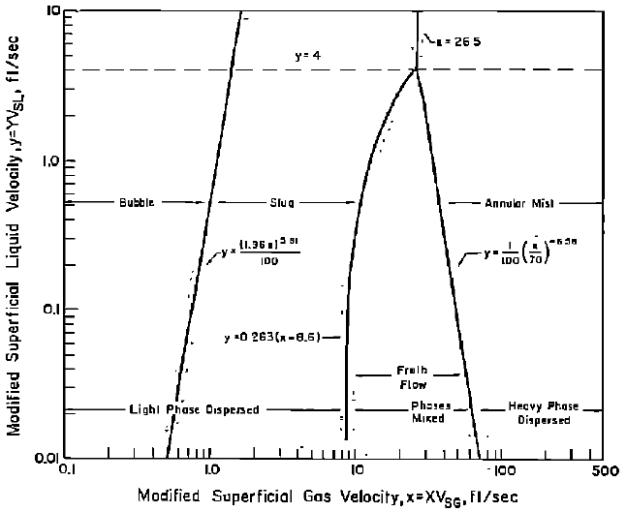

Figure 9.Govier and Aziz (1972) flow pattern map

3) Taitel et al. (1980)

The flow regime map of Taitel el al. (1980) shown in Figure 10 was constructed with air/water mixture flow in 2 in ID vertical tubes with different pipe lengths. They used bubble-rise velocity and slip-velocity to define the boundary between bubble and slug flow by the following expressions:

$$u_{s.b.} = 1.53 \left[\frac{g(\rho_l - \rho_g)\sigma}{{\rho_l}^2}\right]^{0.25} \tag{18}$$

$$u_{s.b.} = u_{slip} = u_g - u_l = \frac{u_{sg}}{\alpha} - \frac{u_{sl}}{(1-\alpha)} \tag{19}$$

where $u_{s.b.}$ is a small bubble-rise velocity and $\propto$ is critical void fraction at which the transition from bubble flow to slug flow occurs by bubble coalescence. Taitel et al. set α equals 0.25 and determined u_{sg} along the bubble and slug flow transition curve A as in Figure 10. For annular flow boundary, they defined gas superficial velocity greater than the velocity in Eq. 20 and presented as curve E in Figure 10.

$$u_{SG} > 3.1\left(\sqrt{\frac{g\sigma(\rho_L - \rho_G)}{{\rho_G}^2}}\right)^{0.25} \tag{20}$$

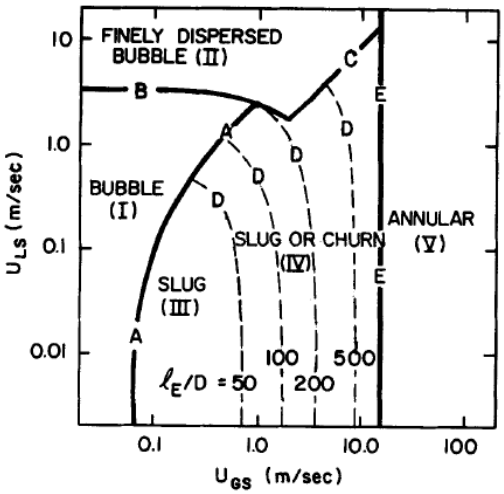

Figure 10. Flow pattern map for air-water flow in 2 in diameter vertical tubes (Taitel et al, 1980)

4) Mukherjee and Brill (1985)

Mukherjee and Brill (1985) proposed a model which is an extension of Beggs and Brill (1973), which can determine liquid hold-up and flow regime transition at any pipe inclination angle. Air/oil (kerosene and light lube oil) and 1 1/2 in ID U-shape pipe were used for the experiments. The U-shaped pipe was placed in the horizontal direction initially and the pipe's inclination angle could be adjusted. Each leg of the pipe was 56 ft long. The density and viscosity of kerosene at 60 °F were 42 ° API and 2 cP, respectively. Corresponding values for lube oil were 35° API and 29 cP. The correlation was verified with Prudhoe Bay and North Sea field data. Mukherjee and Brill created a flow regime map using the liquid and gas number proposed by Duns and Ros (1963). For vertical up flow, bubble, slug, and annular (or mist) flow are presented as Figure 11. Mukherjee and Brill's annular/mist flow regime is similar to Duns and Ros mist flow and transition flow region.

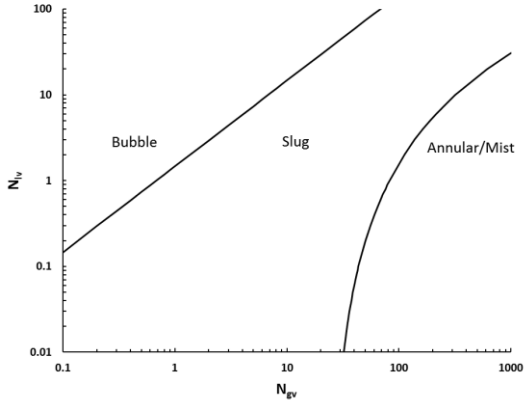

Figure 11. Mukherjee and Brill (1985) flow regime map for up-flow

For flow regime transitions, bubble/slug ($N_{lv\,B/S}$) and slug/mist transition ($N_{gv\,S/M}$) are defined as below:

$$N_{lv\,B/S} = 10^{(logN_{gv}+0.94+0.074sin\theta-0.855\sin^2\theta+3.695N_l} \quad (21)$$

$$N_{gv\,S/M} = 10^{(1.401-2.694N_l+0.521{N_l}^{0.329}} \quad (22)$$

5) Ansari et al. (1990)

Ansari et al. (1990) proposed a mechanistic model for flow regime, liquid hold-up, and pressure drop determination for upward two-phase flow in vertical pipe, using several existing correlations. The flow models they applied were Caetano (1985) for bubble flow, Sylvester (1987) and McQuillan and Qhalley (1985) for slug flow, and Hewitt and Hall Taylor (1969) for annular flow. The model was verified with the Tulsa Fluid Flow Projects (TUFFP) database (1,712 tests). Similar to Taitel et al. (1980), Ansari applied bubble-rise velocity and void fraction of 0.25 to define bubbly/slug flow transition, as seen in Figure 12.

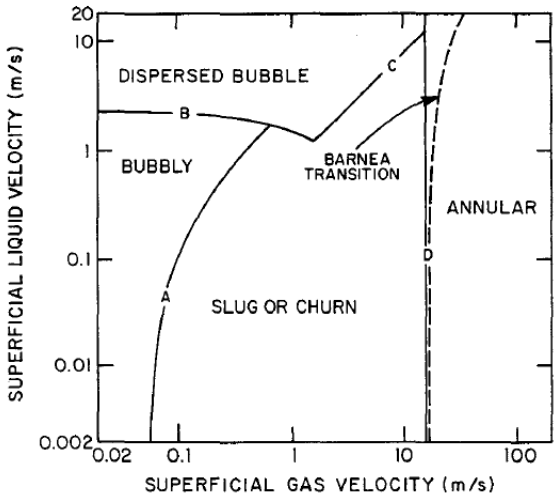

Figure 12. Ansari et al. (1990) flow pattern map

6) Petalas and Aziz (1996)

Petalas and Aziz (1996) presented a mechanistic model for a wide range of pipe geometries and fluid properties. They built the model corresponding to stratified (smooth and wavy), intermittent (slug, elongated bubble, plug), annular-mist (annular flow with dispersed bubble), bubble, dispersed bubble, froth or churn flow regimes. A constant liquid film thickness and no slip velocity between gas and liquid droplets in the gas core were assumed. The model incorporated liquid entrainment and pipe roughness effects for pressure gradient. The correlation was tested against 5,961cases in the Stanford Multiphase Flow Database (SMFD).

7) Chokshi et al. (1996)

The Chokshi et al. (1996) pressure drop model in vertical, upward two-phase flow in wellbores was developed with 324 tests of varying air-water flow rate. The vertical pipe had 2.992 in ID and 1,333ft length. Compressed air up to 750 psig was injected and flow rate, pressure, and temperature at 8 locations were recorded. Gamma-ray densitometer was used to measure non-intrusive hold-up at 490 ft below the surface. The model recognized bubble, slug, and annular flow regimes and was evaluated with 1,712 data sets in the TUFFP databank.

8) Gomez et al. (2000)

Gomez et al. (2000) presented a unified steady-state two-phase flow mechanistic model applicable to horizontal to vertical upward pipe. The model defined unified flow regimes using modifications from previous publications Taitel and Dukler (1976) for stratified flow, Taitel and Barnea (1980) for slug flow and Alves et al. (1991) for annular flow. The model predicted flow regimes as slug, bubble, annular, and dispersed bubble flow. The authors validated the correlation against 1,723 lab and field data sets in the TUFFP databank.

2.5.3. Summary

As described above, a wide variety of flow models and corresponding flow regime maps exist. Most of the flow regimes are expressed in terms of superficial fluid velocities, while some are defined with dimensionless parameters. Flow regime maps (Ansari et al., 1990; Mukherjee and Brill, 1985, Aziz et al., 1972) include slug flow, which is not often observed in large diameter pipes (Ali, 2009). The experimental/field conditions of the described two-phase flow models are summarized in Figure 13 and Table 1. In Figure 13, the range of liquid flow rate (blue bars) and pipe diameters (dark bars) used for steady-state flow model development are presented. A pattern filled bar in Duns and Ross (1963) represents effective diameter for flow in annulus. As it can be seen in Figure 13 and as described above, most of the two-phase flow models were built with a pipe diameter smaller than 4 in with air-water at atmospheric condition.

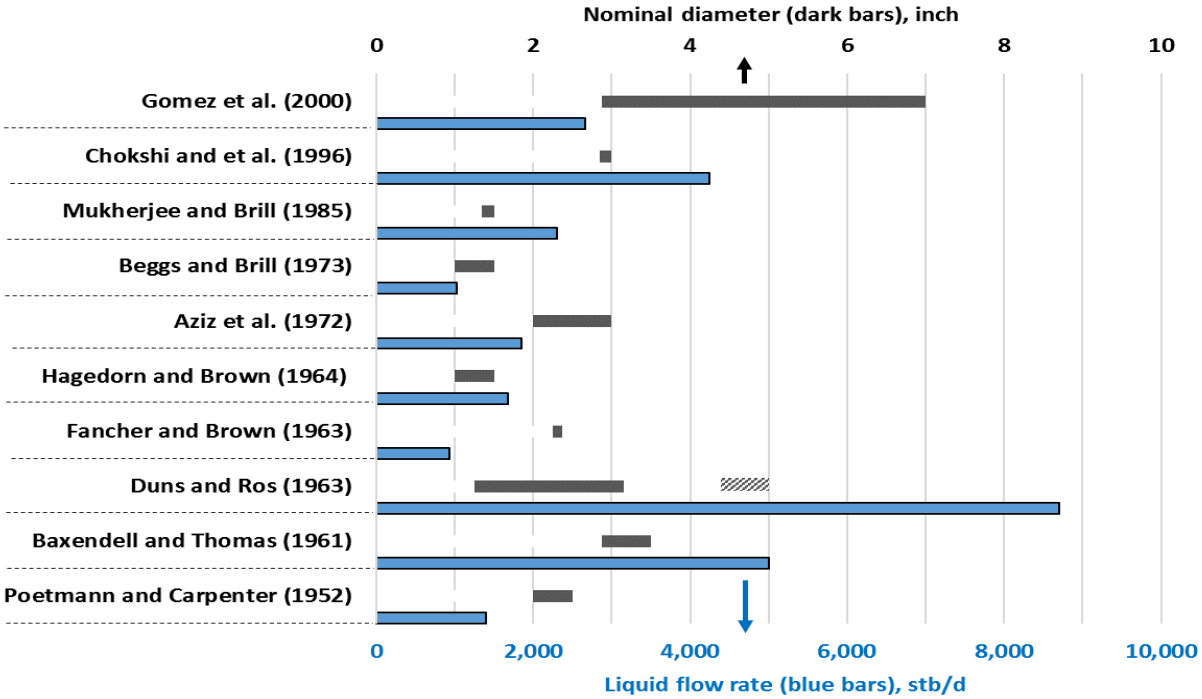

Figure 13. The range of liquid rate and pipe diameters used for steady-state flow model development

Table 1. Experimental /field condition of two-phase flow models for pressure loss estimation

Correlations	Fluids	Pipe nominal diameter (in)	Pipe length (ft)	liquid rate (bbl/day)	Gas rate (Mscf/day)	Fluid properties	Avg. Temp. (°F)	Inclination (degree from horizon)
Poettmann and Carpenter (1952)	oil/gas, gas/oil/water	2, 2.5, 3	1050 – 3,700 3,000-11,000	5 – 80 60-1,400	N/A	30°-54° API 1.1<GLR<41 Mscf/bbl	80	90
Baxendell and Thomas (1961)	gas/oil	2.875, 3.5 OD	6,250	200-5,000	N/A	34° API, 2.58 cP at 160 °F 120 < GOR <160 vol/vol	180	0 and 90
Duns and Ros (1963)	air/oil	1.25, 3.15 (Pipe) 5.6 (Annulus)	33	0 – 8,700 (0-10.5 ft/s)	34- 328 ft/s (0-155mscf/d)	10°-50° API	N/A	90
Fancher and Brown (1963)	gas/oil	2.375 OD	8,000	75- 936	34 – 1,400	34° API, 0.46 cP; gas: 0.65 SG 0.10 <GLR< 9.4 Mscf/bbl Water cut: 0.95	N/A	Any angle
Hagedorn and Brown Original (1964) and Modified (1965)	air/water, air/oil	1, 1.25, 1.5	1,500	30 – 1,680	N/A	26° and 34° API 1, 30, 35, 110 cP 0 < GLR < 3270 scf/bbl	80	90
Orkiszewski (1967)	Tested against Hagedorn and Brown (1964), Poettmann and Carpenter (1952), Fancher and Brown (1963), Baxendell and Thomas (1961), and heavy oil wells (10 to 20° API)							90
Aziz et al. (1972)	gas/oil	2 – 3	4,300 – 12,500	50-1,850	N/A	36°-47° API; 0.15 < GLR< 10 Mscf / bbl; 0 < WOR < 1.38	N/A	90
Beggs and Brill (1973) and Revised	air/water	1, 1.5	2 x 45	0 – 1,030	0 – 300	Air and water at atmospheric condition	N/A	any angle
Gray (1974)	gas/condensate	< 3.5	N/A	N/A	< 50 ft/s	CGR < 50 bbl/MMscf WGR < 5 bbl/MMscf 0.04< WOR < 1.38	N/A	90
Govier and Foragasi (1975)	gas/condensate	1 – 4	3,678 -12,073	N/A	144-27,400	35°-41° API; 0.1 – 0.8 cP 3.9 < GCR < 1,170 Mscf/bbl	60-250	N/A
Mukherjee and Brill (1985)	air/oil	1.5	2 x 32	0-2,300 (0-12 ft/s)	0-95 (0-90 ft/s)	kerosene: 42° API, 2 cP lube oil: 35° API, 29 cP	18 – 132	any angle
Asheim (1986)	gas/oil	Tested with Forties field, Ekofisk field, and Prudhoe Bay flow line data points						0 to 90
Petalas and Aziz (1996)	Verified against selected Stanford Multiphase Flow Database (unknown fluid properties and well conditions)							any angle
Chokshi and et al.(1996)	air/water	2.992	1,348	79-4,250	42-2,800	16-12,685	N/A	90
	Built with above exp. Data and evaluated with selected TUFFP data bank (unknown fluid properties and well conditions)							
GOMez et al. (2000)	gas/oil	2.875-7	N/A	79-2,658	42-23,045	0<Water cut <0.8	N/A	0 to 90

2.6. Drift-Flux Model for Void Fraction Estimation

Drift-flux model developed by Zuber and Findlay (1965) has its advantage over void fraction estimation using two-phase fluid model due to its simplicity. The drift-flux model describes the relative motion between two different phases, and it considers the mixture as a whole. The distribution parameter, C_o, signifies the gas phase distribution on pipe cross section and it assumes no local slippage between gas and liquid phases. Therefore, C_o is related to void fraction distribution and flow regime. The drift velocity, u_d, is the relative velocity of the gas phase to the mixture velocity at the center of a pipe cross section (Zuber and Findlay, 1965).

In this chapter, derivation of drift-flux correlations is described. Volumetric flux density in Zuber and Findlay (1965) is replaced by superficial velocity here to maintain consistency in terminologies.

Zuber and Findlay (1965) defined the relative velocity between the two phases by

$$u_r = u_G - u_L \tag{23}$$

and the drift velocities with respect to the superficial velocity of the mixture by

$$u_{dG} = u_G - (u_{SG} + u_{SL}) \tag{24}$$

Since $u_{SG} = \alpha u_G$,

$$u_{dG} = u_r(1 - \alpha) \tag{25}$$

When relative velocity is zero,

$$u_{dG} = 0 \tag{26}$$

$$u_G = u_{SG} + u_{SL} = u_{SM} \tag{27}$$

Average value over the cross-sectional area of pipe can be defined by

$$< F > = \frac{1}{A} \int F dA \tag{28}$$

and average gas velocity over the cross-sectional area of pipe is

$$< u_G >=< \frac{u_{SG}}{\alpha} >=< u_{SM} > +< u_{dG} > \tag{29}$$

The weighted mean value of quantity F is

$$\bar{F} = \frac{< \alpha F >}{< \alpha >} = \frac{\frac{1}{A}\int \alpha F dA}{\frac{1}{A}\int \alpha dA} \tag{30}$$

whence the weighted mean velocity of gas phase can be obtained

$$\overline{u_G} = \frac{< u_G \alpha >}{< \alpha >} = \frac{< u_{SG} >}{< \alpha >} \tag{31}$$

Therefore,

$$\overline{u_G} = \frac{< u_{SM} \alpha >}{< \alpha >} + \frac{< u_{dG} \alpha >}{< \alpha >} \tag{32}$$

When first term on the right side of Eq. (32) is multiplied and divided by $< u_{SM} >$,

$$\overline{u_G} = \frac{< u_{SG} >}{< \alpha >} = \frac{< u_{SM} \alpha >< u_{SM} >}{< \alpha >< u_{SM} >} + \frac{< u_{dG} \alpha >}{< \alpha >} \tag{33}$$

$$\overline{u_G} = \frac{< u_{SG} >}{< \alpha >} = C_o < u_{SM} > + \frac{< u_{dG} \alpha >}{< \alpha >} \tag{34}$$

where,

$$C_o = \frac{< u_{SM} \alpha >}{< \alpha >< u_{SM} >} \tag{35}$$

Eq. (34) can be expressed in non-dimensional form by diving both side with $< u_{SM} >$,

$$\overline{u_G} = \frac{< u_{SG} >}{< \alpha >< u_{SM} >} = C_o + \frac{< u_{dG} \alpha >}{< \alpha >< u_{SM} >} \tag{36}$$

Therefore, volumetric concentration, void fraction is

$$< \alpha >= \frac{< u_{SG} > / < u_{SM} >}{C_o + \frac{< u_{dG} \alpha >}{< \alpha >< u_{SM} >}} \tag{37}$$

Once general expressions for the average volumetric concentration is obtained, non-uniform flow and distribution concentration effects can be found. Zuber and Findlay (1965) considered axially symmetric flow through a pipe and flow and assumed concentration distributions given by

$$\frac{u_{SM}}{u_{SMc}} = 1 - \left(\frac{r}{R}\right)^m \tag{38}$$

$$\frac{\alpha - \alpha_w}{\alpha_c - \alpha_w} = 1 - \left(\frac{r}{R}\right)^n \tag{39}$$

where subscript c and w refer to pipe center and pipe wall. C_o can be expressed in terms of α_w or α_c

$$C_o = 1 + \frac{2}{m+n+2}\left[1 - \frac{\alpha_w}{<\alpha>}\right] \tag{40}$$

$$C_o = \frac{m+2}{m+n+2}\left[1 + \frac{\alpha_c}{<\alpha>}\frac{n}{m+2}\right] \tag{41}$$

When volumetric concentration is in uniform across the pipe,

$$\alpha_w = \alpha_c = <\alpha> \tag{42}$$

$$C_o = 1 \tag{43}$$

If volumetric concentration at center is larger than that at the wall,

$$\alpha_c > \alpha_w \tag{44}$$

$$C_o > 1 \tag{45}$$

Or if volumetric concentration at center is smaller than that at the wall,

$$\alpha_c < \alpha_w \tag{46}$$

$$C_o < 1 \tag{47}$$

Based on above expressions, C_o can be estimated as function of α_w/α_c, m, and n for vertical upward pipe (Figure 14). From Figure 14, for fully established and constant profile, C_o ranges

between 1.5 and 1.0 depends on α_w/α_c. When α_w/α_c = 1, C_o= 1 for any m and n. For α_w/α_c = 0, C_o is between 1.1 and 1.5 depends on m and n.

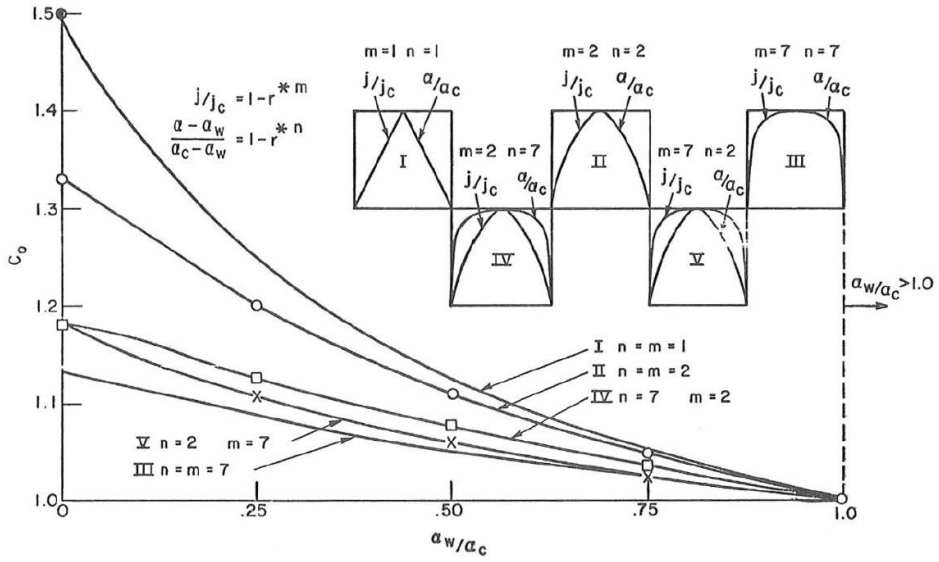

Figure 14. C_o as function of the exponents of concentration profile curves for vertical upward pipe (Zuber and Findlay, 1965)

From a general one-dimensional drift-flux equation, void fraction α, can be determined (Eq. 23). The one-dimensional drift model assumes constant two phase properties across pipe diameter. Therefore, those properties such as void fraction, fluid velocity, drift-flux velocity and drift coefficient are averaged values across pipe cross section. Therefore, Eq. (36) can be expressed by

$$u_G = \frac{u_{SG}}{\alpha} = C_o(u_{SG+}u_{SL}) + u_d \tag{48}$$

Many scholars developed drift-flux models for two-phase upward flow with flow regime-dependent distribution parameter, C_o, and drift-flux velocity, u_d. For bubbly and slug flow, C_o between 1 and 1.3 is used in many studies and corresponds to pipe center peaked void fraction. For Annular flow, C_o close to 1 representing almost flat void fraction across pipe diameter is generally used (Thome, 2006).

In nuclear engineering, drift-flux models are widely used for void fraction prediction in boiling water reactors. In petroleum engineering, some mechanistic pressure loss models (Aziz et al., 1972;

Taitel et al., 1980; Hasan & Kabir, 1988; Ansari et al., 1990; and Hasan et al., 2010) incorporate drift-flux model to predict bubble velocity in fluid column and void fraction, as presented in Table 2. Therefore, it is important to understand that a pressure loss model can be developed with a drift-flux model that estimates void fraction in each flow regime.

Table 2. Pressure loss models applied drift-flux correlations to estimate bubble velocities

Studies	Bubbly flow	Slug flow	Annular flow
Aziz et al, 1972	$u_G = 1.2u_M + v_{BS}$	$u_G = 1.2u_M + v_{TB}$	Non-drift flux
Taitel et al., 1980	$u_G = 1.2u_M + v_\infty$	$u_G = 1.2u_M + v_{TB}$	Non-drift flux
Hasan and Kabir, 1988	$u_G = 1.2u_M + v_\infty$	$u_G = 1.2u_M + v_{TB}$	Non-drift flux
Ansari et al., 1990	$u_G = 1.2u_M + v_{BS}$	$u_G = 1.2u_M + v_{TB}$	Non-drift flux
Hasan et al., 2010	$u_G = 1.2u_M + v_{BS}$	$u_G = 1.2u_M + \overline{v_\infty}$(Slug) $u_G = 1.15u_M + \overline{v_\infty}$ (Churn)	$u_G = u_M$

Studies listed in Table 2 applied rise velocity of bubbles, v_∞, (Harmathy, 1960) or swarm velocity of small bubbles, v_{BS}, in a stagnant liquid column (Zuber & Hench, 1962) as drift velocity, u_d (Eq. 49 and 50) for bubbly flow. For slug or churn flow, Taylor bubble velocity, v_{TB}, (Nicklin et al., 1962) or average bubble rise velocity, $\overline{v_\infty}$, (Hasan et al., 2010) were used as u_d (Eq. 51 and 52). All these studies employed constant C_o = 1.2 for bubbly and slug flow, except Hasan et al. (2010), who used a different C_o for bubbly ($C_o = 1.2$), churn ($C_o = 1.15$), and annular flow ($C_o = 1$). For bubble swarm velocity, v_{BS}, an extra term, $(1-\alpha)^{0.5}$, is added on bubble rise velocity, v_∞. It depicts slower gas bubble movements and lower void fractions thanv_∞. Since v_∞ and v_{BS} are not diameter-dependent, for air and water at 1 atm, v_∞, is about 0.25 m/s (0.82 ft/s) and $v_{BS}$is between 0 and 0.25 m/s.

$$v_{\infty} = u_d = 1.53\left[\frac{g\sigma_L(\rho_L - \rho_G)}{{\rho_L}^2}\right]^{1/4} \tag{49}$$

$$v_{BS} = u_d = 1.53\left[\frac{g\sigma_L(\rho_L - \rho_G)}{{\rho_L}^2}\right]^{1/4}(1-\alpha)^{0.5} \tag{50}$$

$$v_{TB} = u_d = 0.35\left[\frac{gd(\rho_L - \rho_G)}{{\rho_L}^2}\right]^{1/4} \tag{51}$$

$$\overline{v_{\infty}} = u_d = v_{BS}\left(1 - e^{-\frac{0.1v_{GB}}{u_{SG}-v_{GB}}}\right) + v_{TB}\left(e^{-\frac{0.1v_{GB}}{u_{SG}-v_{GB}}}\right) \tag{52}$$

Drift-flux model is theoretically more appropriate when the difference between flowing velocity of each fluid is large or drift velocity is large, which is a bubbly and slug flow regime. However, the proposed drift-flux model shows adequate application to churn and annular flow too.

2.7. Two-Phase Flow Study in Large Diameter Pipes

Although many of the studies on two-phase flow in pipes employ pipe diameters less than 4 in, there are some studies on void fraction estimation for flow in larger pipe diameters in the field of nuclear engineering. In this section, these studies on two-phase flow in large diameter pipes are described. As indicated earlier, the main target of flow models in the field of nuclear engineering is void fraction estimation. Therefore, most of the studies explained in this section do not propose pressure drop calculation methods.

1) Ishii (1977)

Ishii (1977) developed drift-flux model for bubbly, slug, churn, and annular flow, based on a wide range of experiment data using various fluid type (air-water, nitrogen-mercury, steam-water) and geometry (upflow, downflow, round tube, rectangular channel), and pipe diameters (2.36 in – 6.61 in). Ishii argued that the distribution parameter depends on fluid density ratio and assumed 1.2 for

fully developed upward flow in a round pipe. When density ratios equal each other, the distribution parameter becomes 1 (Eq. 53)

$$C_o = 1.2 - 0.2\sqrt{\frac{\rho_G}{\rho_L}} \tag{53}$$

2) Kataoka and Ishii (1987)

Kataoka and Ishii (1987) posited that slug flow seen in small pipes is not sustained in pipe diameter greater than the critical diameter. Above a critical diameter ($D^* \geq 30$) which is about 4 in at atmospheric pressure for air and water, Taylor bubbles are unstable to form slug flow and disintegrate to cap bubbles. The authors developed drift velocity correlation to incorporate the effect of pipe diameter, system pressure, and fluid properties.

For low viscous fluid, $N_{\mu f} \leq 2.25 \text{ x } 10^{-3}$, drift flux velocities are expressed as:

$$u_{d,KI} = 0.03(\rho_G/\rho_L)^{-0.157} N_{\mu f}^{-0.562} N_{nd}, \text{ for} D^* \geq 30 \tag{54}$$

$$u_{d,KI} = 0.00019 D^{*0.809} (\rho_G/\rho_L)^{-0.157} N_{nd,} \text{ for } D^* < 30 \tag{55}$$

For high viscous fluid, $N_{\mu f} \geq 2.25 \text{ x } 10^{-3}$, drift flux velocities are expressed as:

$$u_{d,KI} = 0.92(\rho_G/\rho_L)^{-0.157} N_{nd}, \text{for} D^* \geq 30 \tag{56}$$

$$u_{d,KI} = 0.00019 D^{*0.809} (\rho_G/\rho_L)^{-0.157} N_{nd,} \text{ for } D^* < 30 \tag{57}$$

Non-dimensional parameter N_{nd}, and fluid viscous number, $N_{\mu f}$, are defined as

$$N_{nd} = \left(\frac{\sigma g(\rho_L - \rho_G)}{\rho_L^2}\right)^{0.25} \tag{58}$$

$$N_{\mu f} = \frac{\mu_L}{\left(\rho_L \sigma \sqrt{\frac{\sigma}{g(\rho_L - \rho_G)}}\right)^{0.5}} \tag{59}$$

The authors employed experimental studies of air/water and steam/water in 2 in to 3.78 in column diameter at atmospheric pressure to 2640 psia operating condition.

3) Ohnuki and Akimoto (2000)

Ohnuki and Akimoto (2000) studied the transitions of flow patterns and air/water two-phase distribution in a 7.87 in ID and 40 ft tall vertical pipe (L/D= 61.5). The range of flow rate was 0.03 m/s – 4.7 m/s (0.098 ft/s – 15.4 ft/s) for air superficial velocity and 0.06 – 1.06 m/s (0.19 – 3.48 ft/s) for gas superficial velocity. They visually observed undisturbed bubbly, agitated bubbly, churn bubbly, churn slug and churn froth flows. Ohnuki and Akimoto presented their flow pattern observation at a pipe where L/D=10 and L/D=60 along with the flow transitions of Mishima and Ishii (1984) for comparison and found differences (Figure 15). At L/D=60, the agitated bubbly/churn slug transition of Ohnuki and Akimoto was close to the bubble/slug transition of Mishima and Ishii. However, the slug/churn transition of Mishima and Ishii is located at higher superficial gas velocity, where churn froth was observed in the study of Ohnuki and Akimoto. Unlike Mishima and Ishii, Ohnuki and Akimoto did not observe slug flow in their experiments; hence, flow regime boundaries were quite different from those of Mishima and Ishii.

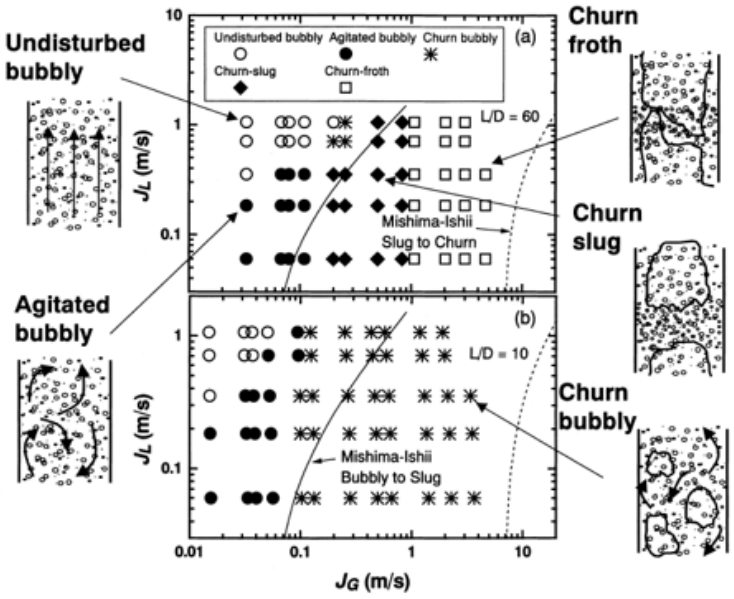

Figure 15. Flow regime map for flow in pipes at (upper) L/D = 60 (lower) L/D = 10 (Ohnuki & Akimoto, 2000)

4) Prasser et al. (2007)

Prasser et al. (2007) generated a comprehensive database for upward air-water flows in a 8 m tall vertical pipe with 7.67 in ID and 2.06 in ID using wire mesh sensor. The testing pressure was from 14.5 psia to 943 psia. The sensor was installed on the top of the test section and gas was injected through holes at 18 different vertical locations. For 7.68 in ID pipe, the testing superficial velocities varied from 0.0025 m/s (0.008 ft/s) to 7.772 m/s (25.5 ft/s) for air and from 0.0405 m/s (0.133 ft/s) to 1.61 m/s (5.28 ft/s) for water. For a smaller 2.06 in ID pipe, the maximum superficial velocities increased to 18.97 m/s (62.2 ft/s) for air and to 4.407 m/s (14.5 ft/s) for water. By interpretation of electro signal from wire mesh sensor, Prasser et al. obtained virtual side projection of void fraction distribution in 2.06 in ID and 7.67 in ID pipes at atmospheric pressure and high pressure.

At atmospheric pressure, as gas superficial velocity increases with fixed water superficial velocity, bubbles in 2.06 in ID pipe coalesce and become bullet-shaped Taylor bubbles that characterize slug flow (Figure 16). Meanwhile, at the same condition, bubbles in 7.67 in ID pipe, do not merge with each other to create Taylor bubbles. Rather, large bubbles become more irregular shaped and are destroyed with higher gas velocity. The flow behavior in larger ID pipe represents flow transition from bubbly to churn turbulent flow without slug flow (Figure 17). Blue represents water and yellow-red represents air bubbles. At higher pressure using steam/water, as pressure increases at fixed water superficial velocity, initially a long Taylor bubble is formed for slug flow in 2.06 in ID pipe is destructed and becomes churn turbulent flow (Figure 18). Similarly, at the same condition, in 7.67 in ID pipe, irregular, large bubbles are dissolved into the mixture and churn turbulent flow becomes more pronounced (Figure 19). Such destruction of large bubbles in the pipes of two sizes is due to the decreasing surface tension and increasing temperature.

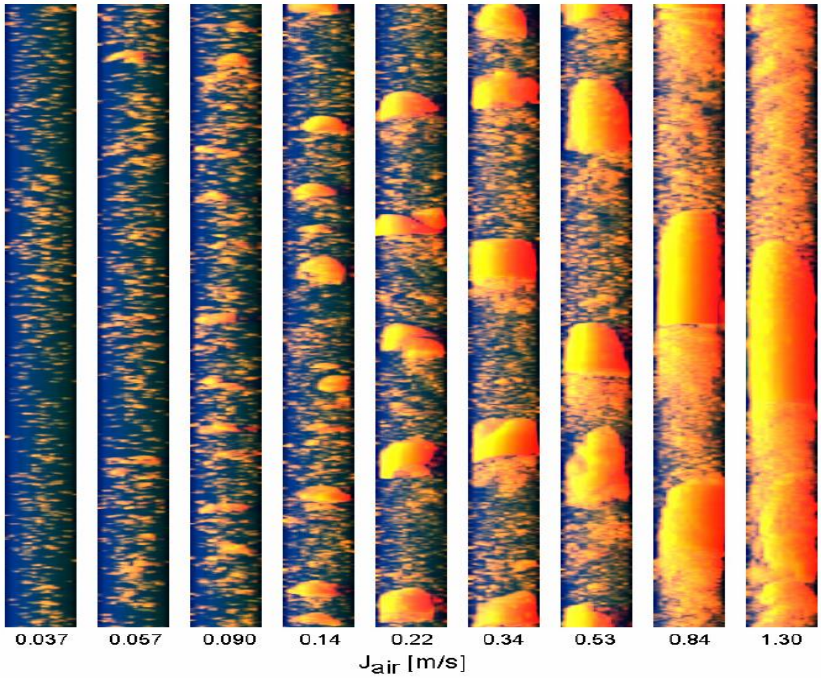

Figure 16. Virtual side fraction of void fraction distribution in 2.06 in ID pipe at water superficial velocity of 1 m/s and atmospheric pressure. (Prasser et al., 2007).

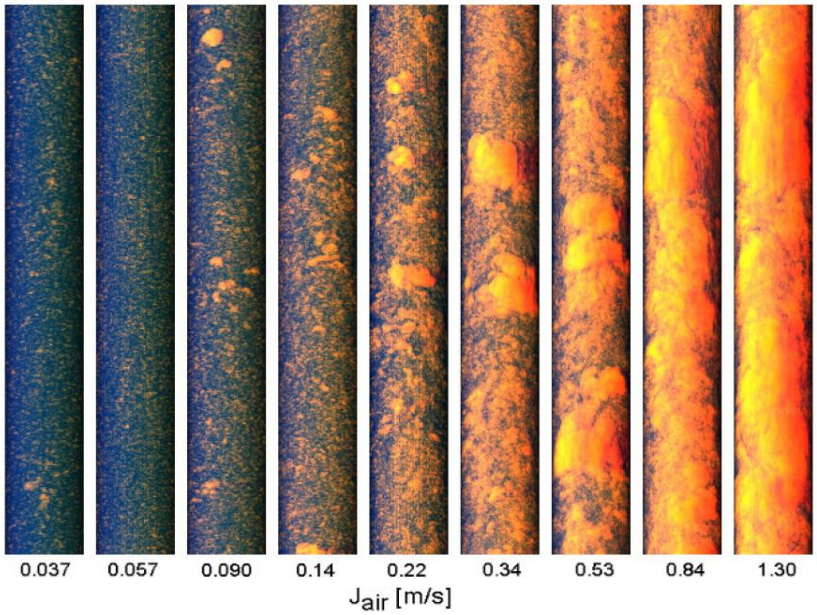

Figure 17. Virtual side fraction of void fraction distribution in 7.67 in ID pipe at water superficial velocity of 1 m/s atmospheric pressure (Prasser et al., 2007).

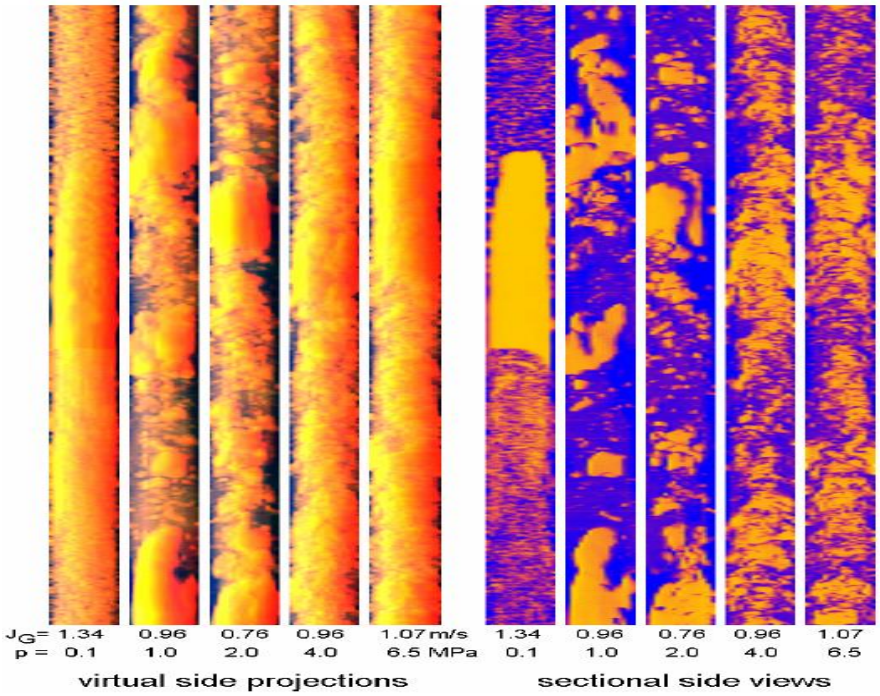

Figure 18. Virtual side fraction and sectional side views of void fraction distribution in 2.06 in ID pipe at water superficial velocity of 1 m/s with increasing pressure (Prasser et al., 2007).

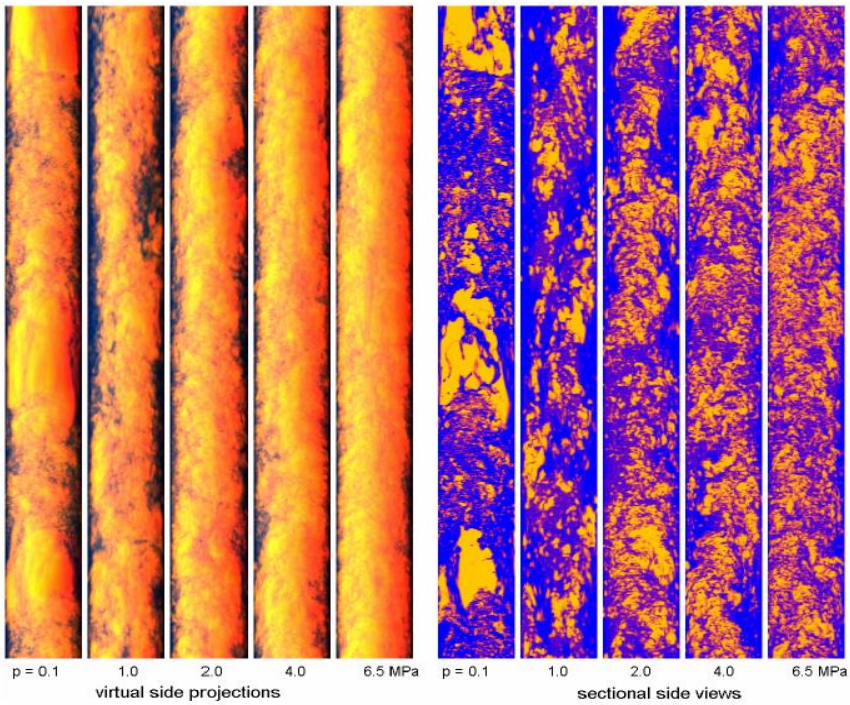

Figure 19. Virtual side fraction and sectional side views of void fraction distribution in 7.67 in ID pipe at water superficial velocity of 1 m/s with increasing pressure (Prasser et al., 2007).

5) Omebere-Iyari et al. (2007)

Omebere-Iyari et al. (2007) experimentally investigated a mixture of naphtha and nitrogen gas flow patterns in a vertical pipe 0.189 m thick and 52 m tall at 290 psig and 1305 psig. Due to the high-pressure experimental condition, visual observation of the flow pattern was not executed. Hence, the authors measured probability density function distributions of void fraction along the pipe using gamma densitometers and determined flow patterns as Bubble, Intermittent, Semi Annular, and Annular flow. The flow transitions created were compared with Taitel et al. (1980) and the results were not satisfactory (Figure 20). To fit bubble/intermittent transition observed in the experiments, Omebere-Iyari et al. modified Taitel et al. bubble/slug transition by increasing critical void fraction from 0.25 to 0.68.

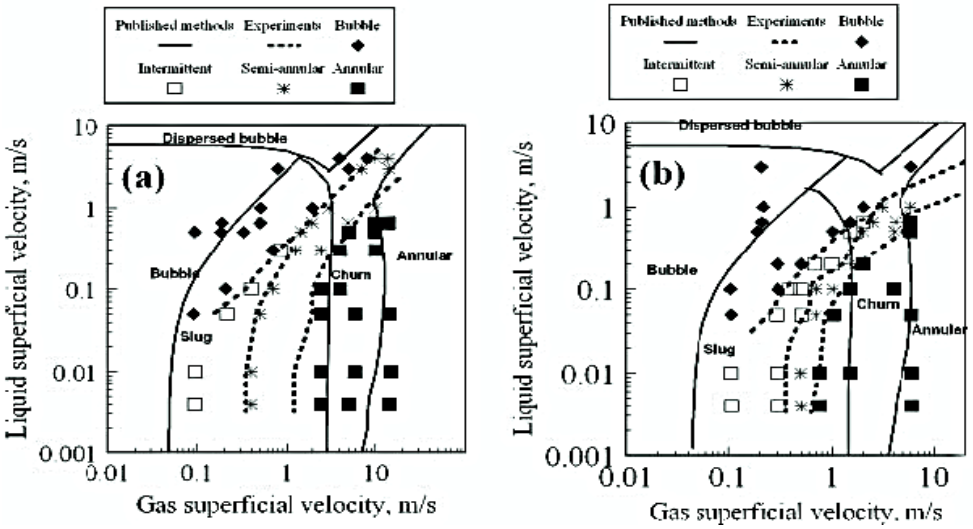

Figure 20. Comparison of bubble/slug transition of Taitel et al. (1980) with experiment data at: (Left) 290 psig (Right) 1305 psig (Omebere-Iyari et al.,2007)

6) Omebere-Iyari et al. (2008)

Omebere-Iyari et al. (2008) performed steam/water experiments at 667 psig, consisting of a vertical test section of a 29.5 ft tall and 7.64 in thick pipe. They employed the same method as Omebere-Iyari et al. (2007) to measure void fraction, bubble size distribution, and flow

visualization in pipe. They classified the flow patterns as either bubble or churn-turbulent by visualization of sectional side views and did not observe conventional slug flow in pipes. They compared steam/water experiments with previously- conducted nitrogen/naphtha experiments (Omebere-Iyari et al., 2007). They found lower mean void fraction during steam/water experiments than nitrogen/naphtha experiments, due to the different physical properties of liquid phases. The steam/water experiments were plotted along with Taitel et al. (1980) bubbly/slug transition. Since the experimentally observed transition did not match Taitel et al. bubbly/slug transition with critical void fraction of 0.25, void fraction was increased from 0.25 to 0.38 and 0.38 was tested. The authors found that the modified transition with critical void fraction of 0.68 matched the experiments the most.

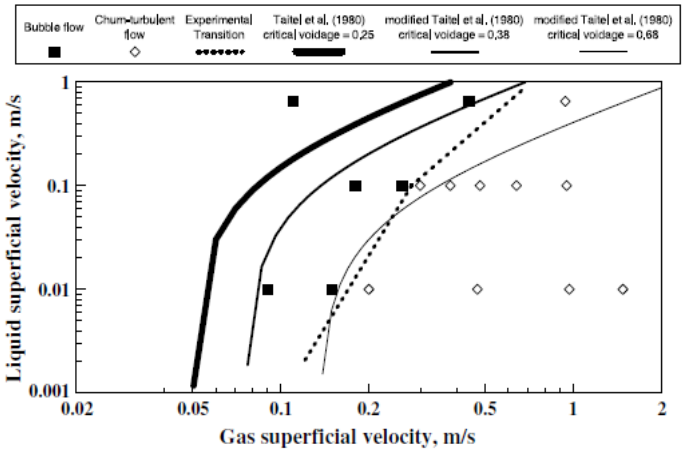

Figure 21. Comparison of Taitel et al. (1980) bubble/slug transition and modified bubble/slug transition with steam-water experimental data (Omebere – Iyari et al., 2008)

7) Ali (2009)

Ali (2009) conducted experiments for air/water mixtures using a 9.84 in ID pipe system, which consisted of a 40 ft long vertical pipe at atmosphere pressure. The gas and liquid superficial velocity range was 0.09 - 2.3 m/s for air and 0.2 - 1.1 m/s for water. Ali visually identified flow regimes as dispersed bubbly, bubbly, agitated bubbly, and churn/froth flow. During the experiment, she did not observe slug flow. Ali compared the results with the existing flow regime models built

with small-diameter pipes such as Taitel et al. (1980), Weisman and Kang (1981), Mishima and Ishii (1984), Barnea et al. (1985), OLGA, Duns and Ros (1963), Beggs and Brill (1973); however, none of them matched her observation (Figure 22). In Figure 22, the dotted lines represent experimentally observed boundaries from bubbly to agitated bubbly and from agitated bubbly to churn-froth boundaries. Ali also compared the measured and predicted values of pressure drop and void fractions. Among the comparisons, the results with popular flow models in the oil and gas industry (Hagedorn & Brown 1964; Duns & Ros 1963; Beggs & Brill 1973; OLGA steady state model) showed large deviations, as high as 50%. A better pressure drop prediction at low gas superficial velocities or at bubbly flow was found. Ali proved that pressure drop models built for small diameter pipe do not have a good performance with respect to large diameter pipes.

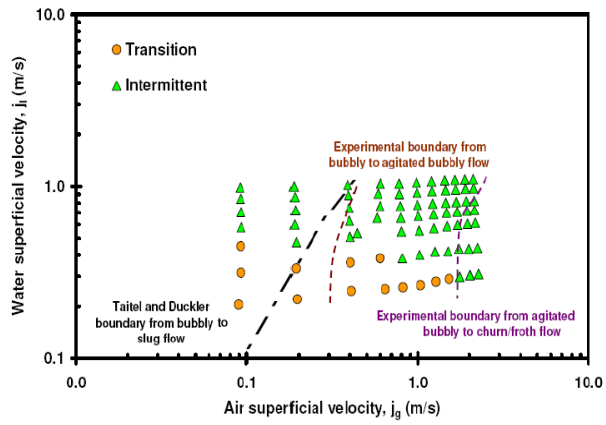

a) Beggs and Brill

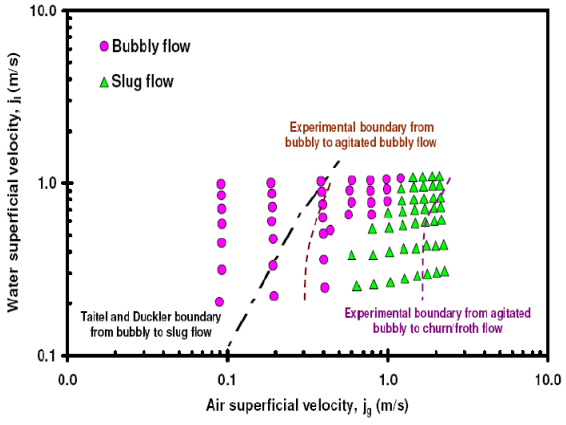

b) Duns and Ros

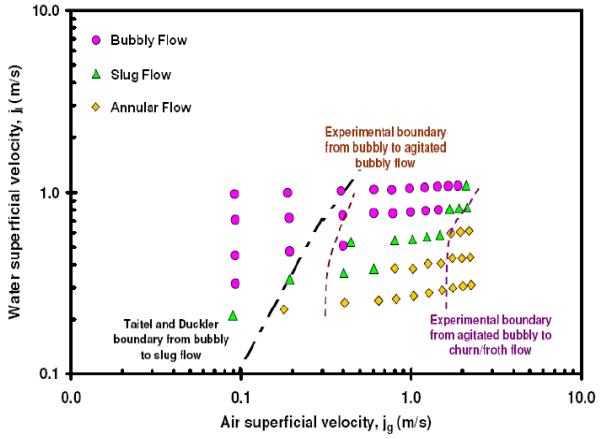

c) OLGA Steady State

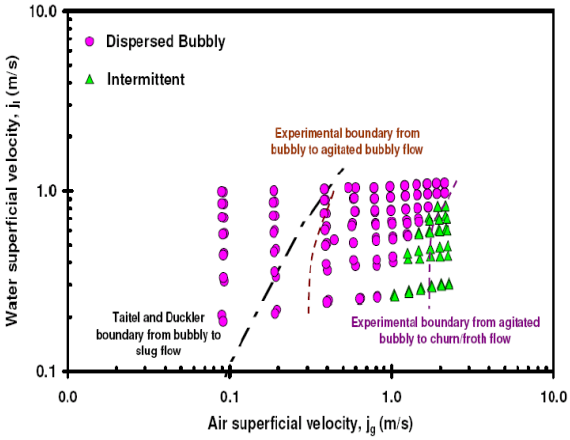

d) Oliemans and Pots

Figure 22. Comparison of flow regime predictions by each flow model (Ali, 2009)

8) Schlegel et al. (2009)

Schlegel et al. (2009) researched the characteristic of air/water two-phase flow in a large diameter vertical pipe. They measured void fraction in a 5.9 in ID and 14.4 ft tall pipe. The applied superficial gas and liquid velocities were from 0.1 to 5.1 m/s and from 0.01 to 2.0 m/s, respectively. They installed 4 electrical impedance meters to measure void fraction. With the void fraction measurement, the cumulative probability density function was established to define the flow regimes as bubbly, cap bubbly, and churn flow. Their bubbly/cap bubbly transition matched well with the transition obtained by Hibiki and Ishii (2003). Further, cap bubbly/churn flow transition followed the predicted transition, as per Kataoka and Ishii (1987). Based on these results, the authors argued that the structure and dynamics of the two-phase flow in a large diameter ($D^* \geq 40$) is significantly different than in small diameter pipes.

9) Fevang (2012)

Fevang (2012) compared pressure drop prediction for flow correlations available in Prosper with the pressure obtained from production tests. The production test data are from the wells in the Statfjord field in the North Sea. TVD and liquid rate of the wells are between 5,580 ft to 8,470 ft and 920 stb/d to 16,000 stb/d. Most of them are completed with 7 in pipes. The absolute average error in pressure drop estimation varies from 5 % (Hagedorn and Brown model) to 40 % (Orkiszewski) with individual error reaching higher than 100 %.

10) Zabaras et al. (2013)

Zabaras et al. (2013) recognized the high uncertainty to the gas/liquid flow behavior in large vertical diameter pipes and carried out an experimental investigation using 40 ft tall and 11 in ID vertical riser connected to 25 ft long and 11 in ID flow line. Their air/water mixture experiment was conducted at atmospheric pressure conditions, and they visually observed bubble, churn,

churn/semi-annular, and semi-annular flow. Zabaras et al. also compared measured pressure gradient and simulated pressure gradient using their own model and commercial multiphase flow simulator, OLGA. Pressure drops were under-predicted by more than 25 % to 80 % and the tested models failed to accurately predict flow behavior where churn flow appeared.

11) Almabrok (2013)

Almabrok (2013) conducted air-water experimental study using u-shaped tubes with 3.9 in ID. Almabrok's objective was to define the effect of 180 º bend pipe on two-phase fluid behavior of upward and downward pipes with large diameter. He found that the bends affected flow behavior considerably and the impacts were air and water flow rates dependent. Almabrok also identified and compared flow regime in the bottom, middle, and top positions of pipe in both directions, as presented in Figure 23. The bottom, middle, and top positions of upward flow pipe correspond to 5D, 28D, and 47D of pipe, respectively. As presented in Figure 23, at the middle and top positions of pipe, flow regimes were identical, but at a lower position, the flow regime was different. Almabrok observed that churn flow area in large diameter is much larger than in a small diameter pipe, while no Taylor bubble was not formed in his large diameter pipe.

In addition, Almabrok identified increasing total pressure drop with higher gas superficial velocity, which was also observed by Capovila et al. (2019). As shown in Figure 24, at a higher liquid superficial velocity, the concave upward trend is more significant than a lower liquid superficial velocity. The churn-annular transition velocity was identified from the minima of each pressure value.

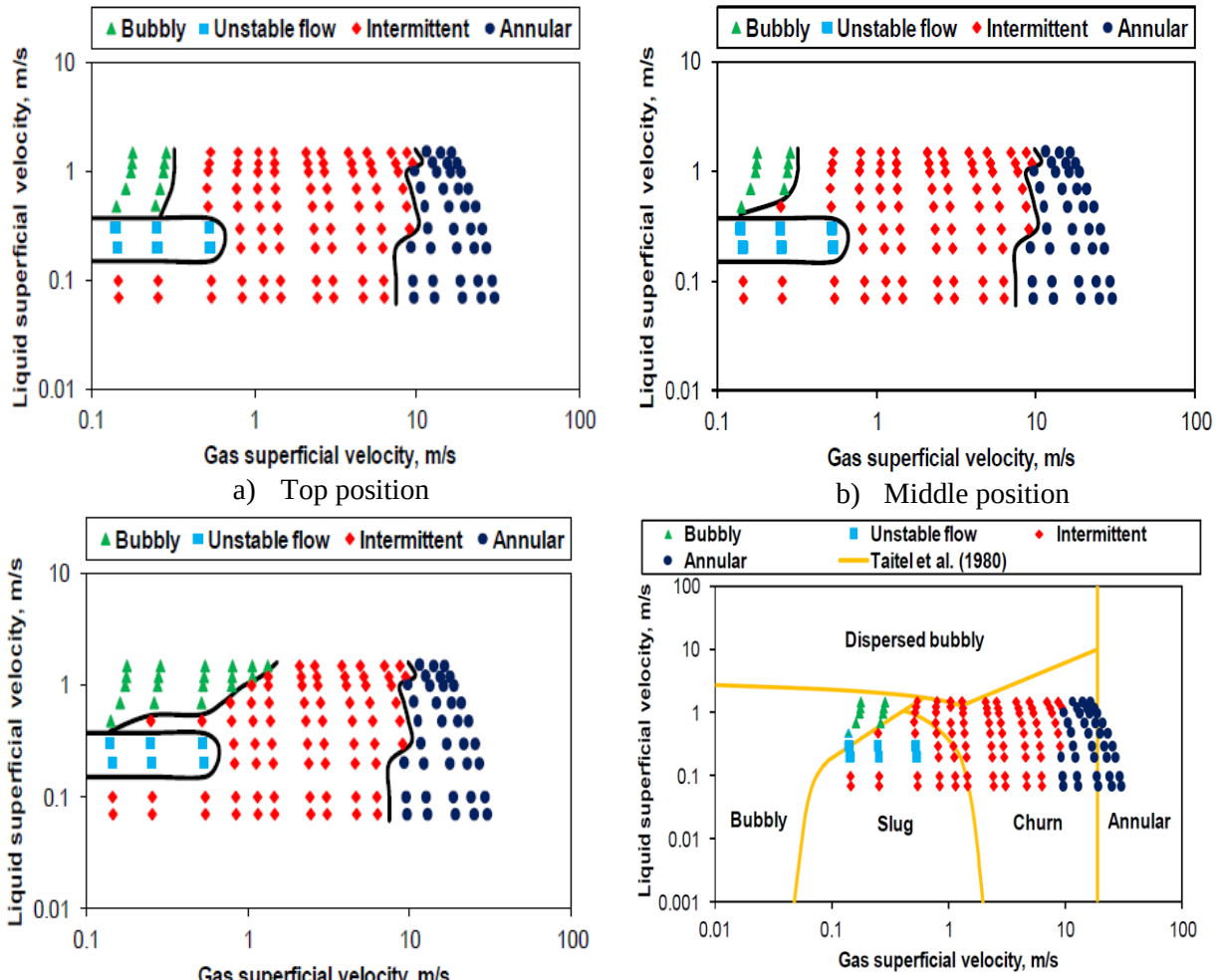

a) Top position

b) Middle position

c) Bottom position

d) Flow regime comparision between flow regime at middle position and Taitel et al. (1980)

Figure 23. (a, b, and c) Flow regime observed in upward flow and (d) flow regime comparison (Almabrok, 2013)

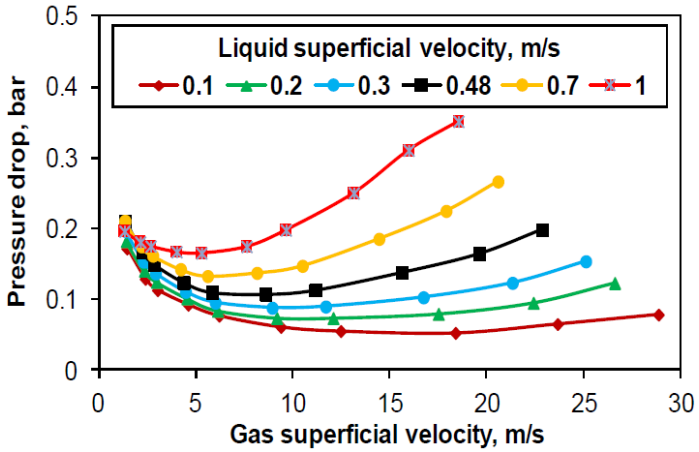

Figure 24. Pressure drops in upward flow pipe (Almabrok, 2013)

12) Bhagwat and Ghajar (2014)

Bhagwat and Ghajar (2014) proposed a flow regime independent drift flux model for void fraction estimation. Distribution parameter and drift velocity were modeled as a function of hydraulic pipe diameter, fluid density, liquid viscosity, system pressure, fluid velocity, pipe orientation, Reynolds number, two phase quality, and void fraction. They tested 8255 data points from 60 sources consisting of air/water, natural gas/water, air/ kerogen, air/glycerin, argon/acetone, argon/alcohol, refrigerants, steam/water, and air/oil combinations. They concluded that their correlation successfully predicts void fraction for hydraulic pipe diameters from 0.02 in to 12 in, system pressure from 14.5 psia to 2625 psia, and pipe orientation from - 90 to 90 degree.

In their model, a distribution parameter is mainly a function of gas-liquid density ratio, two-phase Reynolds number (Re_{tp}), and $C_o, 1$. $C_o, 1$ are also a function of gas-liquid density ratio, Re_{tp}, and two-phase friction factor. As presented in Figure 25, C_o equals 2.0, which is independent of Re_{tp} when Re_{tp}< 1000 at varying $C_o, 1$. In contrast, at varying density ratios, C_o is between 1.6 and 2.0 when Re_{tp}< 1000 and C_o is between 1.0 and 1.3 when Re_{tp}> 10^4. Therefore, at Re_{tp}> 10^4 and at a gas-liquid density ratio of 1, C_o becomes unity.

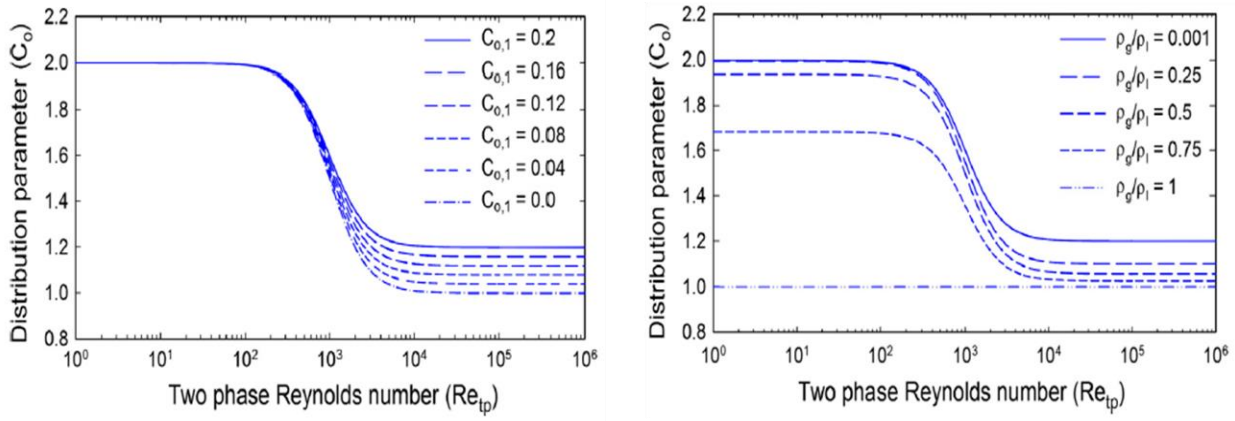

Figure 25. Variation of distribution parameters as a function of two-phase Reynolds number and density ratio in vertical pipes (Bhagwat & Ghajar, 2014)

13) Hewakandamby et al. (2014)

Hewakandamby et al. (2014) conducted a parametric experimental study of churn flow in 5 in thick and 36 ft tall pipes. They employed a wire mesh sensor to map the cross-sectional phase distribution. Air and water and mixture of water/glycerol were used as gas and liquid phases and the maximum gas and liquid superficial velocity were 17 and 1.2 m/s, respectively. The mixture of water and glycerol was used to determine the viscosity effect on the flow regime. They found that viscous fluid had higher void fraction, thinner wall film, higher liquid entrainment in column core, and higher relative velocity than non-viscous fluid, even at the same superficial velocities. Further, large waves and the large liquid wisps entrained in the gas core were found and were increased along the axial distance.

14) Shen et al. (2015)

Shen et al. (2015) studied bubbly – cap bubbly flow transition of air-water flow in a 7.87 in ID and 85.3 ft high vertical pipe. The liquid and gas superficial velocities were from 0.050 to 0.31 m/s and from 0.018 to 0.51 m/s, respectively. Shen et al. (2015) observed bubbly, developing cap bubbly, and fully developed cap bubbly flows using a high-speed camera. The developing cap bubbly lasted long and grew gradually into fully developed cap bubbly flow. This behavior was different than bubbly to slug flow transition in a small diameter pipe where a sudden transition was observed. They found that flow regime transition occurs in a lower void fraction, when axial length is short.

15) Pagan (2016)

Pagan (2016) modeled churn and annular flow regimes in vertical and near-vertical pipes with small and large diameters. Pagan (2016) used experimental data from Skopich et al. (2015) for 2 in and 4 in, Van de Meulen (2012) for 5 in, and Zabaras et al. (2013) for 11 in ID pipes. The main

contributions of her study are 1) to extend Jayanti and Brauner (1994) churn flow model to annular flow, 2) to modify interfacial friction factor of Wallis (1983) for churn flow and adopt Wallis (1983) annular flow for the proposed model 3) to test the model with diameter larger than 1.25 in. For modification in Jayanti and Brauner (1994), Pagan assumed thick liquid film in churn flow regime and thin liquid film in annular flow regime. She also assumed liquid entrainment in the liquid film, not in the gas core. For churn and annular transition model, Pagan used Wallis (1969) and Pushkina and Sorokin (1969) for pipe diameters smaller than 2 in and larger than 2 in, respectively. For bubble and churn flow transition, Pagan applied Omebere-Iyari and Azzopardi (2007) models, which modified Taitel et al.'s (1980) bubbly/slug transition by changing the critical void fraction from 0.25 to 0.68. For future study, Pagan recommended the development of bubbly and slug flow for horizontal and near horizontal well and flow regime transitions for all well inclinations.

16) Ansari and Azadi (2016)

Ansari and Azadi (2016) tested air/water flow in 1.57 in and 2.76 in ID vertical pipes to study the effect of pipe diameter size on flow regime. At the same liquid and gas superficial velocities, Taylor bubble was formed in 1.57 in ID pipe, but churn flow was observed in 2.76 in ID pipe (Figure 26). They observed similar bubble/slug transition for the two pipes, whereas, for a large diameter pipe, slug and annular region were reduced and churn flow occupied the reduced area, as shown in Figure 26. Ansari and Azadi stated that slug region was reduced with increased pipe diameters and disappeared when diameter was about 0.1 m for air/water mixture at atmospheric pressure. This study shows flow behavior change in small diameter ($D^* \leq 18.5$) and transition diameter which is between small and large diameter. For air-water flow at atmospheric pressure, $D^* \leq 18.5$ is approximately 2 in.

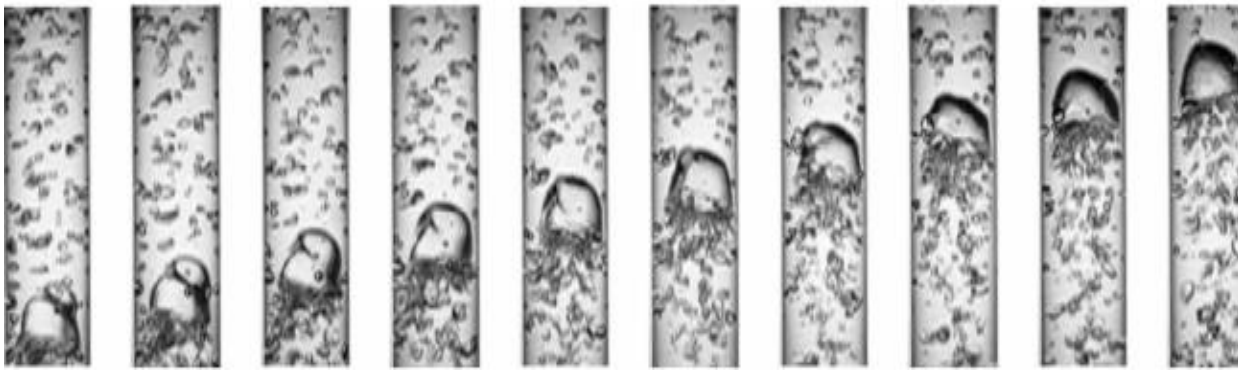

a) Flow structures in 1.57 in ID tube

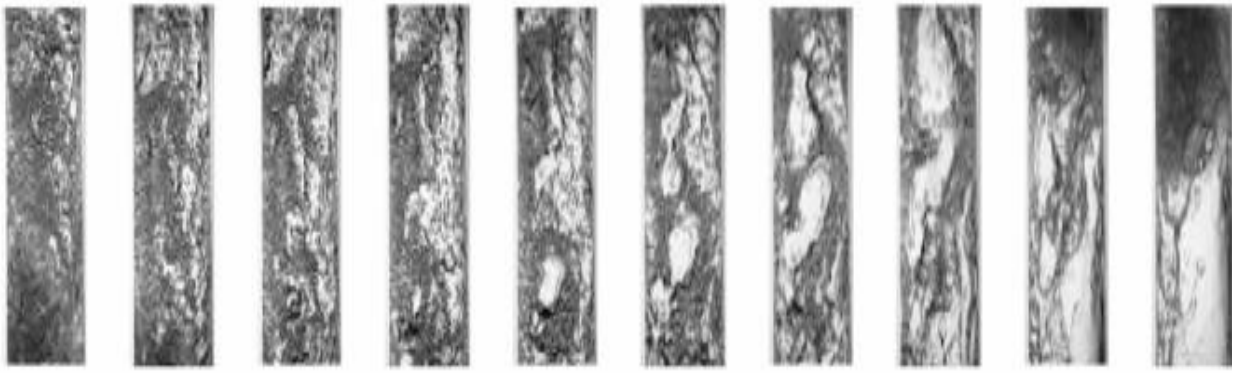

b) Flow structures in 2.76 in ID tube

Figure 26. Flow structures at consecutive frames for tubes with ID (a) 1.57 in (b) 2.76 in at u_{sg} = 0.379 m./s and u_{sl} = 0.368 m/s (Ansari &Azadi, 2016)

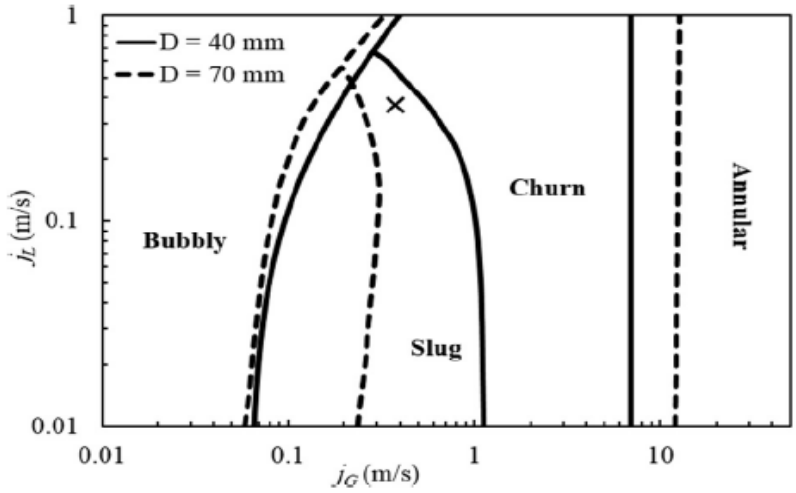

Figure 27. Flow regime map with air/water vertical flow (Ansari & Azadi, 2016)

17) Waltrich et al. (2017)

Waltrich et al. (2017) tested air/water mixture flow from 0.006 to 2.2 MMscf/d and from 215 to 27,430 bbl/d through 20 ft- long vertical pipes for three diameters, 3.9, 7.7, and 11.7 in ID. Two-phase flow behavior was recorded with a high-speed camera and pressure gradient, liquid hold-up, and gas/liquid rates were recorded. Waltrich et al. tested flow models in PIPESIM with their data and observed high pressure gradient errors even higher than 100 % for gas/liquid ratio $1 < u_{sg}/u_{sl} < 100$. However, for low gas/liquid ratios ($u_{sg}/u_{sl} < 1$) where a bubbly flow was expected, all models produced errors of less than 10 %. When the experiment results were plotted on the flow regime of Duns and Ros (1963), all models provided good results for bubbly flow, while the errors increased for churn and annular flow regimes. They also observed that the pressure gradient remained at its minimum at higher gas rates with annular flow (Figure 28).

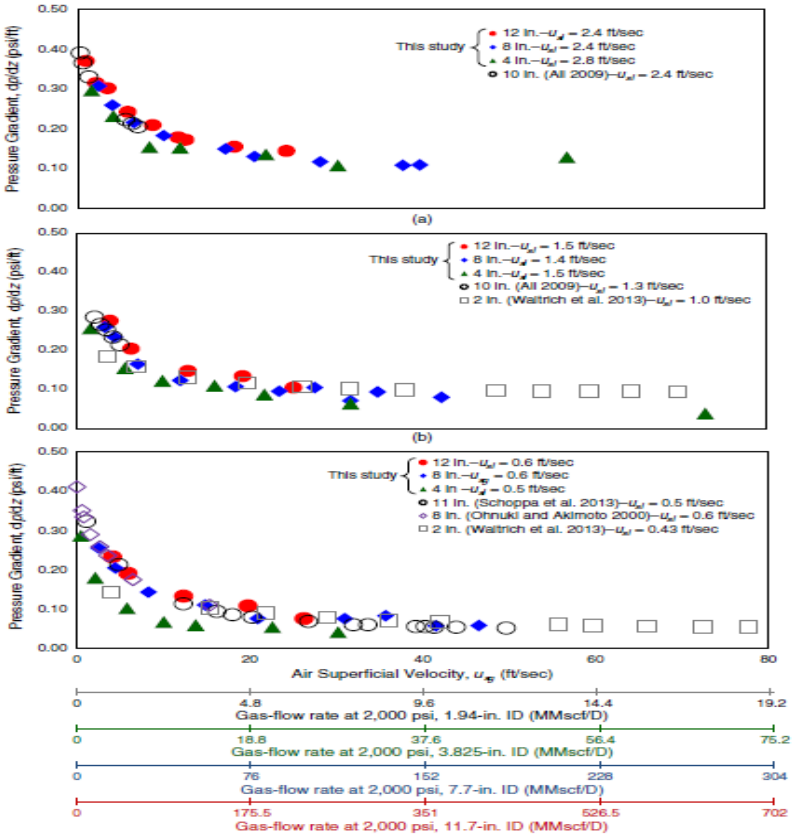

Figure 28. Pressure gradient generated for different diameters and liquid rates at (a) 2.4 ft/s, (b) 1.4 ft/s, and (3) 0.5 ft/s (Waltrich et al., 2017)

18) Teles and Waltrich (2018)

Teles and Waltrich (2018) estimated pressure gradient for bubble, slug, churn, and annual flow using data from Waltrich et al. (2017). Teles and Waltrich (2018) model first determines slip ratio. If it is less than 1, Duns and Ros (1963) is selected. Then, Kataoka and Ishii's (1987) critical diameter ($D^*>40$) is applied to check large diameter. For large diameter, modified Pagan et al. (2017) is applied, and for small diameter, Duns and Ros (1963) is applied.

19) Zhao and Hibiki (2018)

Zhao and Hibiki (2018) studied drift-flux correlation of vertical upward two-phase annulus flow in large diameter pipes. They employed Kataoka and Ishii's (1981) critical diameter equation for large diameter pipes (Eq. 13). They developed drift-flux correlation for bubbly, cap-bubbly, churn, and annular flow in large size annulus using Ozar et al., (2008) which is a modified form of Hibiki and Ishii (2002).

20) Tang et al. (2019)

Tang et al. (2019) built a drift flux correlation for void fraction estimation in all pipe inclinations to implement within a coupled wellbore/reservoir simulation. In their model, they used the distribution parameter of Holmes (1977) and drift velocity of Bendiksen (1984) with adjustment term to implement pipe inclination and Reynolds number. Tang et al. used data sets from TUFFP, whose data is concentrated at high gas fraction range, > 80 %, and from OLGA-S which has more uniformly distributed gas input data. They compared the proposed model with two drift flux models, those of Choi et al. (2012) and Bhagwat and Ghajar (2014), for void fraction estimation. The results showed that Choi et al. predicted less gas volume fraction, if gas fraction is greater than 80 % for upward flow. Bhagwat and Ghajar over-predict gas fraction when it is greater than 50 % for upward flow. Further, Tang et al. (2019) claimed that the major difference among the

models occurs when gas fraction is between 75 % and 100 %. For their model applicability, they restricted the distribution parameter to the range 1 to 1.2 for liquid viscosity lower than 70 cP.

21) Capovilla (2018))

Capovilla (2018) worked on two-phase flow regime map for large diameter pipes and high-velocity flows in his master program. He conducted water-gas flow experiments on large diameter pipes (3.82, 7.8, 11.7 in) and tested flow regime transitions on the experimental data and chose best fit model. Additionally, Capovilla (2019) proposed a flow regime map of a large pipe diameter which consists of bubbly, cap-bubbly, and annular flow (Figure 29). The flow regimet map used transition boundaries from Mishima and Ishii (1984) for bubbly to cap-bubbly and churn to annular flow, and Schlegel et al. (2013) for cap-bubbly to churn flow. Capovilla (2019) recommended to use Duns and Ros (1963) for bubbly flow, Schlegel et al. (2013) for cap-bubbly flow, and Pagan et al. (2016) for churn and annular flow. For future study, Capovilla recommended 1) an experimental study using wire mesh sensors, oil and gas mixture under high pressure, and inclined pipes and 2) investigation on effect of pipe inclinations on flow regime in large diameter pipes for future studies.

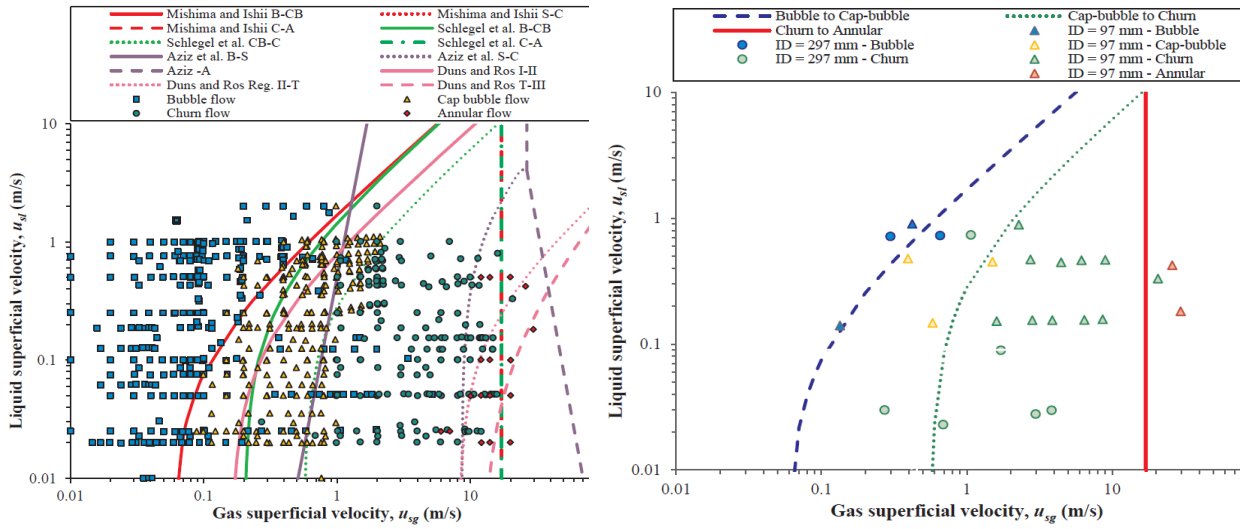

a) Experimental data plotted against flow regime maps

b) Proposed flow regime map

Figure 29. Experiment data on existing and proposed flow regime maps (Capovilla et al., 2019)

22) Tornisiello (2020)

Tornisiello (2020) researched on development and validation of a simplified transient two-phase flow model for any pipe inclinations. Tornisiello modified transient model of Choi et al. (2013) by adopting Bhagwat and Ghajar (2014) drift-flux correlations for void fraction estimation. Choi et al. (2013) employed $C_o$of 1.2 and u_d of 0.3583 for flow in pipes with pipe angle ranges between +90º and -30º. By adopting Bhagwat and Ghajar (2014), Torniseillo extended the model applicability to pipes in any angle. Tornisiello tested the model against Coutinho (2018) for flow in annulus and Waltrich (2012) for flow in tubing. Coutinho's (2018) data were obtained at 2,788 ft deep vertical well with 4.89 in ID inner casing and 2.88 in OD tubing. Waltrich's (2012) data were generated using 1.97 in ID and 141 ft long tubing. The errors for pressure and liquid holdup prediction for bubbly and dispersed bubbly flow regimes were less than 17% for all pipe inclinations. The error for liquid holdup and pressure prediction for slug and churn flow was less than 45% and 24%, respectively. Tornisiello claimed the transition model should work for slow transition flow and low gas oil ratio fluid (black oil). Therefore, Tornisiello recommended future studies to improve drift-flux correlation for high void fraction and to validate the model with field data.

2.8. Summary of Literature Review

In summary, scholars who studied two-phase flow in large diameter pipes observed various flow regimes depending on their experimental conditions. However, many of them did not observe slug flow that is commonly observed in two-phase flow experiments with small diameter pipes. Rather, they observed smother transition from bubbly to churn turbulent-looking flow (Table 3). Although transition from one flow regime to another is a continuous process as observed, two-phase flow models, either for void fraction estimation or pressure drop estimation, have fixed flow boundary

using void fraction, fluid velocity, or dimensionless parameters. To describe this continuous flow transitions more precisely, scholars categorize flow regimes into many sub-flow regimes and have developed correlations for each flow regime. Based on the literature review, flow behaviors in small and large diameter pipes are different and hence, two-phase flow models for small pipe diameters do not represent the difference well. Therefore, it is crucial to evaluate and develop two phase flow models for large diameters.

In comparison to the previous studies of students (Pagan, 2016; Capovilla, 2018; Teles, 2020; Tornisiello, 2020) in Dr. Waltrich's research group, the proposed study has the following differences and uniqueness. First, model validation range is expanded. The proposed model's applicability was validated with extended range of conditions, small and large pipes, low and high void fraction, vertical and inclined pipes, and water-gas and oil-gas field data. Second, the model applied minimum pressure gradient of bubbly flow model for transition of bubbly and non-bubbly flow and minimized number of flow regimes. Third, the model eliminated discontinuity of discrete distribution parameter and drift velocity along with flow regime transitions. Fourth, the proposed study reviewed drift-flux models with different drift-flux parameter estimation methods comprehensively. In addition, the proposed study applied the model for dispersed bubbly flow and WCD case study, and tested friction factor correlations.

Table 3. Literatures presenting flow regimes for large-diameter pipes

Publications	Fluid	Pipe Length (ft)	Pipe ID (in)	Pressure (psia)	Flow pattern observed
Ishii, 1977	No experimental study for flow in large diameter				
Kataoka and Ishii, 1987	No experimental study for flow in large diameter				
Ohnuki and Akimoto, 2000	Air/water	40.35	7.87	14.5	undisturbed bubbly, agitated bubbly, churn bubbly, churn slug, churn froth
Prasser et al, 2007	Air/water	26.2	7.67 2.05	14.5 943	2.05 in ID at 14.5 psia: bubbly, slug 2.05 in ID at 943 psia: bubbly, churn-turbulent 7.67 in ID at both pressure: bubbly, churn-turbulent
Omebere et al., 2007	Naphtha/ nitrogen	176.6	7.44	290, 1305	bubble, intermittent, semi-annular, annular
Omebere et al., 2008	Steam/water	176.6	7.61	667	bubble, churn-turbulent
Ali, 2009	Air/water	40.0	10	14.5	distributed bubble, bubble, agitated bubble, churn froth
Schlegel et al., 2009	Air/water	14.4	5.9	14.5	bubbly, cap bubbly, churn
Fevang, 2012	No experimental study for flow in large diameter				
Bhagwat and Ghajar, 2014	No experimental study for flow in large diameter				
Zabaras et al., 2013	Air/water	40.0	11	14.5	bubble, churn, semi-annular
Hewakandamby et al., 2014	Air/water Air/Water-glycerol	36.1	5	14.5	churn
Shen et al., 2015	Air/water	85.30	7.87	14.5	bubbly, developing cap bubbly, Fully developed cap bubbly
Pegan et al., 2016	No experimental study				
Ansari and Aziz, 2016			1.57 2.76		1.57 in ID: bubble, slug, annular 2.76 in ID: bubble, slug, churn, annular
Waltrich et al., 2017	Air/water	20, 35	3.83,7.7, 11.7	14.5	bubbly, churn, annular
Kiran et al., 2020	Air/water				
Teles and Waltrich, 2018	No experimental study for flow in large diameter				
Capovilla, 2018	Same as Waltrich et al., 2017				
Tang et al., 2019	No experimental study for flow in large diameter				
Tornisiello (2020)	No experimental study for flow in large diameter				

3. MODEL DEVELOPMENT METHODOLOGY

As described in detail in the literature review section, there are many two-phase flow models with their own flow regime transition criterion. Each of these criteria may not be suitable if a laboratory or a field condition is different than the model development conditions. Therefore, it is difficult to choose one flow model appropriate to various conditions. However, as presented by Waltrich et al. (2017), at low superficial gas to liquid velocity ratio ($u_{sg}/u_{sl} \leq 1$), all tested flow models had pressure gradient errors less than 10 %. Further, bubbly/slug flow boundary for small diameter tubes is similar to bubbly/turbulent flow boundary for large diameter tubes (Ansari & Aziz 2016; Ohnuki & Akimoto, 2000; Waltrich et al., 2017). This indicates that for low gas rates where bubbly flow is anticipated, any bubbly flow model can be applied, for either small or large diameter pipes. Beyond bubbly flow regime, at higher gas rates, another flow model should be selected for pressure loss estimations. Regardless of laboratory or field conditions, pressure gradient has a concave-upward trend above certain gas velocity at fixed liquid velocity. This is because the total pressure gradient is the sum of gravitational and frictional pressure gradient and as gas velocity gets higher, frictional pressure becomes larger (Figure 30). The described pressure gradient trend is seen in several experimental studies. As other authors in the literature found for small-diameter pipes, Waltrich et al. (2017) also observed for larger diameters that the total pressure gradient becomes lower as the flow regime changes from bubbly to churn flow and reaches its minimum for churn-annular transition. Zabaras et al. (2013) also found a decreasing pressure gradient from bubbly to churn flow, and churn-annular transition close to the minimum pressure gradient. Hewitt et al. (1985) stated that churn-annular flow transition can be correlated to minimum pressure gradient in small-diameter pipes. Therefore, if a model can simulate this pressure gradient trend along with flow regime transitions, it should be applicable to a wide range of pipe diameters, including large

and small diameters. Thus, the proposed model is developed to present this idea by modifying the drift flux parameters, and is described in the following sections.

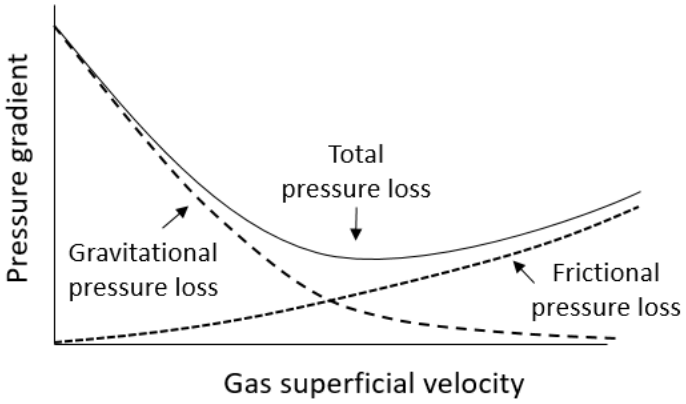

Figure 30. A general total pressure gradient trend

3.1. Description of The Minimum Pressure Gradient Drift-Flux Model

The drift-flux void fraction model of Kataoka and Ishii (1981) is selected for the bubbly flow void fraction estimation for the proposed model. The Kataoka and Ishii model was built for critical diameters greater than 30 ($D^* \geq 40$) and less than 40. Their model also accounts for different fluid viscosities and was recommended for bubbly flow void fraction estimation by many scholars (Hibiki & Ishii, 2003; Schlegel et al., 2010; Mishima & Ishii, 1984).

For non-bubbly flow, beyond gas velocity at minimum pressure estimated by bubbly flow correlation, gradually decreasing the drift coefficient is presented with the void fraction model of Schlegel et al. (2013), who consider a void fraction of 0.3 and 0.51 as transition criteria of bubbly/cap bubble flow and bubbly/churn flow, respectively. Since flow transition criteria are dependent on fluid flow condition (e.g. system pressure, flow rate, pipe diameter, and fluid properties), a fixed value of void fraction would not represent flow transition in various conditions. For example, Taitel et al. (1980) and Hasan et al. (2010) applied α =0.25 as bubbly/slug transition criterion, while Omebere-Iyari et al. (2008) and Pagan et al. (2016) used α = 0.68 as bubbly/churn

flow transition. Hence, instead of using α =0.51, flow rates at minimum pressure gradient estimated by bubbly flow correlation are selected as bubbly/non-bubbly flow transition in the proposed model.

In the proposed model, C_o becomes smaller than 1.2 after bubbly/non-bubbly transition and reaches 1 for ideal annular flow eventually. Through this approach, increasing the slope of the pressure gradient by bubbly flow correlation will follow the actual pressure gradient trend marked with circles (Figure 30). As presented in Figure 31, a limitation of the proposed model is where the total pressure gradient curve becomes significantly concave, when very high gas flow rates are expected and frictional pressure gradient dominates gravitational pressure gradient. This limitation will be examined with field and laboratory data in the next chapter.

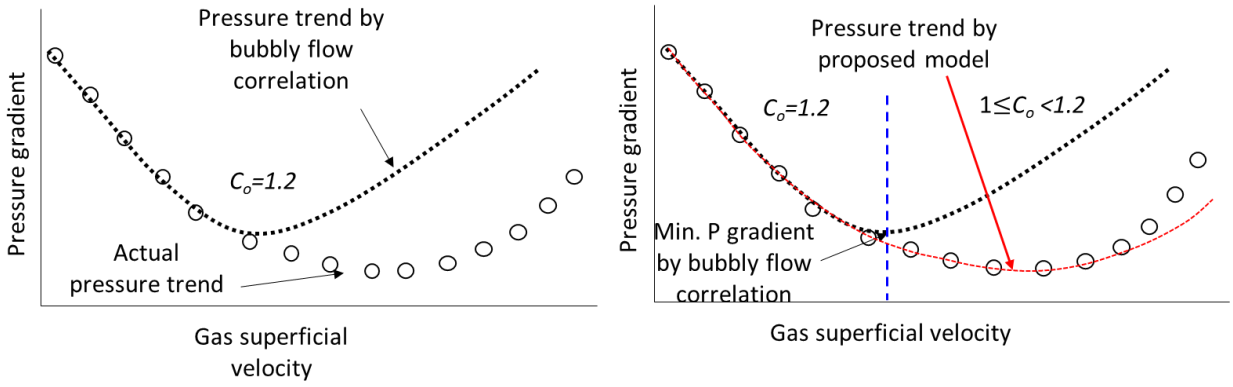

Figure 31. Estimated pressure gradient trends by (Left) bubbly flow correlation (Right) proposed correlation

The model will represent continuous flow regime changes with non-fixed drift-flux parameters. Further, it will describe various bubbly/non-bubbly flow transitions at minimum pressure gradient by a bubbly flow correlation.

3.1.1. Pressure Gradient Estimation Process

Pressure estimation process is presented with a flowchart (Figure 32) and can be summarized as follows:

1. Pressure gradient estimation using bubbly flow correlation
2. Bubbly flow test
3. Re-determination of pressure using updated drift flux parameters for non-bubbly flow.

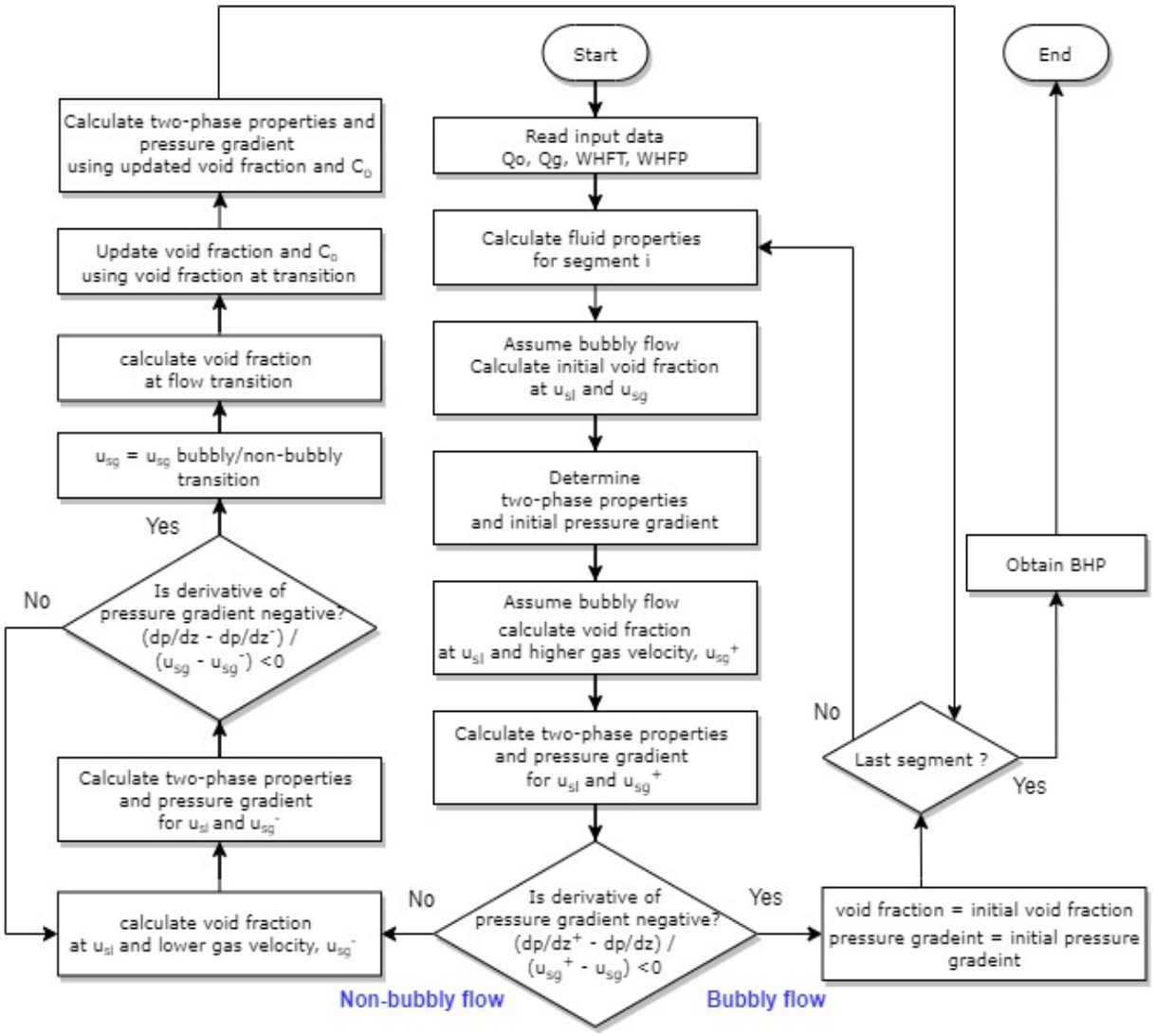

Figure 32. Flow chart of bottomhole pressure estimation process

The detailed process can be explained as follows.

3.1.1.1. Pressure gradient estimation using bubbly flow correlation

First, initial void fraction is estimated by assuming bubbly flow. The drift-flux coefficient of Ishii (1977), $C_{o,ishii}$ and Kataoka and Ishiii (1981) drift velocity, $u_{d,KI}$,presented in Eq. 53 and Eq. 54 are applied to determine initial void fraction,$\alpha_{initial}$, as shown in Eq. 60.

$$\alpha_{initial} = \frac{u_{SG}}{C_{o,ishii}u_M + u_{d,KI}} \tag{60}$$

With the void fraction, two phase parameters such as density, viscosity, and Reynolds numbers are defined as follows:

$$\rho_{TP} = \alpha\rho_G + (1-\alpha)\rho_L \tag{61}$$

$$\mu_{TP} = \alpha\mu_G + (1-\alpha)\mu_L \tag{62}$$

$$R_e = \rho_{TP}u_M D/\mu_{TP} \tag{63}$$

For friction calculation, the Blasius method using Fanning friction factor is applied. Friction factor f for turbulent ($R_e > 100{,}000$), transient ($2100 < R_e \leq 100{,}000$), and laminar flow ($R_e \leq 2{,}100$) are defined as follows:

$$\text{Turbulent flow: } f = 0.046{R_e}^{-0.2} \tag{64}$$

$$\text{Transient flow: } f = 0.079{R_e}^{-0.25} \tag{65}$$

$$\text{Laminar flow: } f = 16\ R_e \tag{66}$$

With the values obtained from the procedures above, considering the deviation angle from horizontal position θ, the total pressure gradient can be calculated as:

$$\frac{dP}{dZ} = \rho_{TP}gsin\theta + 2f\rho_{TP}{u_M}^2/D \tag{67}$$

3.1.1.2. Bubbly flow test

As presented in Figure 34, if a datum point is located on the left side of curvature of pressure gradient curve generated by a bubbly flow correlation, the flow regime remains a bubbly flow. If a datum point is on the right side of the curvature, flow regime is non-bubbly flow. Since experimental data can be acquired systemically, a pressure gradient trend with increasing or decreasing gas rate at fixed liquid rate can be drawn as in Figure 33. However, it is not easy to obtain field data with variant gas rates at fixed liquid rates to get pressure gradient trends. Therefore, a hypothetical datum point at higher gas velocity,$u_{SG}{}^{+}$, than the actual datum point needs to be created. The two data points are at the same liquid rate. Then, updated void fraction, α^{+}, at higher gas velocity, $u_{SG}{}^{+}$, can be estimated as follows:

$$u_{SG}{}^{+} = 2\, u_{SG} \tag{68}$$

$$u_{M}{}^{+} = u_{SL} + u_{SG}{}^{+} \tag{69}$$

$$\alpha^{+} = \frac{u_{SG}{}^{+}}{C_{o,ishii} u_{M}{}^{+} + u_{d,KI}} \tag{70}$$

Applying α^{+} into Eq. 61 and Eq. 62 instead of α, pressure gradient for higher gas velocity, $\frac{dP}{dZ}^{+}$, can be calculated. If a derivative of pressure gradient of the two points, $(\frac{dP}{dZ}^{+} - \frac{dP}{dZ})/(u_{SG}{}^{+} - u_{SG})$, is negative, the datum is in bubbly flow regime. If it is not, it is non-bubbly flow, as described in Figure 31. For bubbly flow, the initial void fraction, $\alpha_{initial}$, from Eq. (60) is the finally determined void fraction to calculate total pressure using Eq. 60 -Eq. 67.

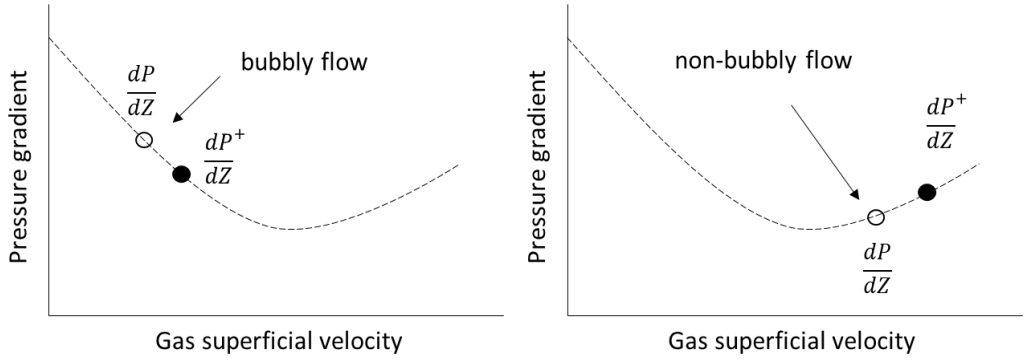

Figure 33. Flow regime determination. If a derivative of pressure gradients is (Left) negative, bubbly flow (Right) positive, non-bubbly flow

3.1.1.3. Re-determination of pressure using update drift flux parameters for non-bubbly flow

For non-bubbly flow, bubbly/non-bubbly flow transition velocity needs to be determined to re-estimate void fraction. New void fraction,α^-, and pressure gradient, $\frac{dP^-}{dZ}$, at a reduced gas velocity, ${u_{SG}}^-$, are determined by the following:

$$u_{SG,interval} = 0.2\, u_{SG} \tag{71}$$

$${u_{SG}}^- = 1 - u_{SG,interval} \tag{72}$$

$${u_M}^- = u_{SL} + {u_{SG}}^- \tag{73}$$

$$\alpha^- = \frac{{u_{SG}}^-}{C_{o,ishii}{u_M}^- + u_{d,KI}} \tag{74}$$

Applying α^- into Eq. 61 and 62 instead of α, the pressure gradient for lower gas velocity, $\frac{dP^-}{dZ}$,is calculated. If a derivative of the two pressure gradients is still positive, another point at lower gas velocity than the previously generated point is created:

$$\text{If} \frac{\frac{dP}{dZ} - \frac{\boldsymbol{dP^-}}{\boldsymbol{dZ}}}{u_{SG} - {u_{SG}}^-} > 0,\ u_{SG} = {u_{SG}}^- \tag{75}$$

$${u_{SG}}^- = u_{SG} - u_{SG,interval} \tag{76}$$

The new derivative can be calculated repeating the above steps. This process is repeated until a derivative of pressure gradients of reduced velocity becomes negative, which is the gas velocity at bubbly/non-bubbly flow transition (Figure 34):

$$\text{if} \frac{\frac{dP}{dZ} - \frac{\boldsymbol{dP^-}}{\boldsymbol{dZ}}}{u_{SG} - u_{SG^-}} \leq 0,\ u_{SG} = u_{SG\_Transit} \tag{77}$$

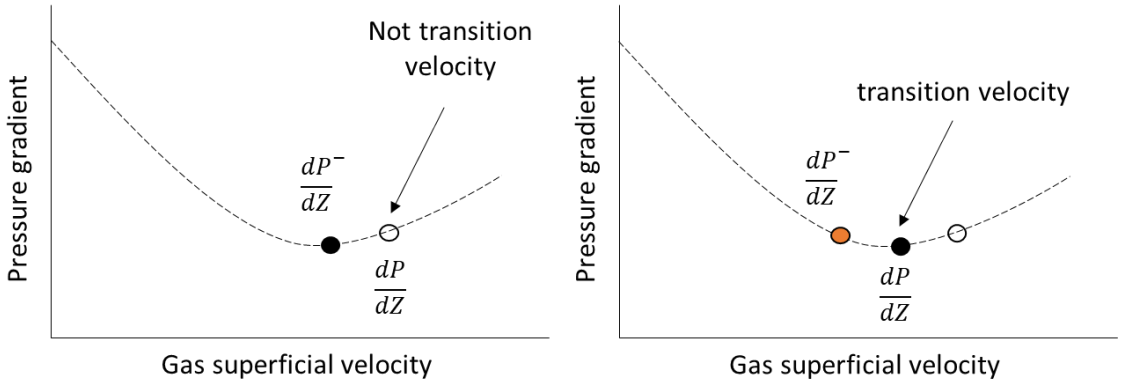

Figure 34. Determination of bubbly/non-bubbly flow transition velocity. (Left) not bubbly/non-bubbly transition (Right) bubbly/non-bubbly flow transition

Once the gas superficial velocity for bubby/non-bubbly flow transition is determined, void fraction at the transition velocity can be estimated. As mentioned, critical void fraction for bubbly/non-bubbly transition is not constant. Schlegel et al. (2013) applied 0.51 and Taitel et al. (1980) and Hasan et al. (2010) used 0.25, while Omebere-Iyari et al. (2008) and Pagan et al. (2016) applied 0.68 for critical void fraction. Therefore, critical void fraction, $\alpha_{Transit}$, is calculated for each datum for the proposed model using Eq. 78 and Eq. 79. Once $\alpha_{Transit}$ is obtained, void fraction at the interest gas and liquid velocity can be calculated using Eq. 80 - 81. Since there are two unknown parameters, C_o and α, it requires iterations. Further, $C_{o,ishii}$ is for bubbly flow and is approximately 1.2. Hence, C_o for non-bubbly flow cannot be larger than $C_{o,ishii}$. With the acquired α, mixture properties and pressure gradient can be attained using Eq. 61 – Eq. 67.

$$u_{M\_Transit} = u_{SL} + u_{SG\_Transit} \tag{78}$$

$$\alpha_{Transit} = \frac{u_{SG\_Transit}}{C_{o,ishii} u_{M\_Transit} + u_{d,KI}} \tag{79}$$

$$C_o = C_{o,ishii} - (C_{o,ishii} - 1)\left(\frac{\alpha - \alpha_{Transit}}{1 - \alpha_{Transit}}\right) \tag{80}$$

$$\text{If } C_o \geq C_{o,ishii}, C_o = C_{o,ishii} \tag{81}$$

$$\left(\frac{u_{SG}}{\alpha} - u_{d,KI}\right)/u_M = C_{o,ishii} - (C_{o,ishii} - 1)\left(\frac{\alpha - \alpha_{Transit}}{1 - \alpha_{Transit}}\right) \tag{82}$$

The above steps are repeated for the number of segments of pipe n, to determine BHP. For an optimized n, different number of segments are tested. When n is greater than 10 for experimental data and n is greater than 100 for field data, the calculated pressures are almost identical to the pressure with smaller n. Therefore, for experimental data, n = 10 and for field data, n = 100 are applied for this study.

$$BHP = P_{Top} + \sum_{i=1}^{n} \frac{dP}{dZ} \tag{83}$$

For air/water two phase flow experiment at near atmospheric condition, interfacial tension,σ, can be treated as a fixed value, 0.072 N/m for approximation. However, for a field condition where pressure and temperature of fluid in pipes are much higher than the experiment condition, interfacial tension between oil and gas decreases and thus it should be considered into the model. Abdul-Majeed (2000) updated the Baker and Swerdloff (1956) correlation by testing 18 crude oils covering temperatures from 60 to 130 °F and their model is used for this study (Eq. 84 and 85).

$$\sigma_{dead\_oil} = (1.17013 - 10^{-3} T_f 1.694)\ (38.085 - 0.259\, API) \tag{84}$$

$$\sigma_{oil} = \sigma_{dead_{oil}}\left(0.056379 + 0.94362\, Exp\left(-10^{-3} Rs\ 3.8491\right)\right) \tag{85}$$

For other fluid property calculations, the following correlations are applied.

- Gas solubility, bubble point pressure: Standing, 1981

- Oil formation volumetric factor: Vazquez and Beggs (1980)

- Oil viscosity: Beggs and Robinson (1975)

4. MODEL VALIDATION

In this chapter, the proposed model and existing flow models are compared for BHP estimations. The data and models for comparison are described and the results are presented here.

4.1. Tested Data Sets

Drift-flux models (Hasan et al., 2010; Bhagwat & Ghajar, 2014) and well-known empirical and mechanistic two-phase flow models available in PIPESIM (Table 5) are tested with the proposed model for pressure estimation. The tested models were selected since they represent different types of models well. For instance, each tested drift-flux model uses a different approach to estimate void fraction. Those models in PIPESIM has unique flow regime maps or has no flow regime map. By testing those models, the factors that contribute to model accuracy or deficiency would be determined systemically. For this study, lab and field data that cover the widest range of flow rate, pressure, and pipe diameter size in the literatures are employed for the test (Table 6). The data includes flow condition at liquid flow rate (up to 27,700 stb/d), gas flow rate (55,700 Mscf/d), GOR (up to 1,400,000 scf/stb), pressure (up to 7,000 psia), and fluid type (oil/gas, water/air, dry gas), pipe diameters (2–11.7 in), and geometry (vertical – deviated wells). In Figures 35 and 36, the range of testing data sets are expressed. Almost all the field data have GOR > 100 scf/stb and superficial velocity ratio (u_{SG}/u_{SL}) > 1. It is worth mentioning that the tested field data set is a comprehensive set to test flow models for high flow rates in large diameter pipes, which is close to WCD conditions.

Table 4. Tested flow correlations and their abbreviations

Wellbore flow model	Abbreviation
Proposed model	Lee &Waltrich
Hasan et al. (2010)	HASAN
Bhagwat and Ghajar (2014)	Bhagwat
Ansari et al. (1990)	ANS
Beggs and Brill (1973)	BB
Duns and Ros (1963)	DR
Gray (1974)	GRAY
Hagedorn and Brown (1964)	HB

Table 5. Experimental and field data used to evaluate pressure drop estimation.

Source	Fluids	Pipe Length (ft)	Pipe ID (in)	Liquid rate (Stb/d)	Gas rate (Mscf/d)	GLR (Scf/Stb)	Outlet Pressure (psig)
Waltrich et al., (2017)	Water/air	20 35 20	3.83 7.72 11.7	3,300-27,700	0.006- 2 (Few data up to 102)	1 – 1,000	0
Almabrok(2013)	Water/air	11	4.00	440-4,400	30 – 700	10-1580	0
Fancher and Brown(1963)	Oil/Gas	465 – 2685	2.0	200-1,050	80-940	520-7,300	89 – 349
Reinicke et al. (1987)	Oil/Gas	5413 – 15988	3.976	10-500	1,600-34,000	7700 - 1,404,000	1300 – 7000
Asheim (1986) – Ekofisk field	Oil/Gas	9900 – 14330	2.11, - 4.90	720-17,000 (mostly 10,000)	1670 – 55,700 (mostly 10000-20000)	450-5,930 (mostly 1000 – 2500)	650 – 4420 (mostly 1000-2300)
Asheim (1986) – Forties field	Oil/Gas	6899 – 10289	3.96 – 6.184	2,300-27,000 (mostly 12000-23000)	2,000-9,000 (mostly 2000 – 5000)	320-340	140 – 390
Espanol et al. (1969)	Oil/Gas	4304 – 12450	2.38	50- 1,600 (mostly less than 500)	30-1,450 (mostly less than 200)	170-9,980 (mostly 500 – 1000)	10 – 1740 (mostly less than 900)
Petrobras	Oil/Gas	15513 – 15739	3.74 – 4.5	718-3262	4070 -8703	2668-6183	2190 – 3225
Equinor F-01C	Oil/Gas	8810	6.182	4000 – 9800	3000-7000	790-820	940-1600
Equinor F-15D	Oil/Gas	9650	6.182	1200-2800	1000-2300	780-930	500-700

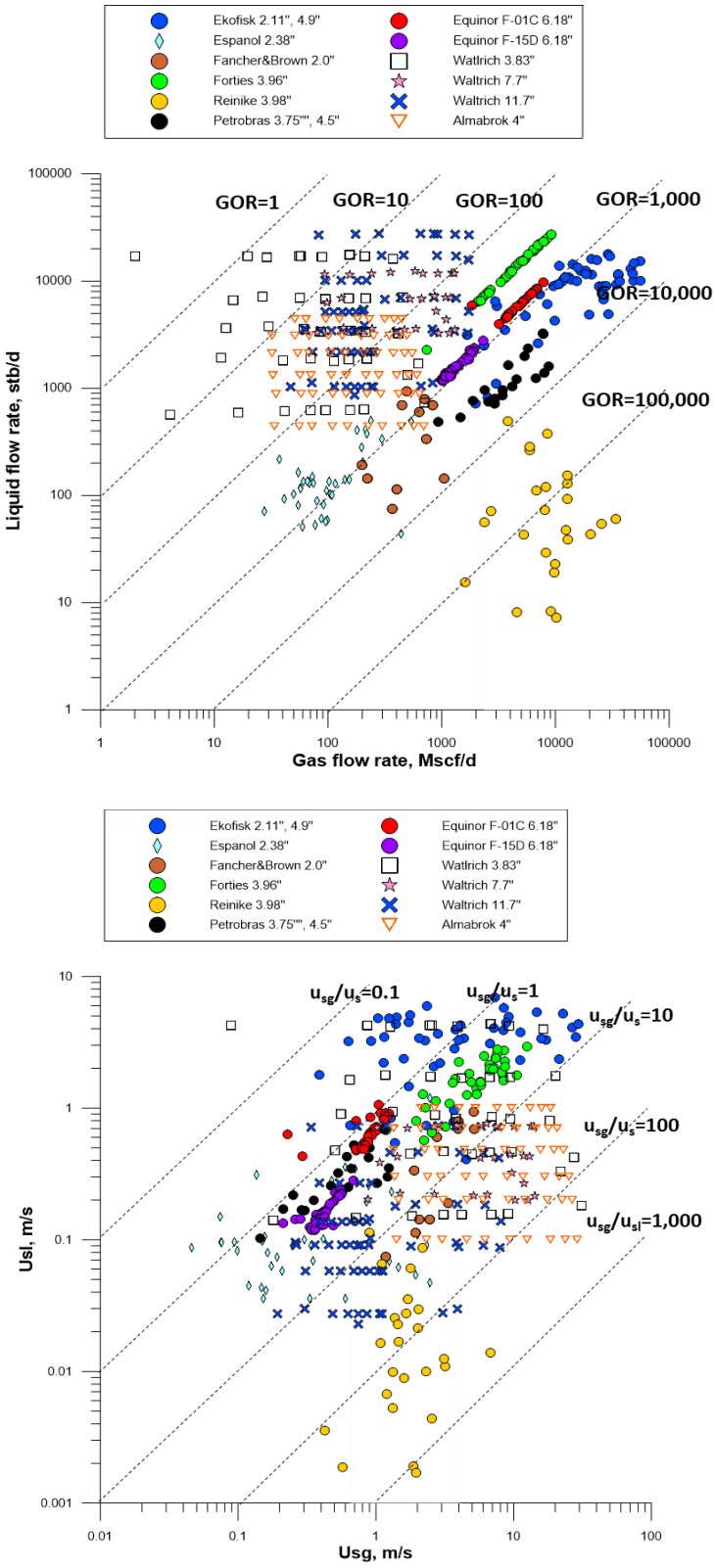

Figure 35. The range of tested experimental and field data in field unit and SI unit

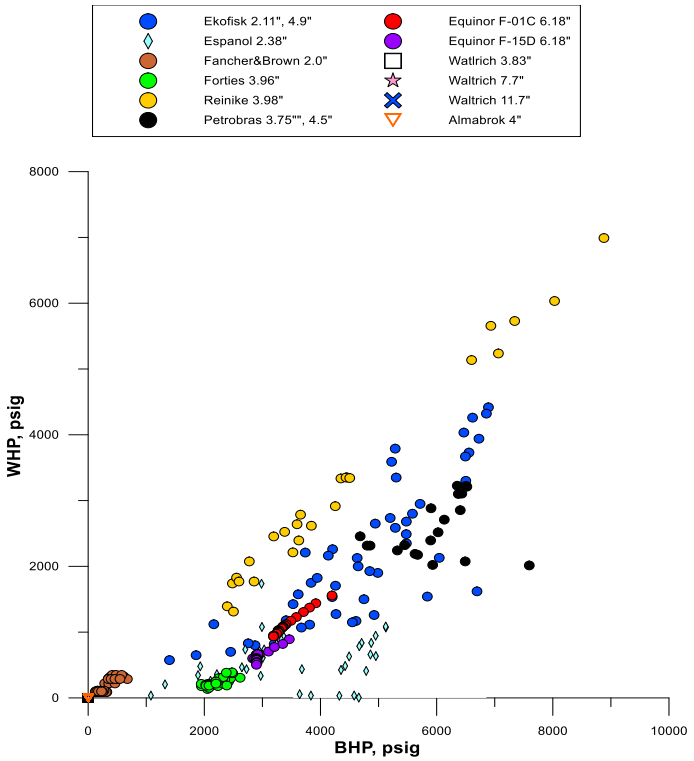

Figure 36. Measured wellhead and bottomhole pressure of tested data

Before using the lab data (Waltrich et al., 2017; Almabrok, 2013), two sets of data are compared with each other for validation. As seen in Figure 37, data from the two sources are similar, and it confirms that the tests from the two studies have valid data as an input for this study. As the outlet pressure of the fluid column is not specified in Almabrok (2013), the atmospheric pressure was assumed for pressure drop estimation.

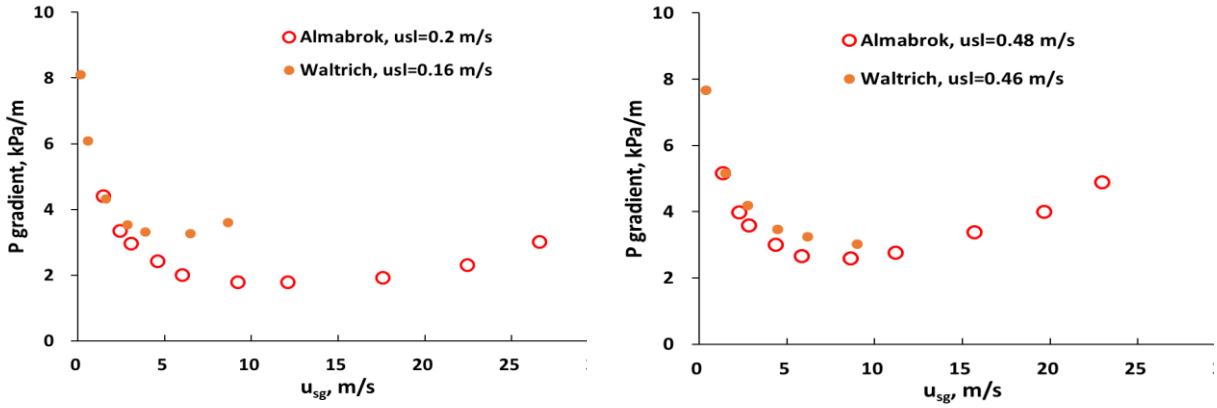

Figure 37. Lab data cross-validation

4.2. Comparison Method of Flow Model Accuracy

Each tested flow model is compared with the measured pressure loss between BHP and WHP. The results are expressed with pressure drop (BHP-WHP) differences and standard deviation of errors. The error is defined as:

$$error = \frac{calculated\ pressure\ drop - measured\ pressure\ drop}{measured\ pressure\ drop} \times 100\ (\%) \tag{86}$$

Since errors can be positive or negative, the average of errors may not describe the ability of a model. Therefore, absolute error and the average of absolute errors are also obtained as:

$$\text{Absolute error} = |error| \tag{87}$$

$$\text{Average absolute error, } |\overline{error}| = \frac{1}{n}\sum_{i=1}^{i=n}|error| \tag{88}$$

Since standard deviation of absolute errors may yield a lower result that overestimates the accuracy of a model, standard deviation of errors is calculated as:

$$\text{Standard deviation of errors, } \overline{\sigma} = \sum_{i=1}^{n}\sqrt{\frac{(error - \overline{error})^2}{n}} \tag{88}$$

For laboratory data, pressure gradient errors are presented.

4.3. Results of Flow Model Comparisons with Laboratory Data

Flow correlations listed in Table 4 were tested against laboratory data from Waltrich et al. (2017) and Almabrok (2013) and the results are presented in this section.

4.3.1. Flow Model Comparisons Against Waltrich Et Al. (2017) Data

From Figure 38 to Figure 43, the red circles are measured data and lines are simulated results. Figure 38, 39, and 40 show the results for pressure gradient for 3.8 in, 7.8 in, and 11.9-in pipe diameters. Among the lines, dashed lines are results of drift-flux correlations of Bhagwat and Ghajar (2014), Hasan et al. (2010), and the proposed model (Lee and Waltrich). In Figure 38, the

trend of pressure gradient estimation along the increased gas superficial velocity for 3.8 in diameter pipe is presented. Throughout Figures 38 to 40, the pressure drop predictions of drift-flux models (dashed lines) are closer to the measured data than other mechanical and empirical models are, in general. Only when the results of drift-flux models are compared, distinctive differences are presented and the differences are more evident at high gas and liquid superficial velocities.

In Figure 39, the results of Hasan et al. (2010) show that the pressure gradient suddenly decreases to zero. Bhagwat and Ghajar (2014) show an earlier concave upward trend and over-predicted the experimental pressure gradient. The results of the Lee and Waltrich model follow the measured pressure data, the best among the tested models. For pipe diameters 7.8 in and 11.7 in Figures 40 and 41, the differences among the three drift-flux models are less than shown in Figure 38, due to lower gas superficial velocities.

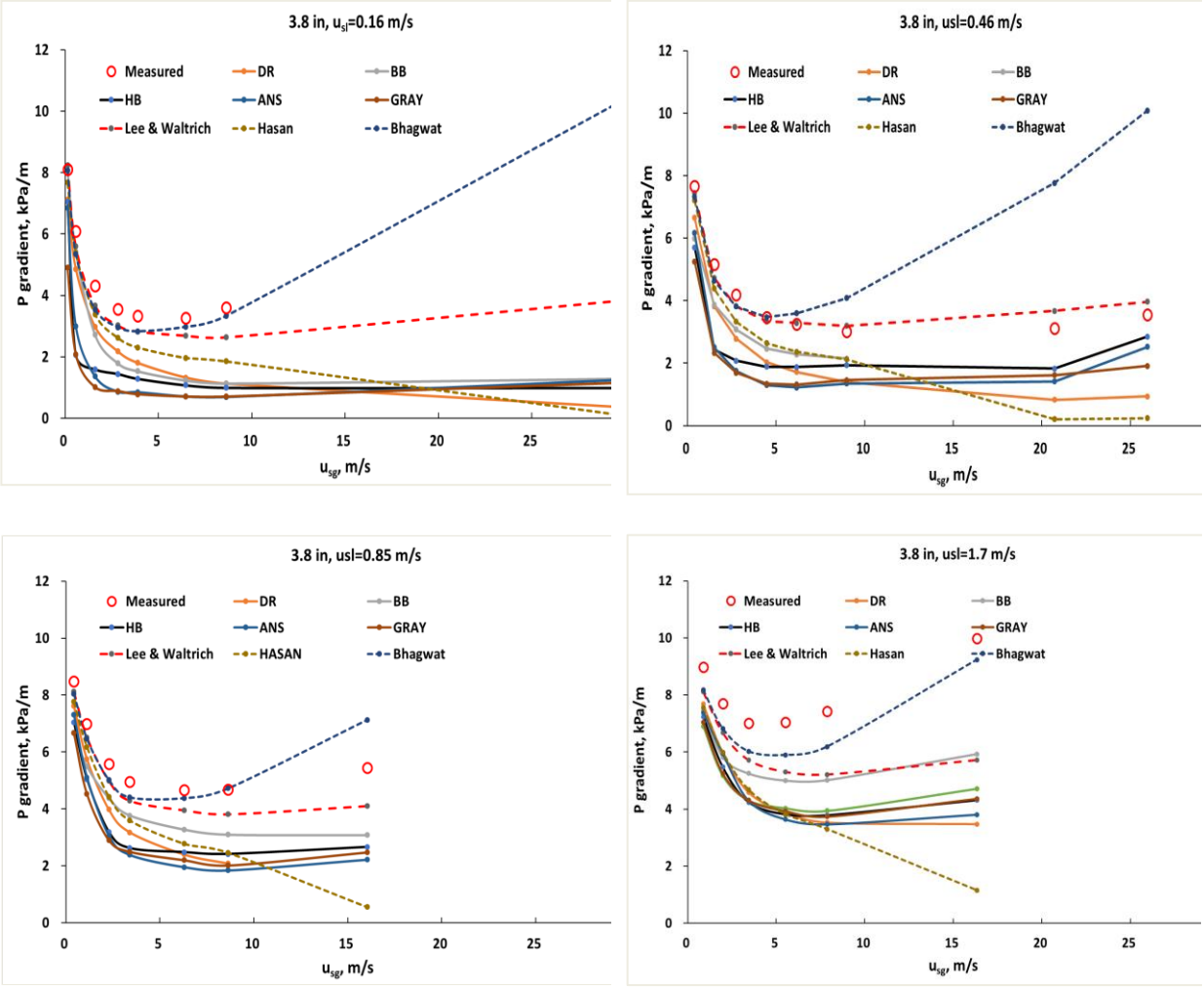

Figure 38. Pressure gradient estimation against Waltrich et al's (2017) 3.8 in ID pipe data

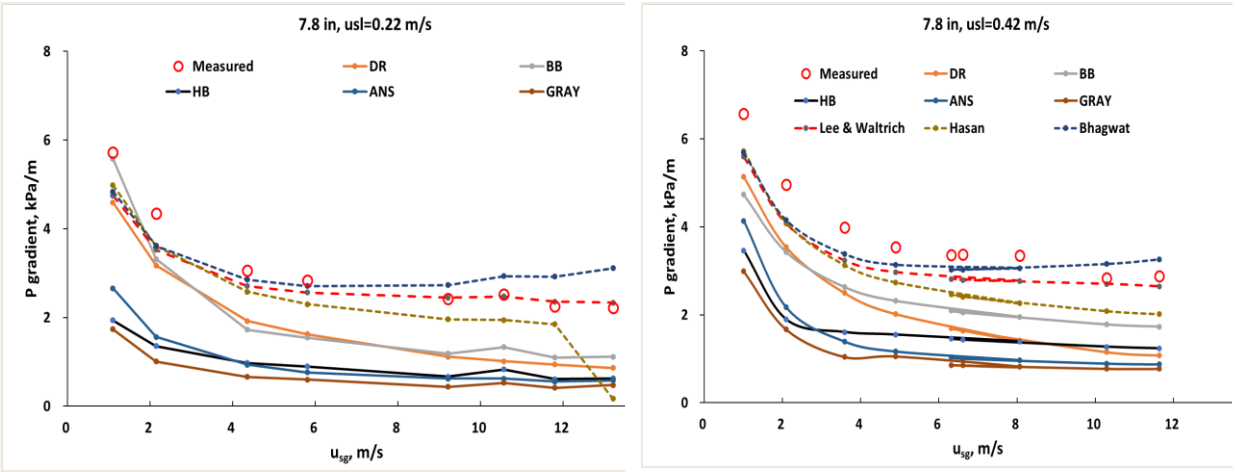

Figure 39. Pressure gradient estimation against Waltrich et al's (2017) 7.8 in ID pipe data

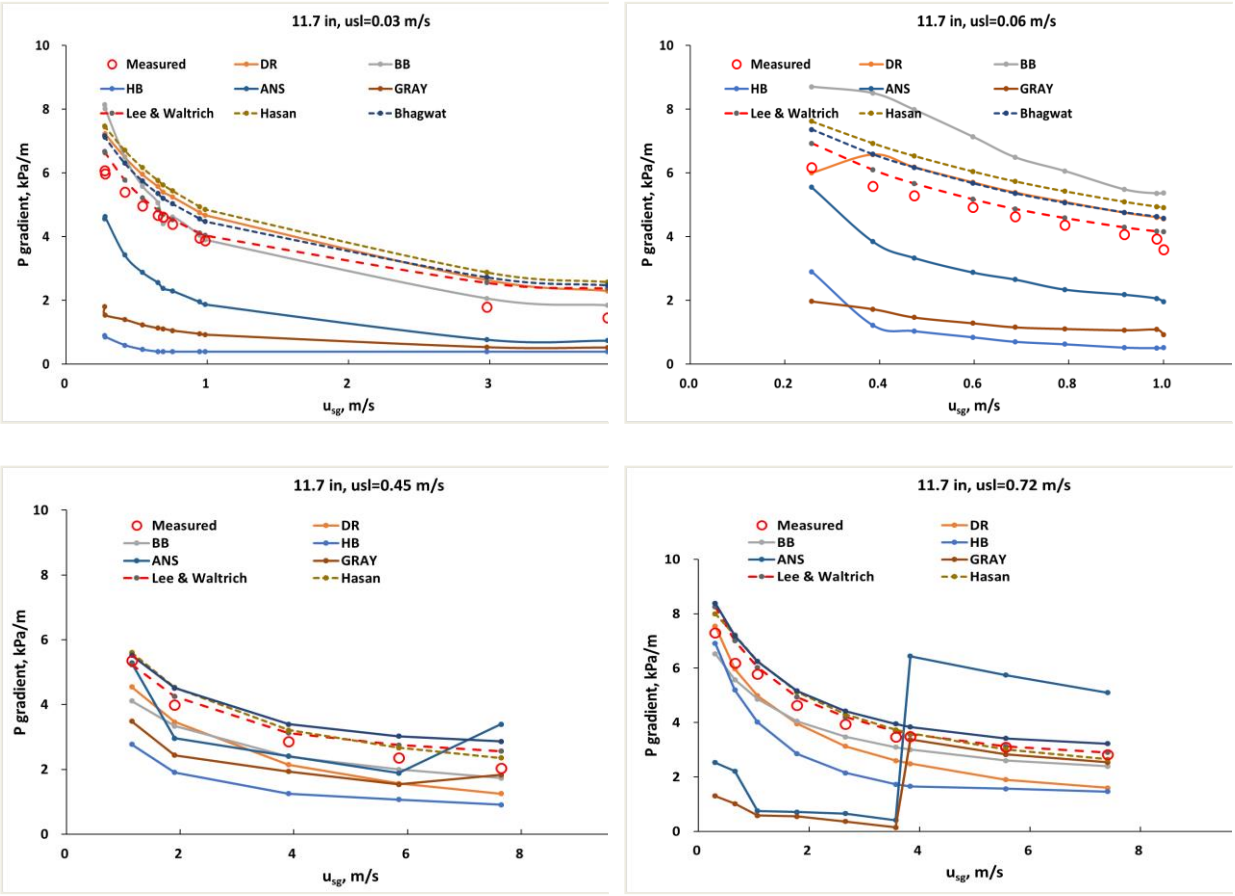

Figure 40. Pressure gradient estimation against Waltrich et al's (2017) 11.7 in ID pipe data

To compare the differences in the results of the three drift-flux models, their distribution parameters, C_o, are plotted in Figure 41 - Figure 43. As indicated in Eq. 21, at higher velocity, drift velocity, u_d has lesser contribution to void fraction and pressure drop estimation than the distribution parameter does. Therefore, only C_o is presented here. The left side of Figure 41 - Figure 43 indicates pressure gradient estimations and the right side of the figures are C_o estimations of the models.

As pressure gradient trend differences are evident at higher fluid velocity, the variance of C_o is dramatic. In Figure 41, C_o of Bhagwat stays near 1.2, while C_o of the others varies from 1.2 to 1.0. In many drift-flux studies (Ishii, 1977; Kataoka et al, 1987; Hibiki et al, 2003; and Hasan et al,

2010) C_o =1.2 and C_o=1.0 are applied for bubbly flow and annular flow, each. Although Bhagwat and Ghajar (2014) do not employ the flow regime for their model, calculating $C_o$around 1.2 for all data points produced a result that their model predicted bubbly flow. As presented in Figure 31, when bubbly flow model is applied to higher gas velocity, the predicted pressure curve becomes concave earlier and over predicts the pressure drop. The same trend as presented in Figure 31 is shown with the results of Bhagwat in Figure 38. As depicted in Figure 24, in Bhagwat and Ghajar (2014), model $C_o$varies along with two-phase Reynolds number and gas-liquid density ratio. When two-phase Reynolds number is greater than 5 x 103, approximately, and gas-liquid density ratio is 0.001, C_o stays near 1.2. Since tested data from Waltrich et al. (2017) satisfy these two conditions, the Bhagwat and Ghajar (2014) model predicts $C_o$around 1.2 for all velocity ranges of data that result in over-predicted pressure drops.

The results of Hasan are also distinctive: sudden pressure gradient drops to near zero and corresponding $C_o$reductions to 1.0 are observed. Since Hasan et al. (2010) apply the flow regime to their model, these sudden variations of pressure and C_o are related to flow regime changes. As shown in Table 2, Hasan et al.(2010) employ the flow regime dependent drift-flux parameters. C_o for bubbly, slug, churn, and annular flow is 1.2, 1.2, 1.15, and 1 respectively. For slug to churn flow and churn to annular flow regime transition criteria, Hasan et al. (2010) utilized the flow regime map of Taitel et al. (1980) as presented in Figure 2. Consequently, C_o reductions from 1.2 to 1.15 and 1.0 imply that the model predicts bubbly, slug/churn, and annular flow in sequence in Figure 41. This discrete allocation of C_o and application of Taitel et al. (1980) flow regime map, which was built with small diameter pipes, result in an abnormal pressure prediction. To minimize the sudden pressure drops, continuous and smooth transition across the flow regime and corresponding C_o should be applied.

Compared to the results of Hasan and Bhagwat, the results of the proposed model (Lee and Waltrich) show better pressure prediction in Figure 41; the primary reason therefore can be continuous reduction of C_o without discrete flow regime transition. As explained in Chapter 3.1 and Figure 31, the proposed model uses the bubbly flow correlation until it predicts the minimum pressure. At gas velocity higher than the velocity at the minimum pressure, the model applies non-bubbly flow correlation. The non-bubbly correlation re-calculates C_o and void fraction. The re-calculated $C_o$lies between 1.2 and 1.0, as shown in Figure 41. As stated above, Bhagwat and Ghajar (2014) predicted $C_o$around 1.2, which made the pressure curve like that generated by a bubbly flow drift-flux correlation. For that reason, the pressure curve of Lee and Waltrich deviates from the minimum pressure of Bhagwat as presented in Figure 41. However, at u_{sl} = 1.7 m/s, the proposed model does not follow pressure gradient as well as Bhagwat. Flow regime or friction factor may be the reason for this under-representative pressure gradient. This is further described in Chapter 4.3.3.1 and 4.3.3.2.

In larger diameter pipes as shown in Figure 42 and 43, the difference in pressure predictions among the three models looks smaller. However, this is due to lower superficial velocity at the same volumetric flow rate in larger diameter pipes. Although the difference is not as significant as in Figure 41, pressure curves begins to part from each other around u_{sg} = 5 m/s in Figure 42 and 43. Since $C_o$effects pressure prediction directly, similar $C_o$between 1.15 and 1.20 among the three models can be observed in Figure 42 and 43. Although $C_o$are is in similar range, Lee and Waltrich present $C_o$variance along with gas velocity. Predicted flow regimes of each drift-flux model are plotted along with flow transitions by Capovilla et al. (2019) in Figure 44 and 45.

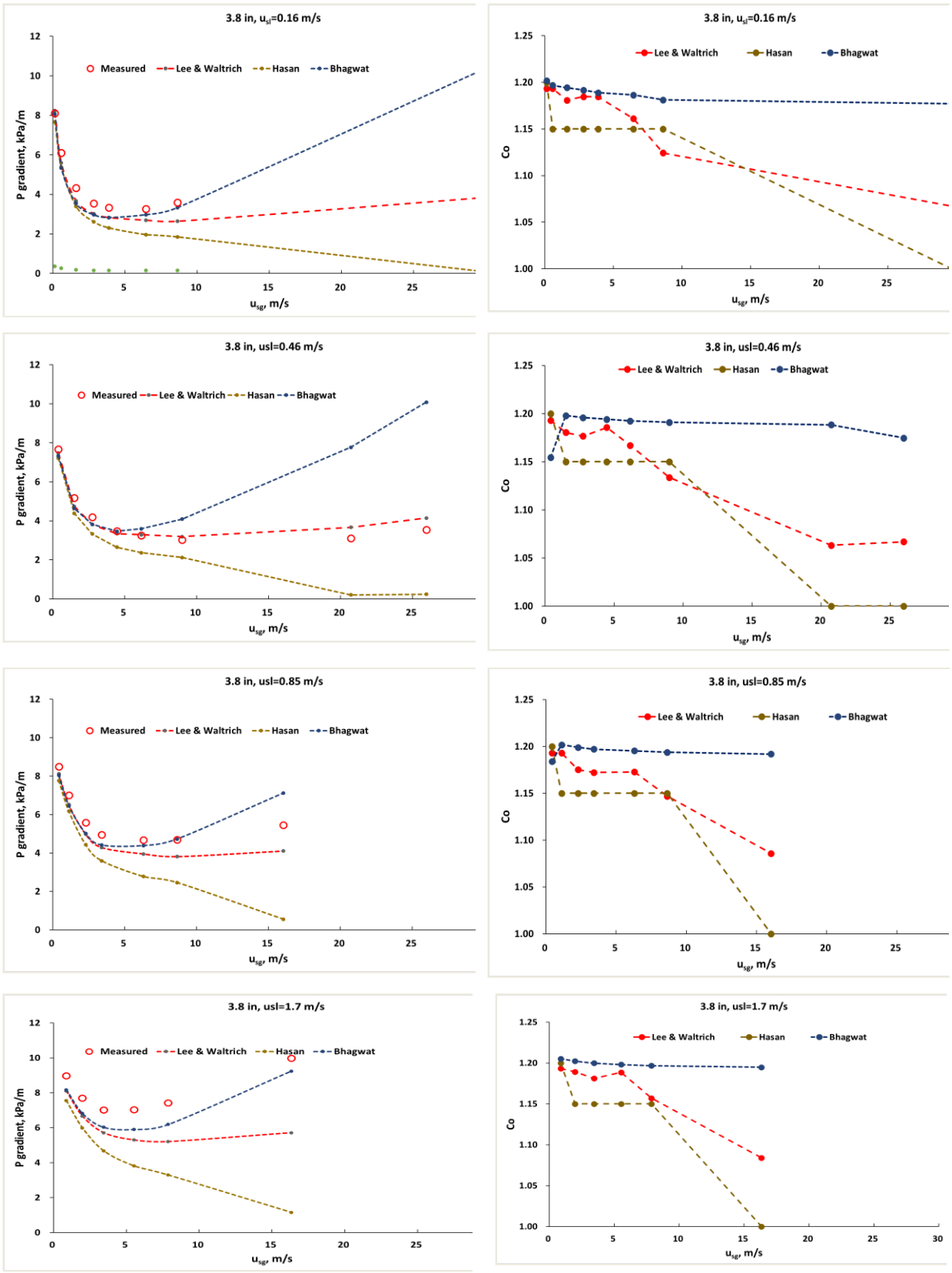

Figure 41. C_o of the tested drift-flux models against Waltrich et al's (2017) 3.8 in ID pipe data

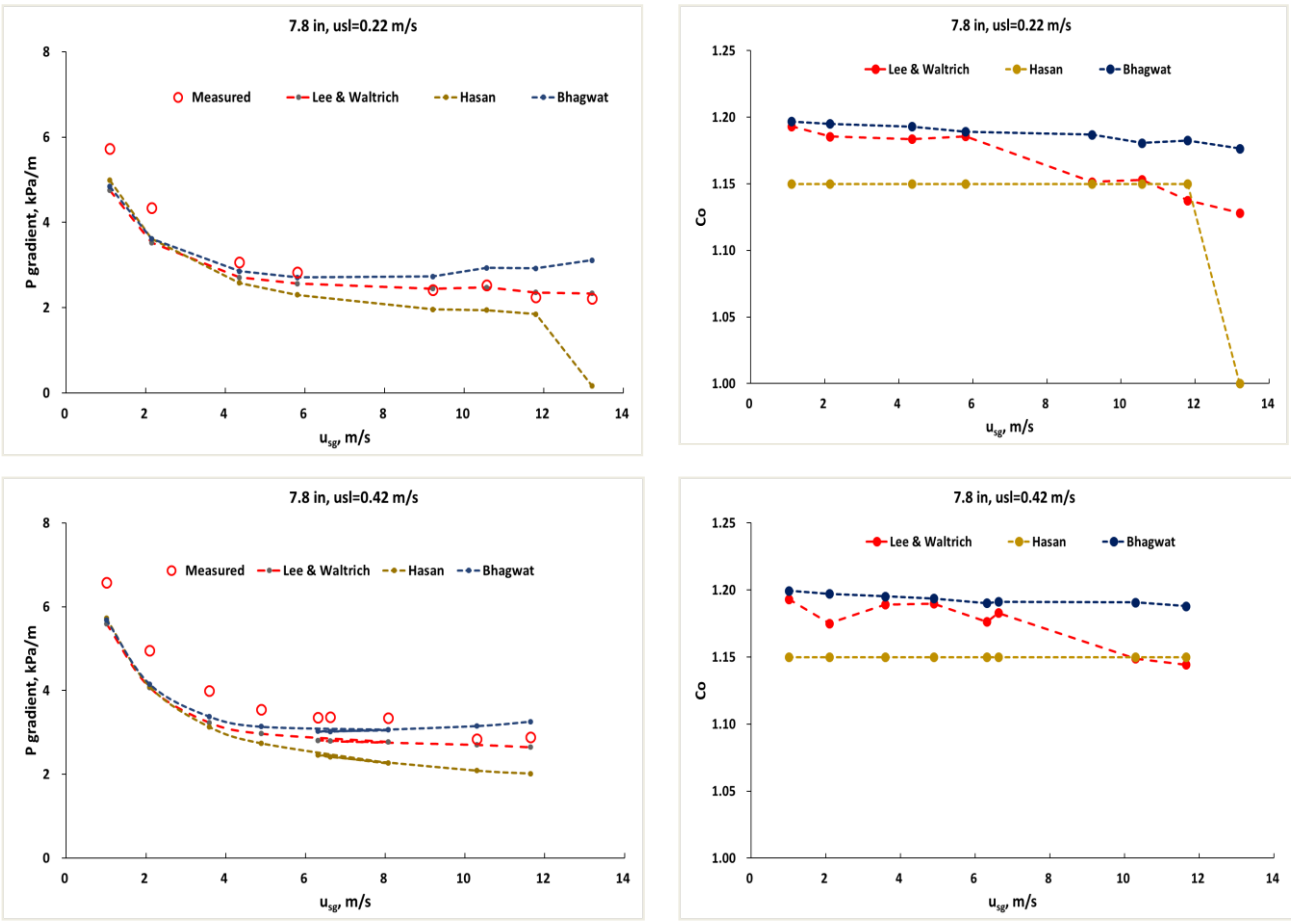

Figure 42. C_o of the tested drift-flux models against Waltrich et al's (2017) 7.8 in ID pipe data

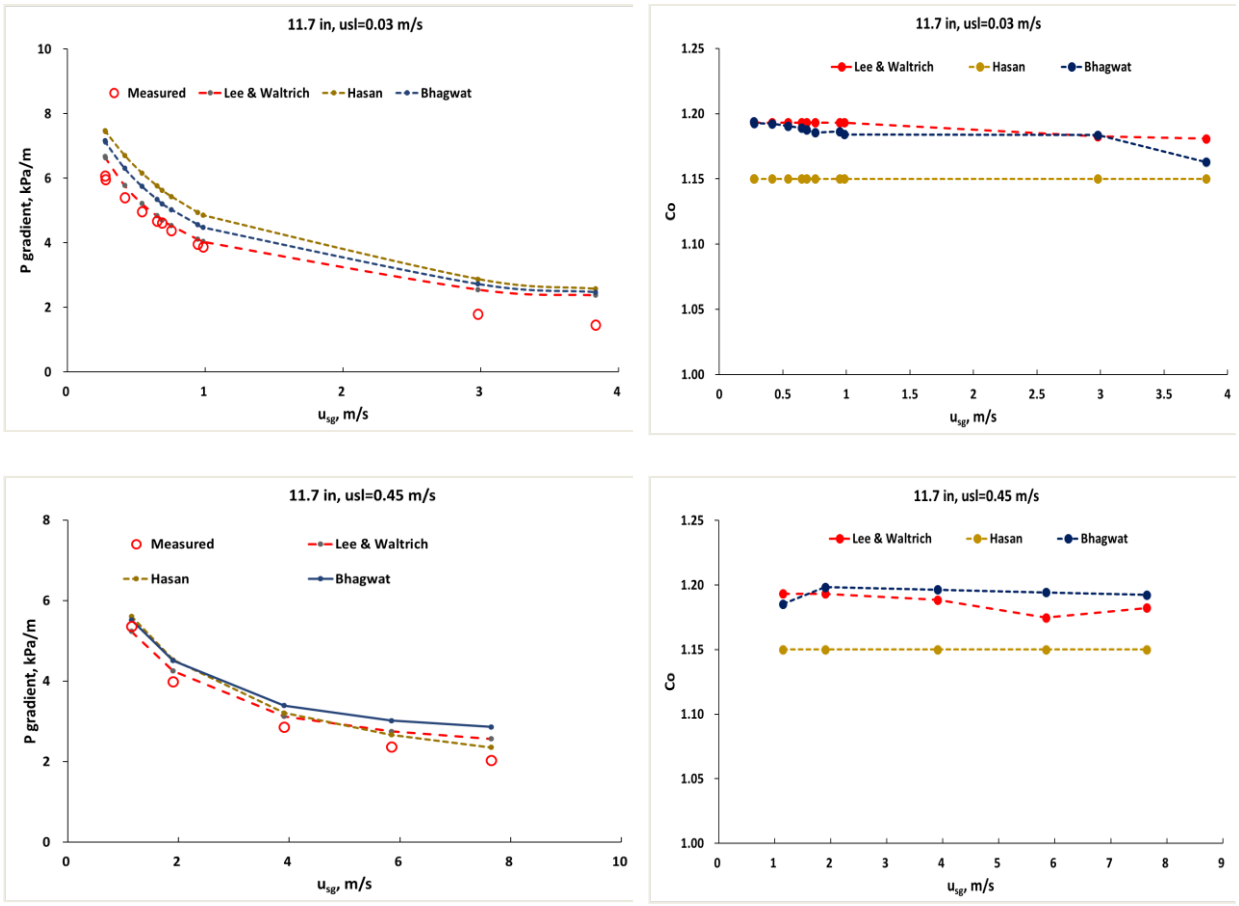

Figure 43. C_o of the tested drift-flux models against Waltrich et al's (2017) 11.7 in ID pipe

In Figures 44 and 45, dashed lines are flow regime transitions suggested in the study of Capovilla et al. (2019). B-CB, CB-C, and C-A represent bubbly to cap-bubbly, cap-bubbly to churn, churn to annular and flow transition respectively. The green, orange, and black symbols are the predictions for 3.8, 7.8, and 11.7 in diameter pipes. Circles and triangles in Figure 44 represent bubbly and non-bubbly flow predicted by Lee and Waltrich. Circles, crosses, triangle, and asterisks in Figure 45 are bubbly, slug, churn, and annular flow predicted by Hasan et al. (2010).

In Figure 44, till the cap-bubbly to churn flow transition, Lee and Waltrich predict bubbly flow for 11.7 and 7.8 in pipes while the model predicts non-bubbly flow for 3.8 in ID pipes. In the same area, Hasan et al. (2010) predict churn flow mostly. Since cap-bubbly flow is transition between

bubbly and churn flow, it cannot be said that either the churn flow prediction by Hasan et al. (2010) or bubbly flow prediction by the proposed model is wrong. However, both of models predict churn flow area well. The annular flow prediction of Hasan et al. (2000) matches the annular flow regime of Capovilla et al. (2019). This is because Capovilla et al. (2019) adopted the churn to annular flow transition of Mishima and Ishii (1984) that is nearly identical to the churn to annular flow transition of Tietel et al. (1980) (Eq. 20) which Hasan et al. (1980) adopted. Tietel et al. (1980) used 3.1 as a constant as shown in Eq.20, while Mishima and Ishii (1984) used fluid viscosity number in Eq. 58 which becomes 3.1 for air-water flow at atmospheric condition. Further, Hasan et al. (2010) arbitrarily set the minimum void fraction of 0.7 as an extra rule to be annular flow. The Lee and Waltrich model pressure predictions for the data in annular flow regime are closer to the measured values than those of Hasan et al. (2010) and any other tested flow model, as proved in Figure 41. Therefore, it is important to state that the proposed model with two flow regimes with proper drift-flux parameters can perform better than models with many flow regimes and corresponding parameters.

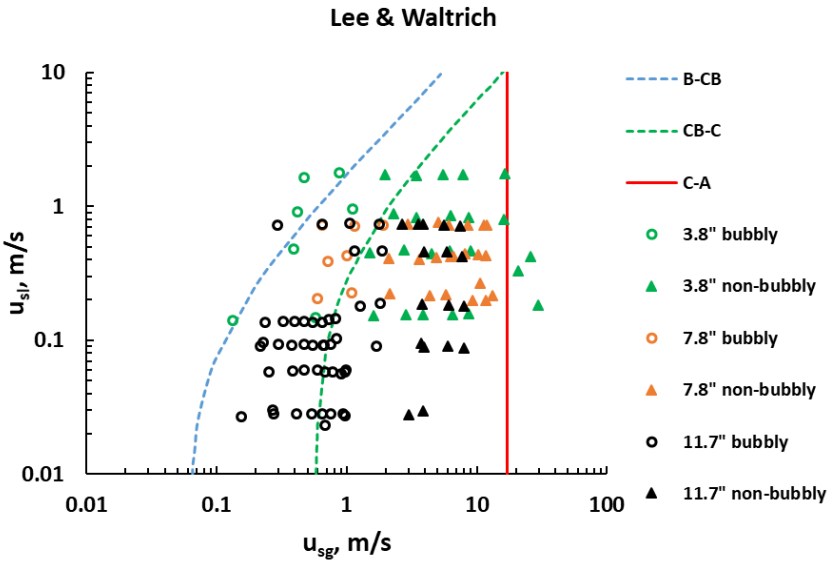

Figure 44. Predicted flow regime of Lee and Waltrich on Capovilla et al. (2019) flow regime map

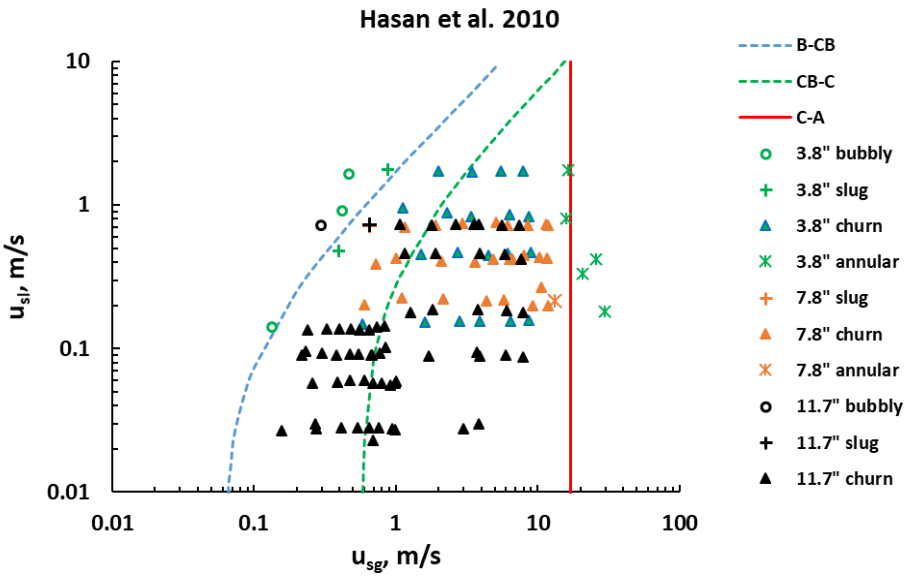

Figure 45. Predicted flow regime of Hasan et al. (2010) on Capovilla et al. (2019) flow regime map

The average absolute errors, $|\overline{error}|$, of pressure gradient estimations and standard deviations of the errors, $\overline{\sigma}$, are presented in Figure 46. For each diameter size, the Lee and Waltrich model has the lowest errors, less than 20 %, and standard deviations of less than 20%. For 7.8 in, the error difference between Lee and Waltrich and Bhagwat is only 0.3 %, which is negligible. Bhagwat has low errors overall, but has high standard deviations due to over-predicted pressure as presented in Figures 38 and 41. Overall, drift-flux models perform better than empirical and mechanistic models tested against Waltrich et al. (2017). For larger diameters, 11.7 in, the $|\overline{error}|$ for each model is quite variant from those for smaller diameter, 3.8 in. Among the tested non-drift-flux models, that of Beggs and Brill shows the best result. The details of each model will be discussed with field data in Chapter 4.4.

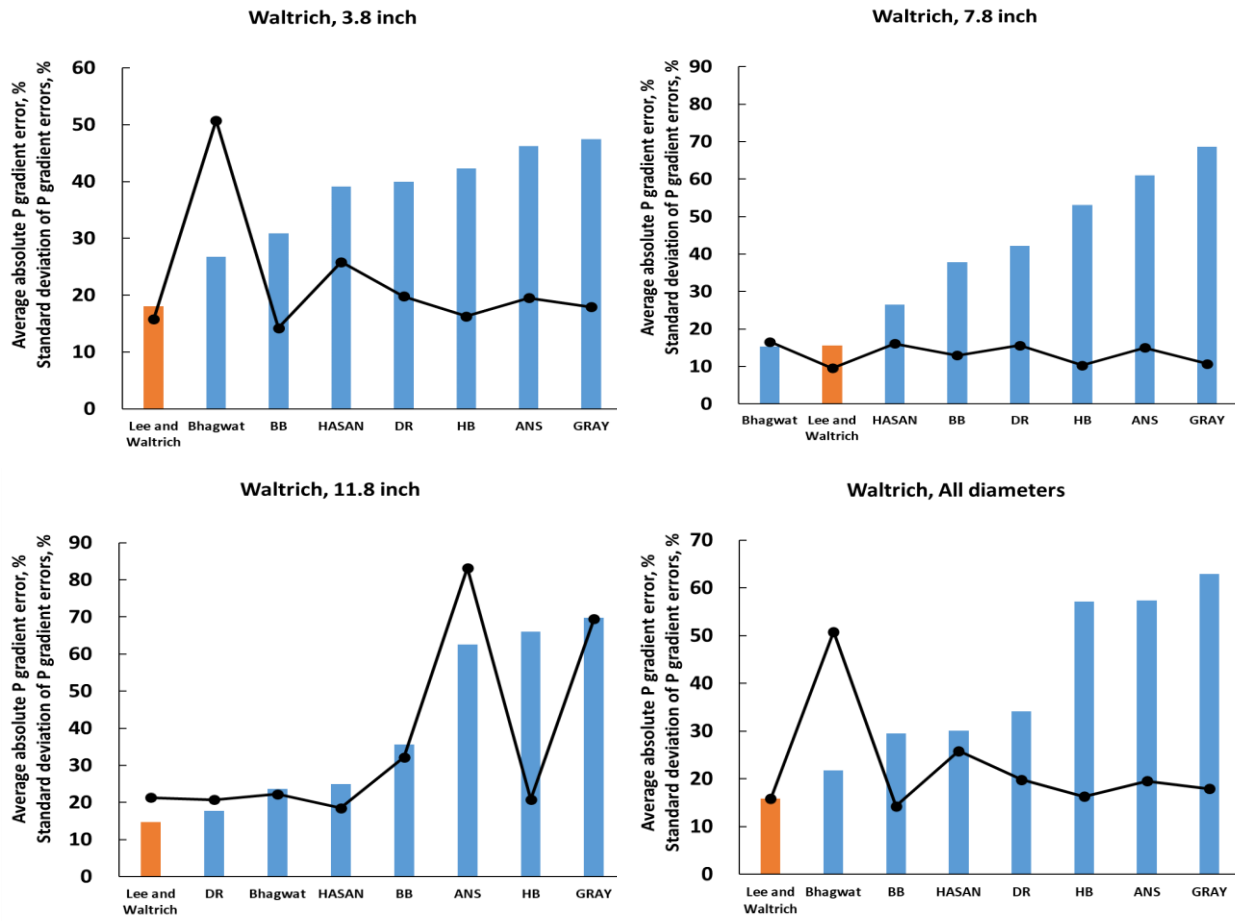

Figure 46. Average absolute pressure gradient errors (bars) and standard deviation of pressure gradient errors against laboratory measurements.

4.3.2. Flow Model Comparisons Against Almabrok's (2013) Data

In Figures 47 and 48, the red circles are measured data and lines are simulated results. Figure 47 is pressure gradient versus gas superficial velocities for different liquid superficial velocities. Figure 48 is to compare pressure drop and related C_o of the tested drift-flux models.

Pressure trends similar to those shown in Figure 38 are observed in Figure 47. The results of Bhagwat concave upward significantly and those of Hasan drop suddenly to near zero. The results of Lee and Waltrich are positioned between Hasan and Bhagwat. Other flow models under-predict pressure drop overall. Although the results of Bhagwat show early concave upward and over-

predicted pressure, the results at u_{sl} = 0.7 m/s and 1.0 m/s match the measured data better than those at other liquid superficial velocities. However, as seen in Figure 39, the measured pressure increases substantially with higher liquid superficial velocity and all tested flow models including that of Bhagwat fail to follow the measured value. For instance, the measured pressure gradient ranges from 8 kPa/m to 4 kPa/m at u_{sl} = 0.85 and from 13 kPa/m to 17 kPa/m at u_{sl} = 4.2 m/s respectively. Therefore, the results of Bhagwat are expected to be under-predicted at u_{sl} greater than 1.0 m/s.

In Figure 49, the three drift-flux models are plotted along with the measured data from Waltrich et al. (2017) and Almabrok (2013). The distinctive differences of the models are well presented in the figure. Their pressure gradient curves are close to each other at the beginning of the curves, and they deviate from each other as velocity gets higher.

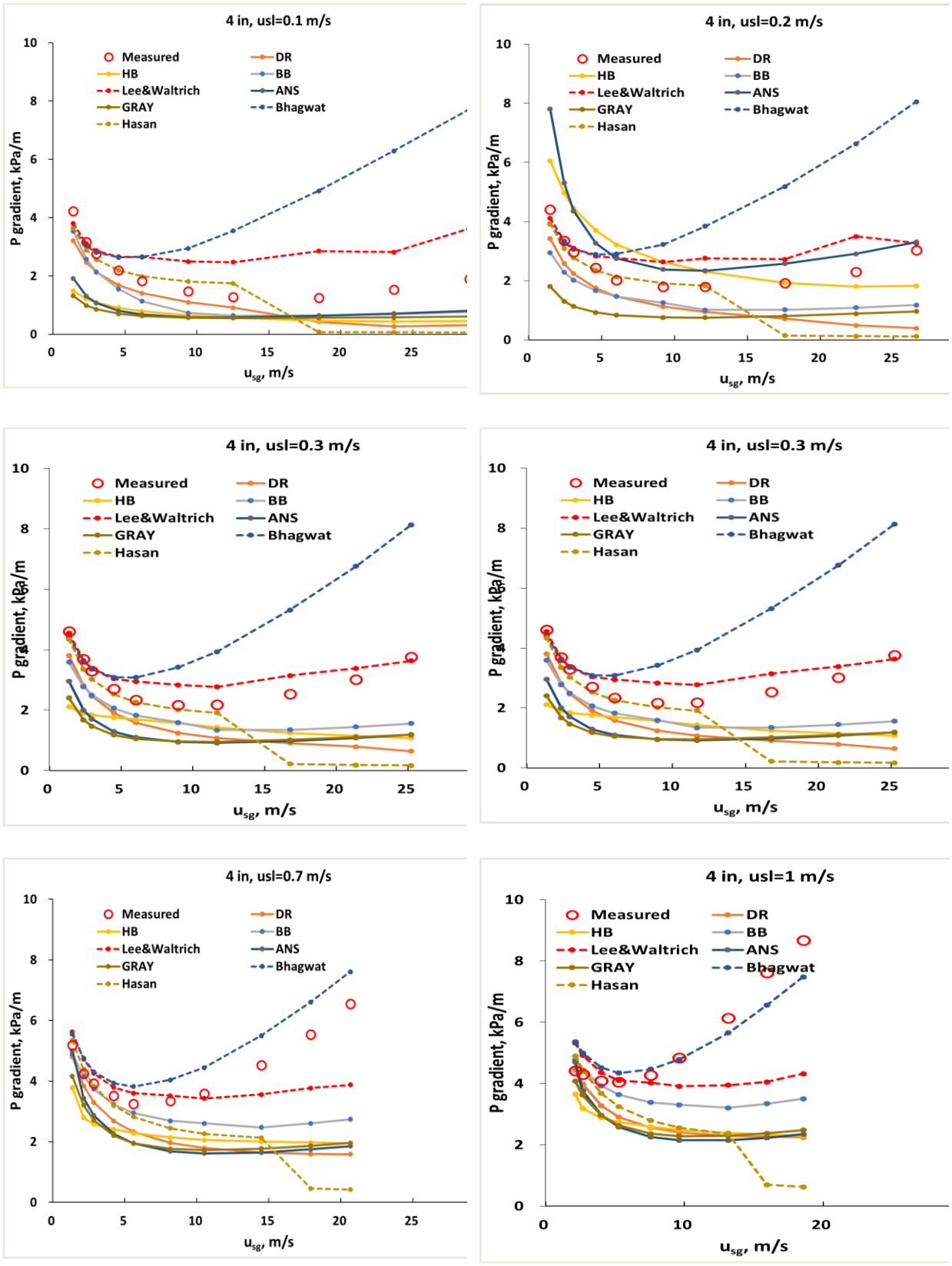

Figure 47. Pressure gradient estimation against Almabrok's (2013) 4.0 in ID pipe data

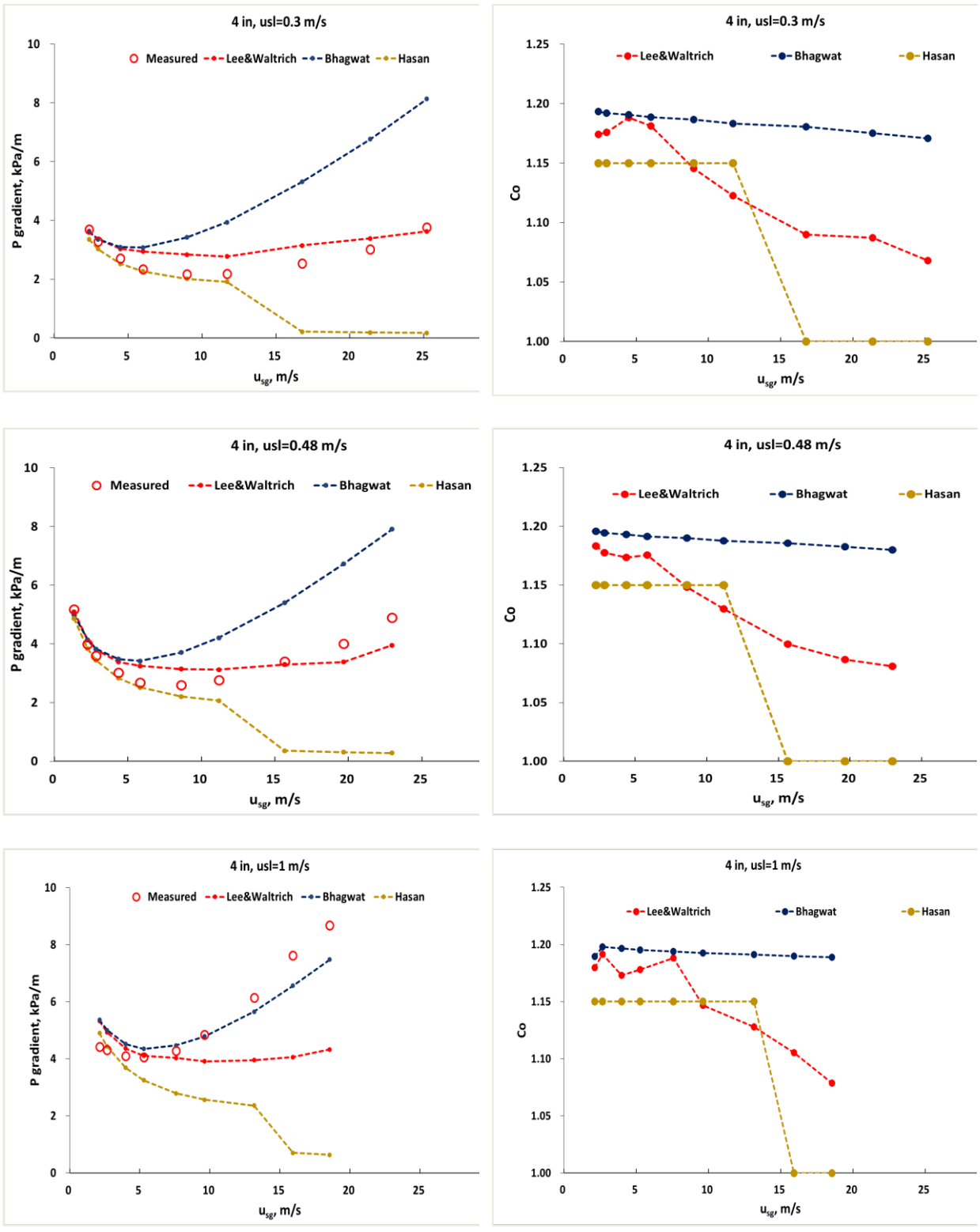

Figure 48. C_o of the tested drift-flux models against Almabrok's (2013) 4.0 in ID pipe data\

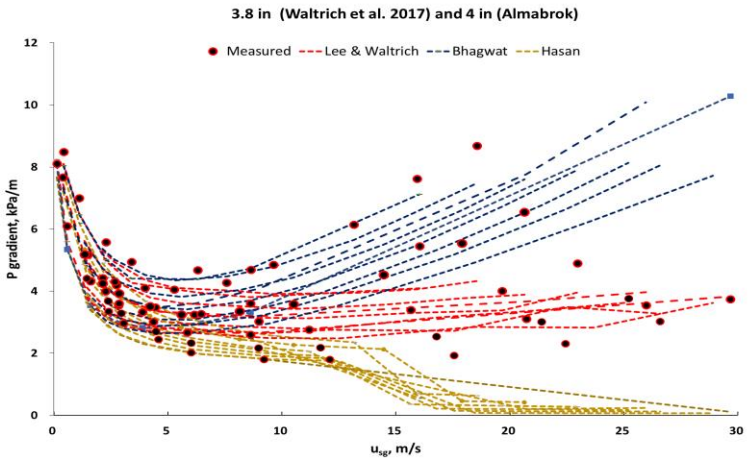

Figure 49. Pressure gradient trends estimated by drift-flux models for laboratory data

4.3.3. Investigation of Model on High Liquid Flow Rates

In previous chapters, the proposed model showed good performance in terms of average error. However, at certain liquid velocity (u_{sl}=1m/s in Almabrok (2013) and u_{sl}=1.7 m/d in Waltrich et al., (2017) the model under-estimated pressure loss and did not follow the measured pressure well. This under-estimation might be from improper friction factor. Also, interestingly, those data have relatively higher liquid velocity and are located near dispersed bubbly flow regime of Taitel et al. (1981). Therefore, the model's relatively low accuracy at higher liquid velocity is investigated with dispersed bubbly flow regime and friction factor in this chapter.

4.3.3.1. Dispersed Bubbly Flow

Bubbly flow can be sub-divided into dispersed bubbly and bubbly flow. Dispersed bubbly flow is observed at high liquid rate with uniformly distributed gas bubbles in continuous flowing liquid (Chen et al., 1997; Taitel et al., 1980; Shoham, 1982; Ali, 2009). Taitel et al. (1980) argue that when turbulent forces are high enough to break the bubbles into smaller bubbles, dispersed bubble flow exist. But dispersed bubble flow cannot exist for a void fraction larger than 0.52. Above 0.52, Taylor bubbles, which represent slug flow are formed. Bubble to dispersed bubble flow transition

for air-water flow at standard condition in 2 in (0.051m) and 1 in (0.0254m) pipes is expressed as follows:

$$2\left[\frac{0.4\sigma}{(\rho_L-\rho_G)g}\right]^{0.5}\left(\frac{\rho_L}{\sigma}\right)^{0.6}\left[\frac{2*0.046}{d}\left(\frac{\rho_L d}{\mu_L}\right)^{-0.2}\right](u_M)^{1.12}=0.725+4.15(\frac{u_{SG}}{u_M})^{0.5} \quad (89)$$

The transition ends when $u_{SG}/(u_{SL}+u_{SG})$= 0.52.

Chen et al. (1997) assumed if turbulent kinetic energy of the liquid phase is less than surface free energy of dispersed spherical bubble, dispersed bubble flow exists. The bubble to dispersed bubble flow transition was tested with Shoham's (1982) experimental data of air-water flow in 1 in (0.0254 m) vertical pipes at standard condition:

$$Y_L=\frac{(\rho_L-\rho_G)g}{\frac{4C_L}{d}\left(\frac{d_H u_{SL}}{\mu_L/\rho_L}\right)^{-n}\frac{\rho_L u_{SL}^2}{2}} \quad (90)$$

$$E_O=\frac{(\rho_L-\rho_G)g d_H^2}{\sigma} \quad (91)$$

$$\frac{u_{SL}}{u_{SG}}=12.65\frac{Y_L}{E_O^{0.5}} \quad (92)$$

where C_L = 0.046, n=0.20, and d_H is hydraulic diameter.

Weisman and Kang (1981) stated that turbulent forces are high enough to break bubbles dispersed bubble flow occurs and the forces can be expressed as pressure drop. In their model, the transition is independent of pipe orientation and gas rate but dependent of diameter and surface tension. Bubble to dispersed bubble flow transition of Weisman and Kang (1981) is:

$$\left[\frac{(\frac{dP}{dZ})_L}{(\rho_L-\rho_G)g}\right]^{0.5}\left[\frac{\sigma_L}{(\rho_L-\rho_G)gd^2}\right]^{-0.5}=9.7 \quad (93)$$

where $(\frac{dP}{dZ})_L$ is single phase frictional pressure drop.

Dispersed bubbly flow regime of Taitel at al. (1980), Chen et al. (1997), and Weisman and Kang (1981) were tested with laboratory data. In Figure 50, bubbly-dispersed bubbly flow boundaries are plotted along with Waltrich et al. (2017) data. For 3.8 in, 7.8 in, and 11.7 in ID pipe, no method predicts dispersed flow regime. n addition, bubbly-dispersed bubbly transitions are plotted on Almabrok's (2013) data in Figure 51 and no method predicts dispersed bubbly flow.

Ali (2019) observed dispersed bubbly flow in air-water flow in 10 in (0.254 m) diameter vertical pipe at u_{SL} > 0.7 m/s and u_{SG} < 0.2 m/s. Ali (2019) stated that Chen et al. (1997) and Weisman and Kang (1981) are more representative to her experimental data than Taitel et al., (1980) although all of them estimated higher liquid velocity for bubbly-dispersed bubbly flow transition than the observation. It indicates that bubbly-dispersed bubbly flow transition for large diameter is at a lower liquid superficial velocity than the estimations built with small diameter pipes. Therefore, there is a chance that u_{SL} around 1 m/s in Waltrich et al. (2017) might be dispersed bubbly flow. However, due to high fluid velocity, it might be very difficult to differentiate dispersed bubbly flow with other flow regime with naked eyes. Hence, bubbly-dispersed bubbly flow transitions in large diameter pipes should be compared with more data in future.

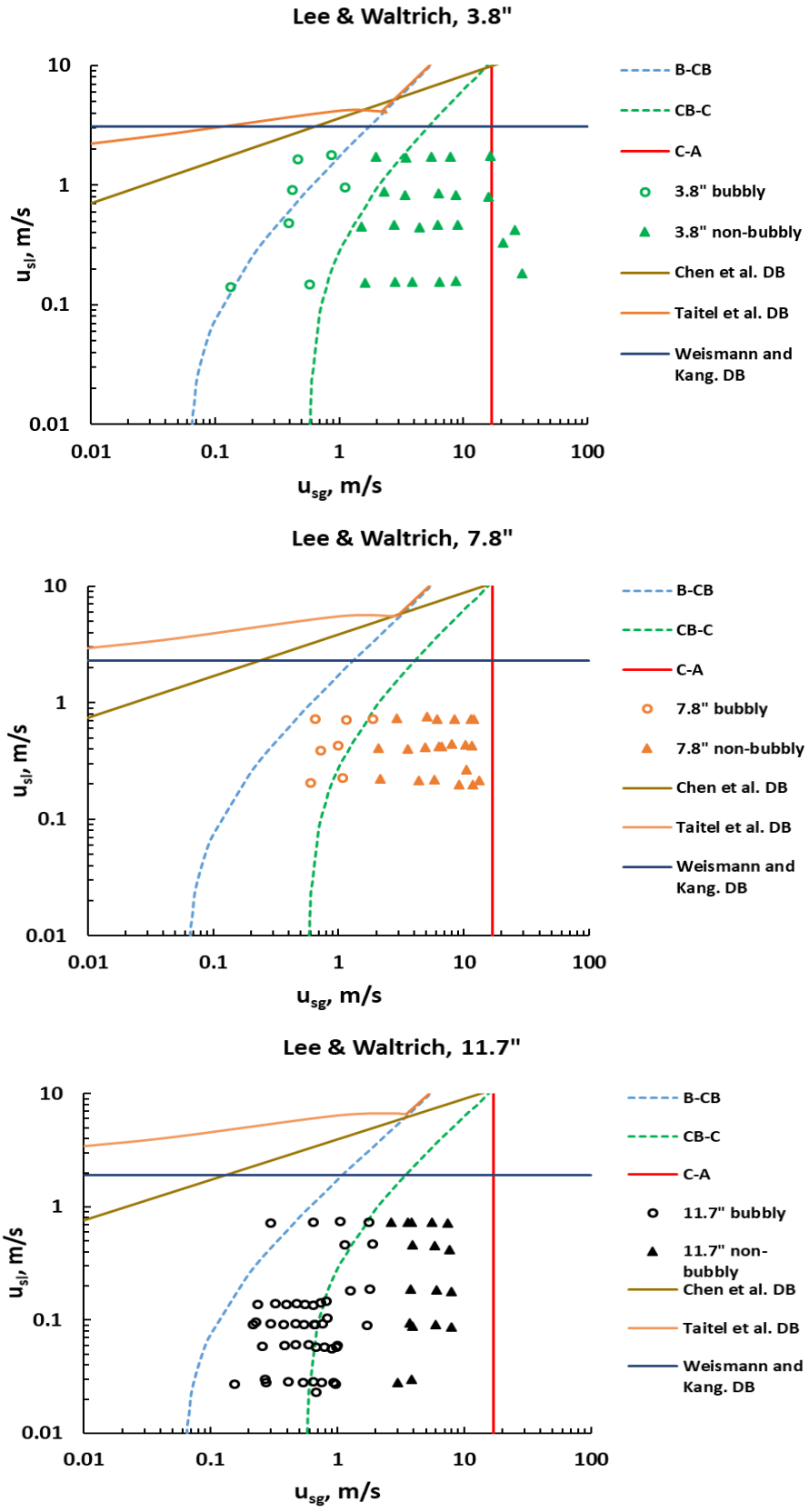

Figure 50. Bubbly- dispersed bubbly flow transition of different models

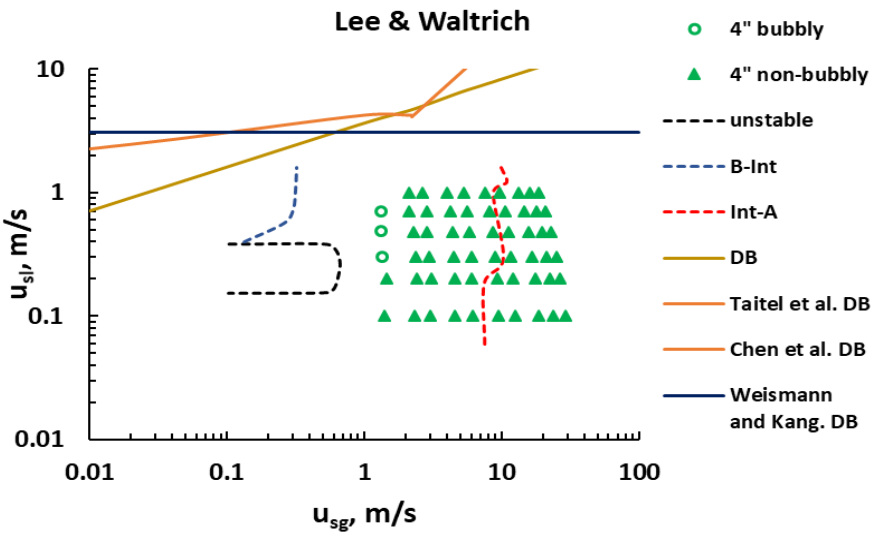

Figure 51. Bubbly- dispersed bubbly flow transition on Almabrok (2013)

Since dispersed bubbly flow represents uniformly distributed fine gas bubbles in a continuous liquid phase, drift velocity relative to the liquid phase can be neglected, and it can be treated as a homogeneous flow (Chen et al, 1997). Therefore, drift velocity should be close to 0 for fully developed dispersed bubbly flow. Meanwhile, distribution parameter, C_o, should be close to 1.2 rather than 1.0. This is because the major phase of dispersed bubbly flow is liquid, and nature of flow is closer to bubbly flow than annular flow. Implementation of C_o = 1 for ideal gas flow with negligible liquid phase would result in underestimated pressure gradient for dispersed bubbly flow. The model validation results of Hasan et al. (2010) in Chapter 4 demonstrates underestimated pressure when C_o = 1 and u_d = 0. Therefore, the proposed model for bubbly flow regime should be reasonable for dispersed bubbly flow, but it needs to be tested.

4.3.3.2. Friction Factor Correlations

Friction factor correlations of Colebrook (1939), Blasius (1908), Zigrang and Sylvester (1982), Fang et al. (2010), and Noriyuki and Terao (2017) are compared against Almabrok (2013) and Waltrich et al.'s (2017) data. For the comparison, the gas velocity is extended to 30 m/s to check

how friction factor impacts pressure gradient at high gas rates. Since friction factor correlations of Blasius (1908) and Noriyuki and Terao (2017) are for smooth pipes and the others are for smooth and rough pipes, pipe roughness is set to 1.5x10-3 mm (6x10-5 in), which represents PVC pipe commonly used in laboratory experiments. For the pressure gradient estimations, drift-flux model with Co = 1.2 and single phase Reynolds number is used to minimize the effect of void fraction change.

The Reynolds numbers for Almabrok's (2013) data are between 2x105 and 2.2 x106, and it is within the range of the Reynolds number that Colebrook et al. (1939) and Noriyuki and Terao (2017) had for their models. Until u_{sg}= 5 m/s or Reynolds number of 105, all models have almost the same pressure gradient, which implies gravitational pressure drop dominant flow.

In Figure 52, The estimated pressure gradients match well with the measurement from Almabrok (2013) at usg < 10 m/s. Although estimated pressure gradients are lower than the measured values at u_{sg} > 10 m/s or at Reynolds number greater than 106, pressure gradient trends do follow the measured pressure. Figure 64 indicates that the pressure drop estimations using Blasius (1908) and Noriyuki and Terao (2017) for smooth pipes are almost identical. Between two explicit approximation of Colebrook equation, Fang et al. (2010) shows closer approximation to Colebrook's implicit equation. In addition, at low pipe roughness for PVC pipes, pressure estimations using all friction factor equations are close each other, especially at Reynolds number less than 106.

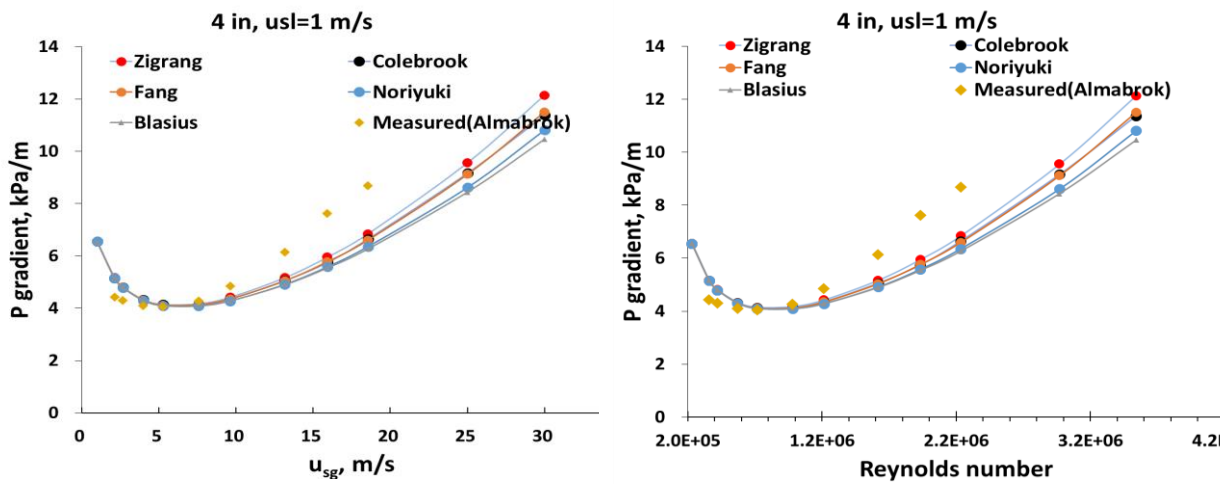

Figure 52. Pressure gradient estimation on Almabrok (2013)

As presented in Figure 38–48, Bhagwat and Ghajar (2014), which had C_o close to 1.2 for all tested experimental data, generally overestimated the pressure gradient. However, it seems to predict the pressure gradient better at a relatively smaller diameter pipe, 4 in, and u_{sl} > 0.8 m/s and u_{sg} > 10 m/s approximately. Meanwhile, at a relatively larger diameter pipe of 7.8 in, and u_{sl} > 0.8 m/s and u_{sg} > 10 m/s, Bhagwat's estimation is not as good as Lee and Waltrich's (Figure 39). In Figure 53, pressure estimations at u_{sl} = 1 m/s are presented. As presented in Figure 53, initial pressure estimation by Lee and Waltrich under-predicted the pressure gradient, while it predicted non-bubbly flow. Since u_{sl} = 1 m/s is close to dispersed bubbly flow (Figure 50) and dispersed bubbly flow behavior is more similar to bubbly flow than churn or annular flow, bubbly flow is assumed, and pressure gradient is calculated. Lee and Waltrich, with the bubbly flow application, shows the improved pressure gradient estimation at the given condition. The main difference between bubbly flow correlation and non-bubbly flow correlation of Lee and Waltrich is C_o value, not friction factor. Hence, an extra flow regime to assign C_o for higher liquid velocity may be needed and should be studied in future.

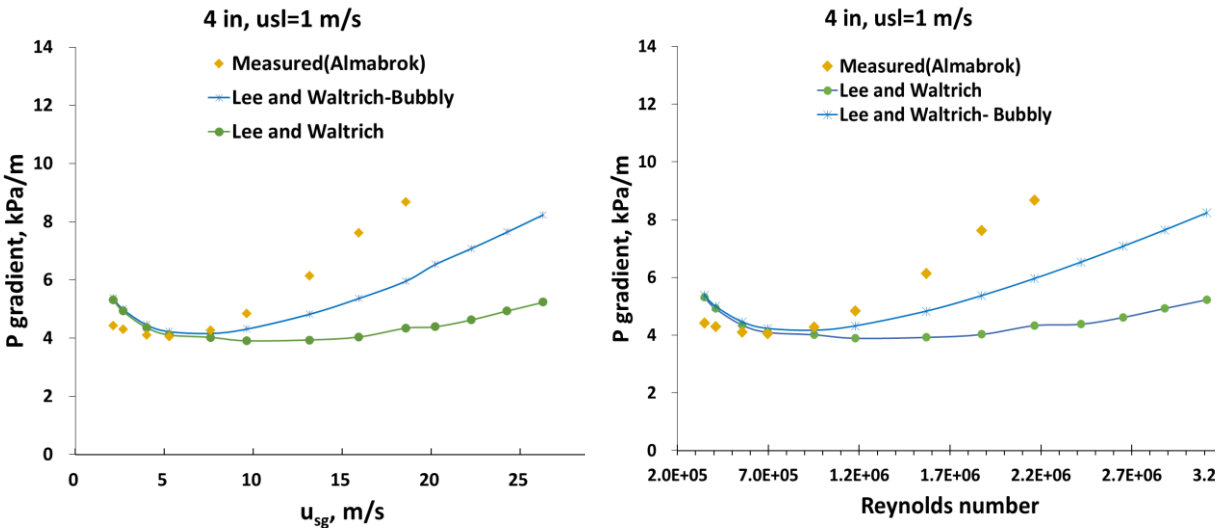

Figure 53. Pressure gradient estimation on Almabrok (2013)

4.4. Results of Flow Model Comparison With Field Data

All flow models listed in Table 5 are tested against field data listed in Table 6. Pressure drop errors are expressed along with superficial gas-liquid velocity ratio in Figure 54. In general, pressure drop errors become larger as u_{sg}/u_{sl} approaches from 0.1 to 10. At u_{sg}/u_{sl} higher than 10, each model's performance varies widely, which signifies that most of tested models do not represent certain flow condition well. Low u_{sg}/u_{sl} indicates that the mixture flow is close to bubbly flow and high u_{sg}/u_{sl} means that the mixture flow is close to the churn or annular flow. Since most of the tested flow models have relatively smaller pressure loss errors at u_{sg}/u_{sl} <1, they predict flow behavior at u_{sg}/u_{sl} <1, where bubbly flow is likely to occur. Low errors – u_{sg}/u_{sl} <1 – was also observed by Waltrich et al. (2017) and Teles and Waltrich (2018). However, the tested models do not predict flow behavior at higher u_{sg}/u_{sl}, which implies less accurate flow behavior prediction in more turbulent flow than bubbly flow.

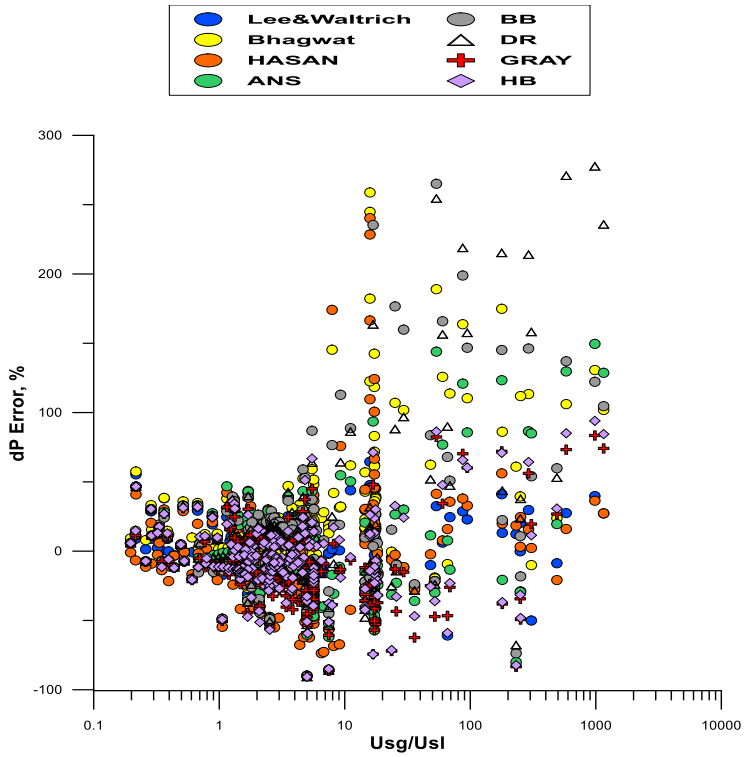

Figure 54. Pressure drop errors versus u_{sg}/u_{sl} for all tested flow models on field data

To demonstrate each model's performance on pressure estimation in relation to superficial velocity ratio (u_{SG}/u_{SL}), Figure 55 is plotted. The sizes and colors of circles in each plot of Figure 55 represent the magnitude of absolute pressure drop errors ($|error|$). The smallest white circles are $|error|$ less than or equal to 10 %, whereas the biggest black circles are $|error|$ greater than 100%. Unlike other circles, the size of the dark circles varies depending on the magnitude of errors.

The color scheme is described in Figure 51. The 4 diagonal lines represent u_{SG}/u_{SL} = 0.1 to u_{SG}/u_{SL} = 1,000 each and y-axis and x-axis are u_{SL} and u_{SL}respectively. The colors and sizes of circles represent magnitude of absolute pressure drop. By checking the emptiness of each plot, instinctive judgment can be made. Further, the strength and weakness of each model can be found from the plots too. For example, the Lee and Waltrich model has the emptiest space without circles, which means that the circles are smaller and therefore, errors are also smaller across all ranges of

u_{SG}/u_{SL}.The bubble distribution of Lee and Waltrich is more uniform than that of other flow models, which indicates the reliability of the model across all u_{SG}/u_{SL} or flow regimes.

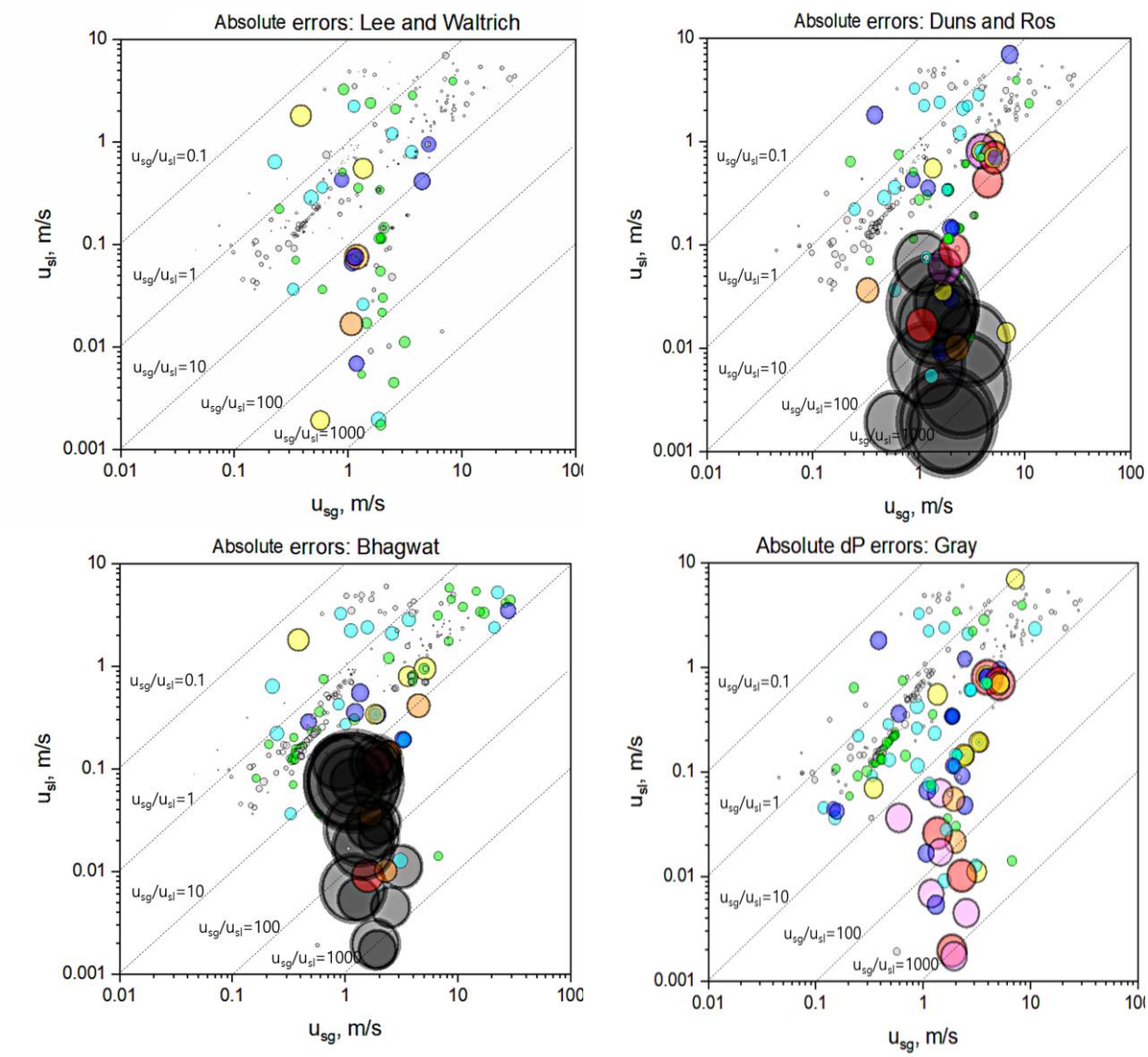

Figure 55. Absolute pressure drop errors along with superficial velocity ratios.

Figure continued.

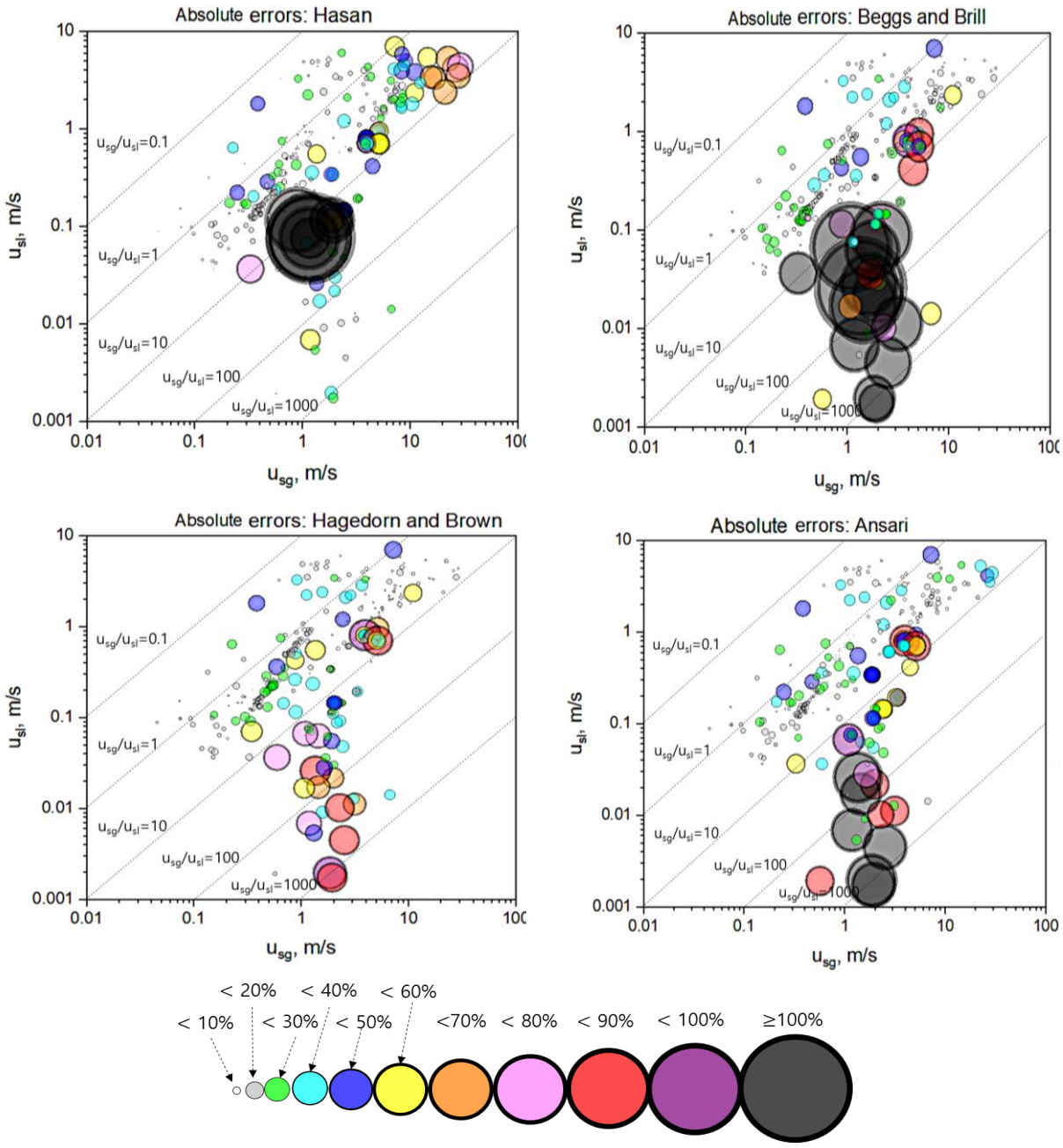

Although the sizes and colors of circles for each tested model vary widely, the circles located between 0.1 $<u_{SG}/u_{SL}<$ 1 and close to u_{SG}/u_{SL} = 1 are smaller, while circles located above u_{SG}/u_{SL} = 1 are larger across all the models in general. More white, gray, green and blue circles are observed where 0.1 $<u_{SG}/u_{SL}<$1, while more yellow, red and dark circles represent errors less than 60 and 90, and greater than 100 % are observed where $u_{SG}/u_{SL}>$ 1. The circles in Hagedorn

and Brown and Gray are smaller in overall. Those two models show relatively better performance, where all models except Lee and Waltrich have large dark circles, high pressure drop errors.

The model of Gray (1974) was developed with wet gas well data and is hence expected to give lower pressure drop errors on data with high gas rates such as data from Reinike et al. (1987) and Ekofisk field (Asheim et al., 1986). As described in the literature review, Hagedorn and Brown (1964) employed the dimensionless parameters of Duns and Ros (1963) and created liquid hold-up correlation plot to match their measured pressure with liquid hold-up. As presented in Figure 6, the liquid holdup plot was built with tubing sizes of 1 to 2 in ID and the pipe diameter number has an inverse relationship with liquid hold-up. Therefore, with larger diameter pipes, liquid hold-up will be smaller and void fraction will be larger. Further, unlike other tested flow models that define slug flow rather than churn flow, Hagedorn and Brown (1964) did not utilize flow regime. These may cause relatively lower errors where u_{SG}/u_{SL}> 10 and churn flow is expected. When the errors of Beggs and Brill (1973) are plotted on their own horizontal flow pattern map, relatively higher errors in segregated flow and middle of intermittent flow regime are observed (Figure 55). In Beggs and Brill (1973), stratified, wavy and annular flows are segregated flow and plug and slug flow are intermittent. Most of the data in segregated flow regime are the data from Reinike, which is likely to be annular flow. Therefore, it shows that when liquid content in horizontal pipe in stratified flow is converted to liquid hold-up in vertical flow to estimate pressure gradient, high errors exist in the model. Further, slug and plug flow predictions that would not occur in large diameter pipe cause high errors.

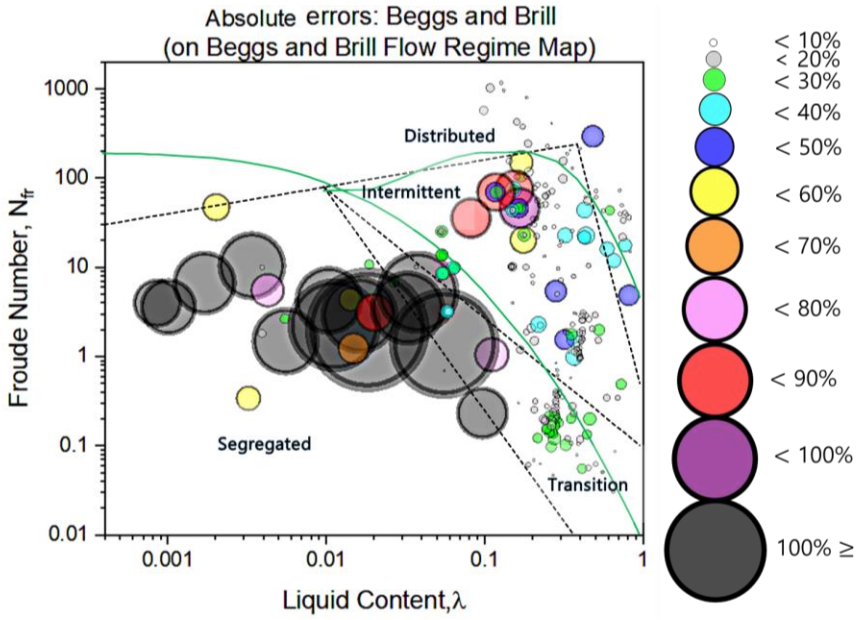

Figure 56. BHP errors of Beggs and Brill (1973) displayed on their flow pattern map

Ansari et al. (1990) considered churn flow as a part of slug flow rather than develop a churn flow model due to its complexity. For void fraction estimation of bubbly and slug flow, Ansari employed bubble rise velocity and Taylor bubble velocity as drift velocity to estimate gas velocity as presented in Table 2. Therefore, most of the field data are predicted as slug flow according to Ansari's flow regime map (Figure 12) and may cause high pressure drop errors. Similar to all other tested correlations, the results of Duns and Ros (1963) lower BHP errors for the data with u_{sg}/u_{sl} less than 1. The errors get higher where u_{sg}/u_{sl} is between 10 and 1,000, especially 100 and 1,000. The higher errors in a certain range of u_{sg}/u_{sl} or liquid and gas superficial velocities can be explained with Duns and Ros (1963) flow regime map in Figure 57. Liquid and gas superficial velocities are converted to liquid and gas dimensionless numbers. As shown, absolute pressure drops are lower in Region I, where bubble flow and plug flow exist. In Region II, where slug and froth flow exist, the errors are greater than those in Region I. The errors are the greatest in slug flow and the area beyond flow regime map. The high level of errors implies that the Duns and Ros

(1963) correlation is not suitable for flow at low liquid velocity with high gas velocity, which results in high u_{sg}/u_{sl}.

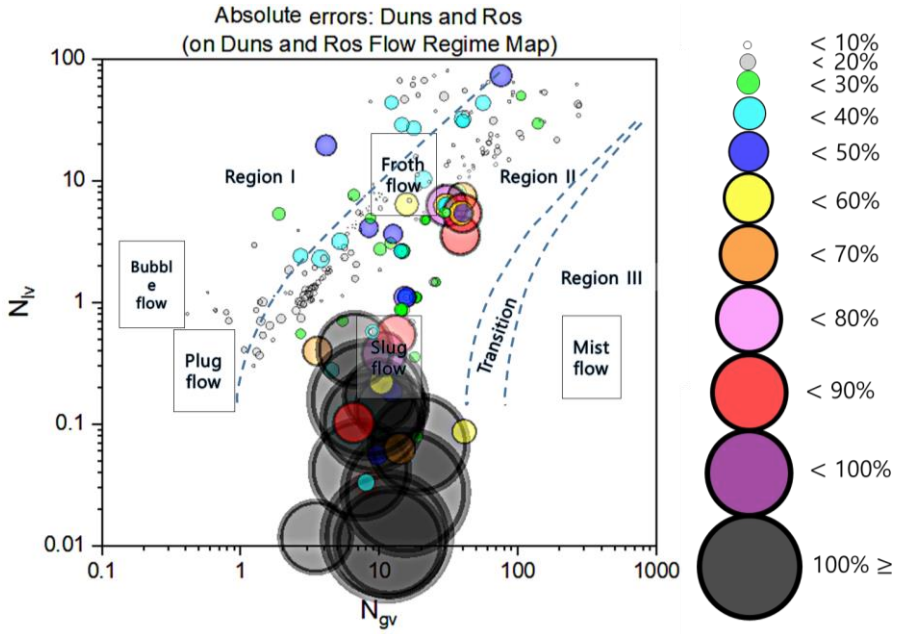

Figure 57. Abs. pressure drop errors on flow regime map of Duns and Ros (1963)

For Hasan, particularly larger errors are observed in the middle of the plot, where Fancher and Brown data are located. The results of Bhagwat also show higher errors for high u_{sg}/u_{sl} data. To compare the performance of drift-flux models with flow regime prediction along depth change, measured pressure from Fancher and Brown (1963) is plotted with the models' pressure predictions in Figure 55. Drift coefficient of the three models are also plotted. The symbols and dash lines in red, gold, and blue represent the C_o and pressure predictions by Lee and Waltrich, Hasan et al (2010), and Bhagwat and Ghajar (2014), respectively.

As observed through comparisons of pressure estimations by the three drift-flux models on laboratory data, the difference of the models is distinct here. In the experimental data, the pressure estimation by Bhagwat is higher than the estimation by Hasan and the estimation by Lee and Waltrich is between them (Figure 58).

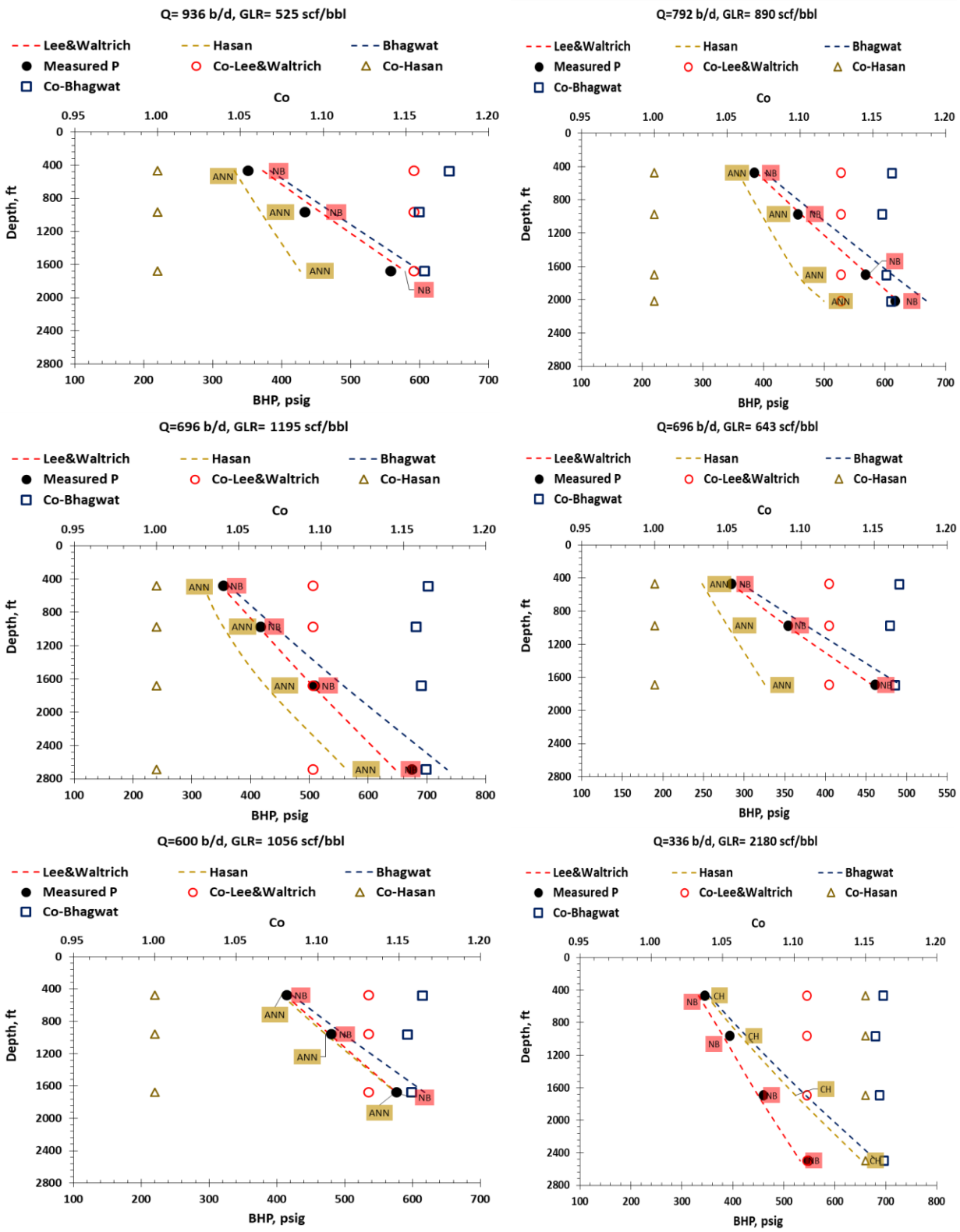

Figure 58. Pressure estimation and C_o of drift-flux models for Fancher and Brown (1963)

Figure continued.

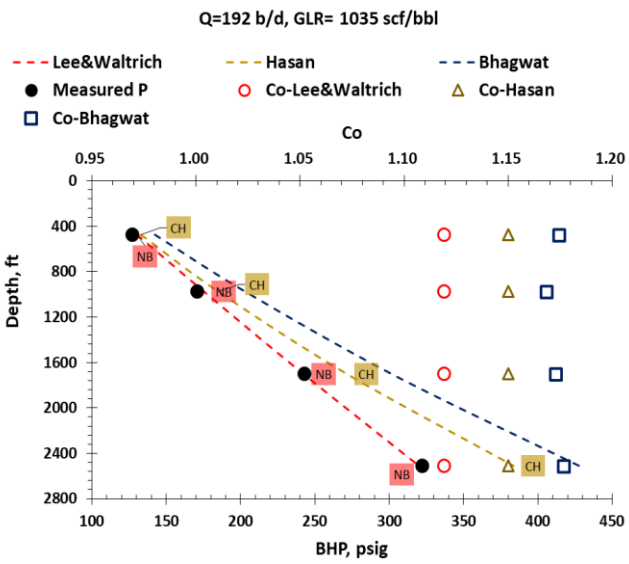
Q=192 b/d, GLR= 1035 scf/bbl
Lee&Waltrich
Hasan
Bhagwat
Measured P
Co-Lee&Waltrich
Co-Hasan
Co-Bhagwat
Co
0.95 1.00 1.05 1.10 1.15 1.20
Depth, ft
0 400 800 1200 1600 2000 2400 2800
100 150 200 250 300 350 400 450
BHP, psig
CH
NB

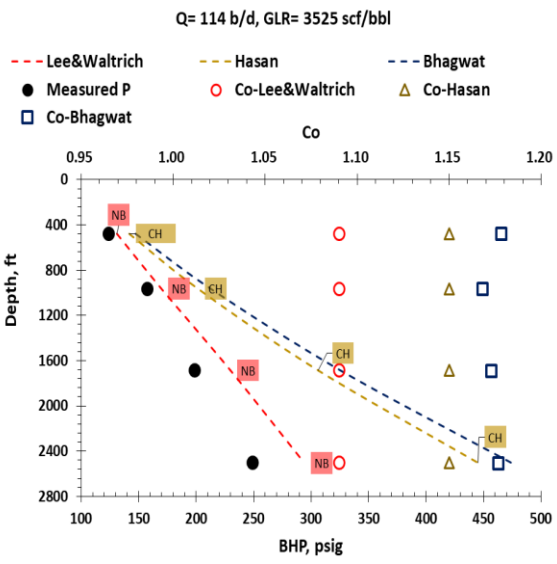
Q= 114 b/d, GLR= 3525 scf/bbl
Lee&Waltrich
Hasan
Bhagwat
Measured P
Co-Lee&Waltrich
Co-Hasan
Co-Bhagwat
Co
0.95 1.00 1.05 1.10 1.15 1.20
Depth, ft
0 400 800 1200 1600 2000 2400 2800
100 150 200 250 300 350 400 450 500
BHP, psig
CH
NB

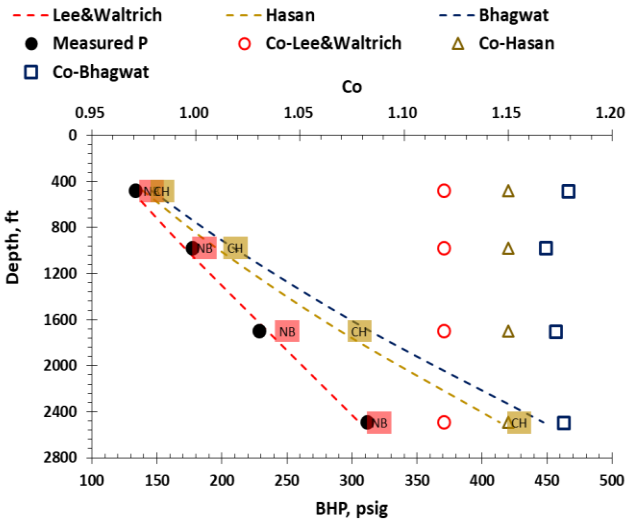
Q=144 b/d, GLR= 1541 scf/bbl
Lee&Waltrich
Hasan
Bhagwat
Measured P
Co-Lee&Waltrich
Co-Hasan
Co-Bhagwat
Co
0.95 1.00 1.05 1.10 1.15 1.20
Depth, ft
0 400 800 1200 1600 2000 2400 2800
100 150 200 250 300 350 400 450 500
BHP, psig
CH
NB

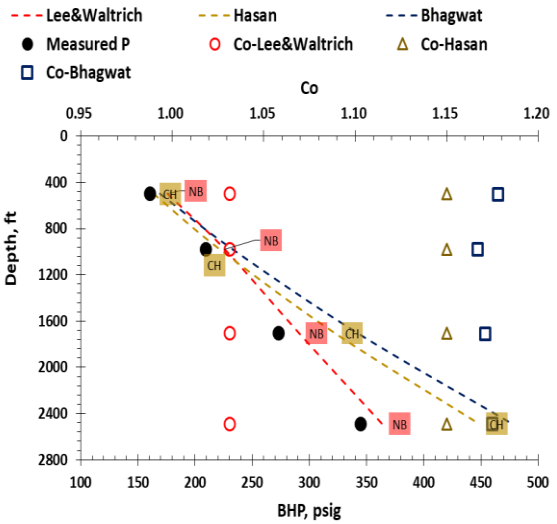
Q=144 b/d, GLR= 7283 scf/bbl
Lee&Waltrich
Hasan
Bhagwat
Measured P
Co-Lee&Waltrich
Co-Hasan
Co-Bhagwat
Co
0.95 1.00 1.05 1.10 1.15 1.20
Depth, ft
0 400 800 1200 1600 2000 2400 2800
100 150 200 250 300 350 400 450 500
BHP, psig
CH
NB

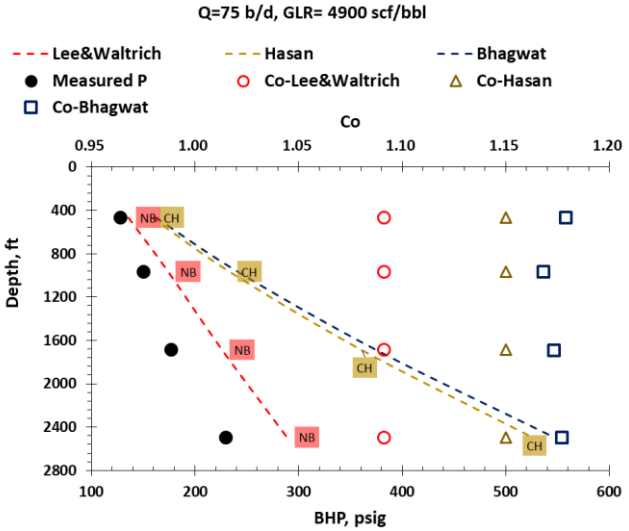
Q=75 b/d, GLR= 4900 scf/bbl
Lee&Waltrich
Hasan
Bhagwat
Measured P
Co-Lee&Waltrich
Co-Hasan
Co-Bhagwat
Co
0.95 1.00 1.05 1.10 1.15 1.20
Depth, ft
0 400 800 1200 1600 2000 2400 2800
100 200 300 400 500 600
BHP, psig
CH
NB

The tested models, except those of Lee and Waltrich, Hagedorn and Brown (1964), and Bhagwat and Ghajar (2014), apply flow regime-specific parameters and those parameters of a flow model remain constant in the same flow regime. This approach would cause abrupt change in estimation of flow behavior, especially for data located near the flow regime boundaries. This behavior is presented in the previous chapter by pressure predicted by Hasan et al. (2010) using experimental data (Figures 38 - 43). Inappropriate flow regime prediction can also result high pressure estimation errors as described with the results of Duns and Ros and Beggs and Brill in Figures 56 and 57. Hadedorn and Brown (1964) do not utilize the flow regime map and have relatively fewer errors where churn flow is anticipated as shown in Figure 55. Although Bhagwat does not specify the flow regime, density and Reynolds number, dependent C_o cause overestimated C_o for high flow rates, as presented in Figures 38 - 43.

Compared to the results of other models from Figure 55 - 58, Lee and Waltrich has the least variance in error distribution along all ranges of u_{sg}/u_{sl}, Q, GLR, and tested data sets as shown in Figure 56. It shows substantially lower errors at $10 < u_{sg}/u_{sl}$ where other flow models have high errors. The low errors can be a result of the uniqueness of the model compared to other flow models. Lee and Waltrich has non-fixed bubbly/non-bubbly flow boundary and gradual reduction of drift flux coefficient with higher gas velocity, which represents the actual physical behavior of fluid flow. Therefore, it can be applied to different conditions of pressure, rates, fluid properties, and pipe geometry.

4.5. Summary of Results

The average of absolute errors of bottomhole pressure and average standard deviation of bottomhole pressure errors against field data are plotted in Figure 59. Bars and lines represent the errors and standard deviations, respectively. Although, in Figure 59 no model has constantly higher

or lower errors across all tested data set, Lee and Waltrich results look more reliable than any other models for all the data sets. The highest error and standard deviation of Lee and Waltrich area about 25 % and most of them are less than 15 %. All other models show errors and standard deviations higher than the proposed model, going above 50 % for some of the data sets. The errors of all the models except Lee and Waltrich are around 20 % for all tested data, as shown in the last plot in Figure 59. This averaging of errors may lead to the wrong conclusion that all the models are quite reliable in predicting pressure for all the tested field data. This is a biased result due to the high amount of data of Equinor F-01C and Equinor F-15D. Standard deviations of all the tested models other than Lee and Waltrich range between 30 % and 50 % in the last plot. This clearly indicates that 20% errors of other models are skewed value and Lee and Waltrich is the most reliable pressure estimation model for all the tested data.

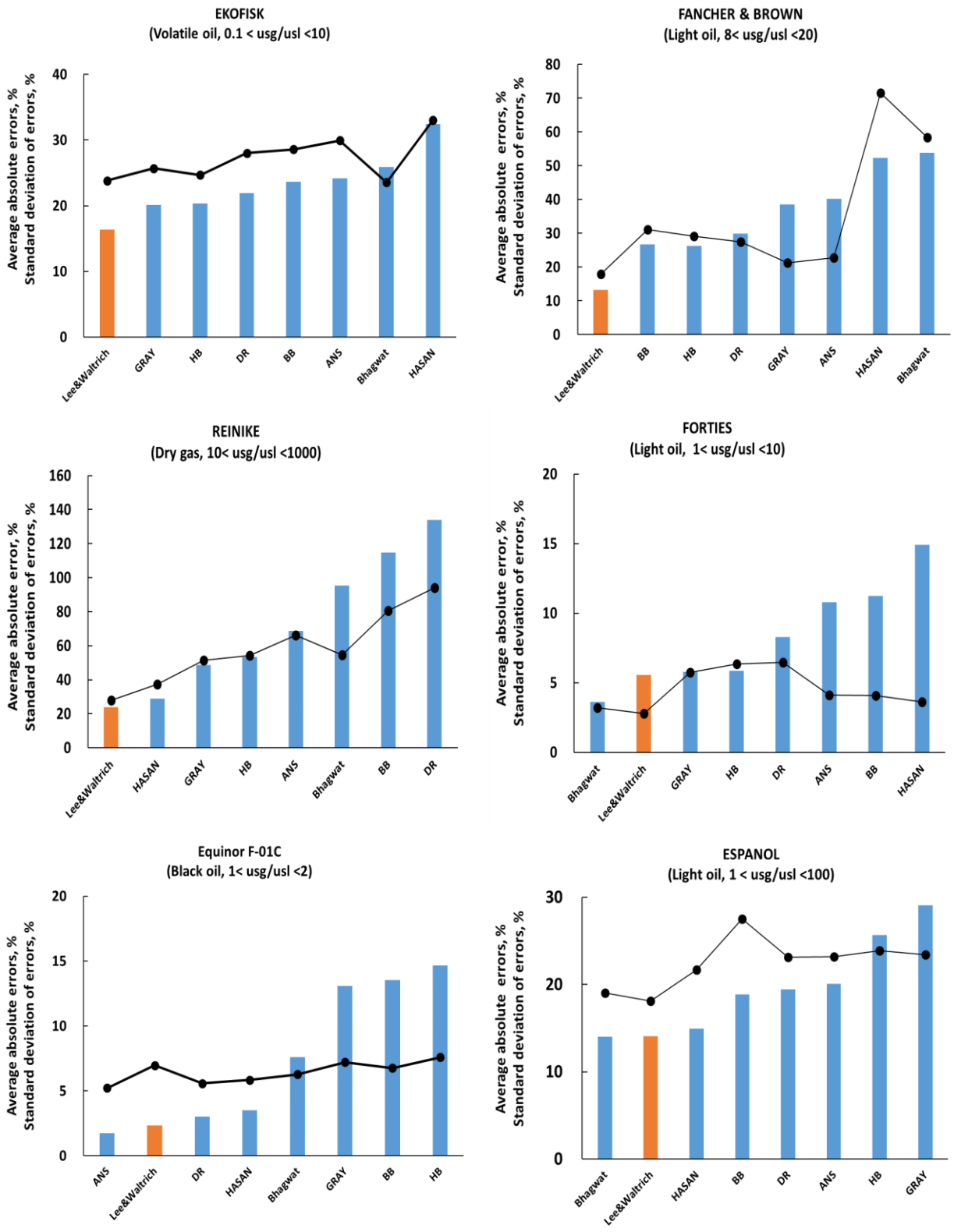

Figure 59. Average abs. errors and average std. dev. of bottomhole pressure errors

Figure continued.

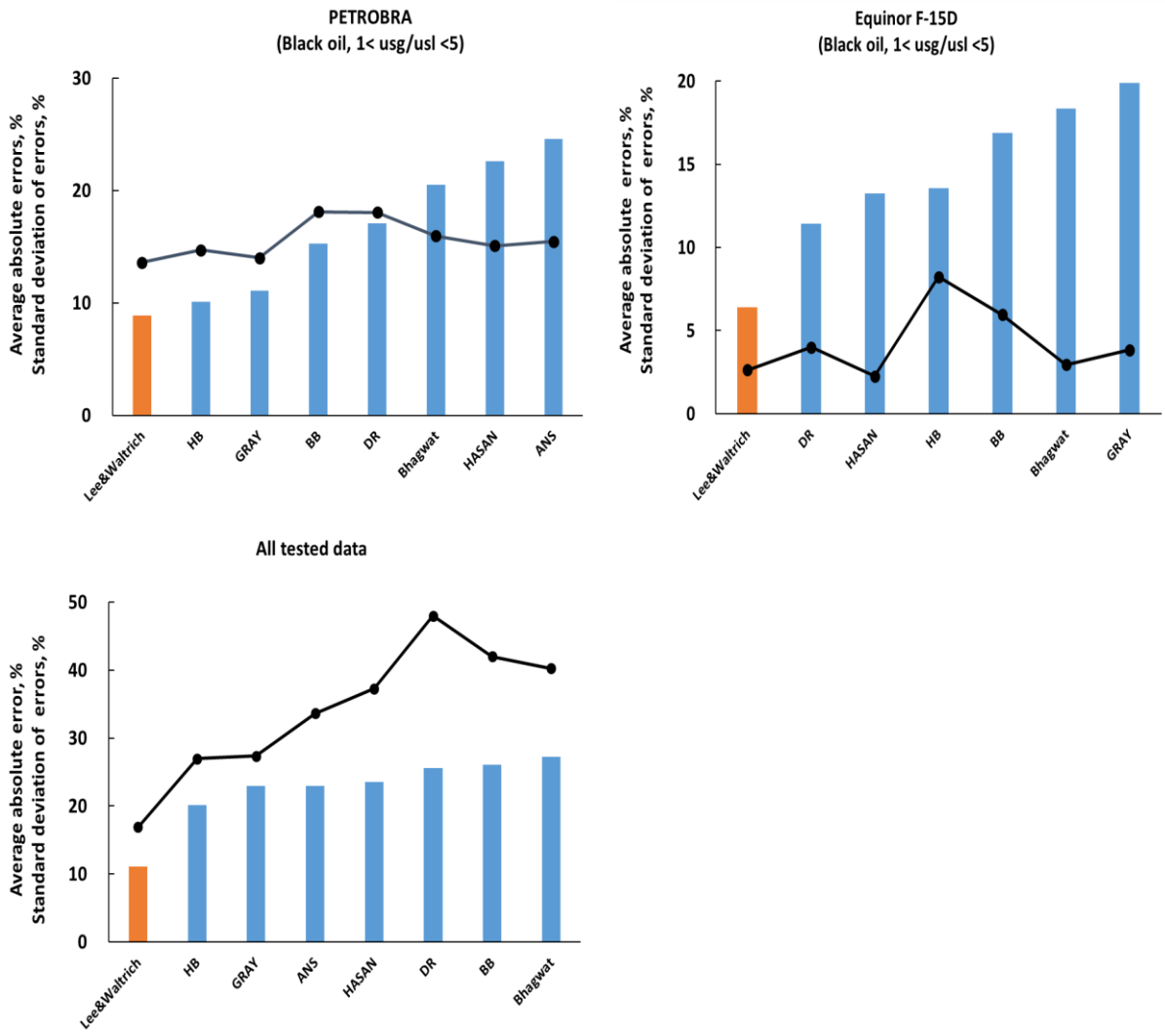

The results presented in Figure 59 are rearranged by model and field in Figures 60 and 61, from which the performance of each model by field is more clearly identified.

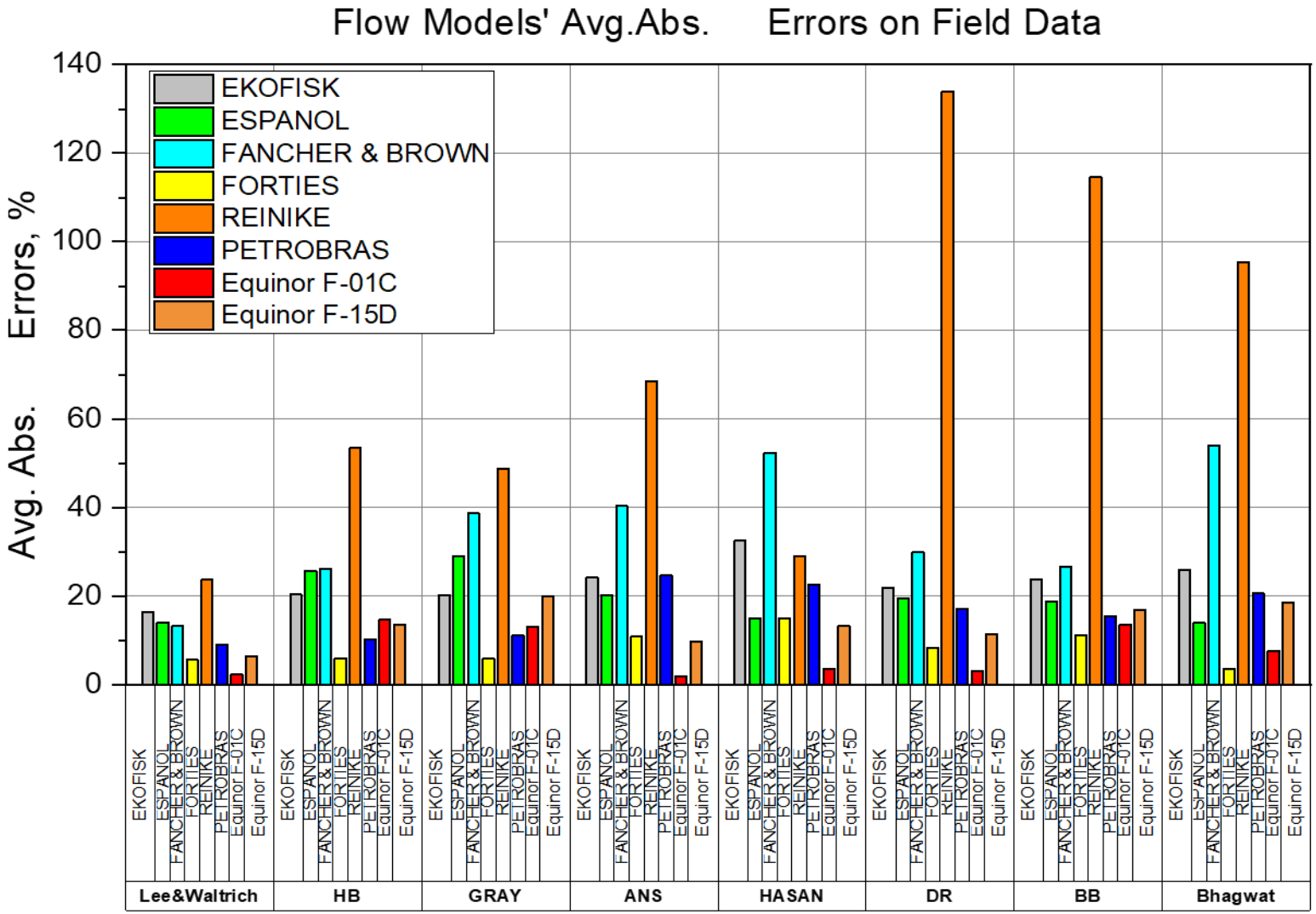

Figure 60. Flow model's average absolute bottomhole pressure errors on field data

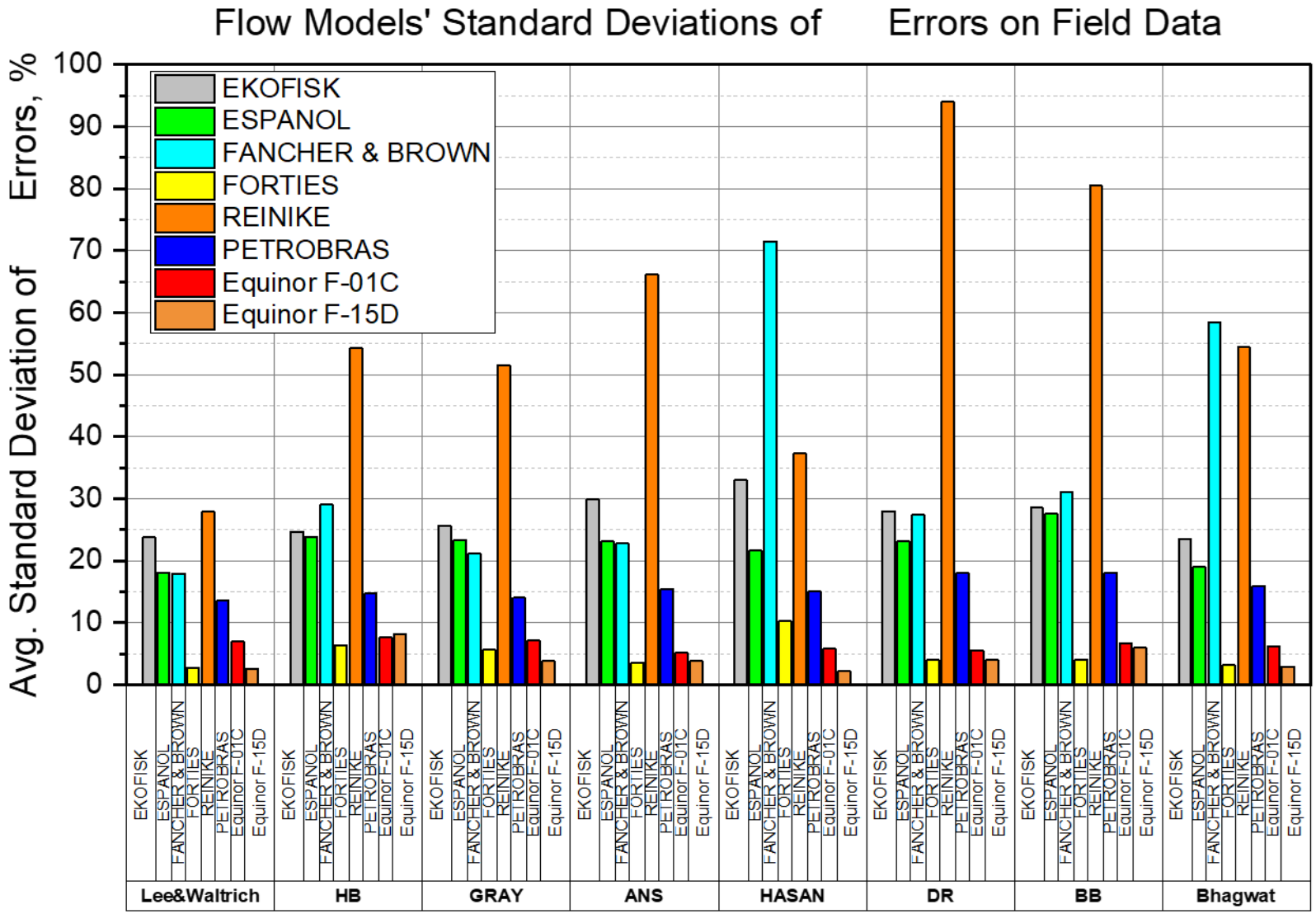

Figure 61. Flow model's average standard deviation of bottomhole pressure errors on field data

5. MODEL APPLICATION

An average of absolute bottomhole pressure errors was as high as 130% for the tested field data in Figure 60. Since bottomhole pressure is one of the main factors estimate flow rate (Figure 1), high error in BHP estimation would cause inadequate flow rate estimation. To check the effect of BHP estimation on flow rate for WCD calculation, a WCD scenario was built based on Zulqarnain (2014). Zulqarnain (2014) presented a method to select a representative well configuration and reservoir based on a statistical analysis of existing wells in the Gulf of Mexico. Figure 62 depicts the most probable base-case for wellbore configuration in Gulf of Mexico, U.S., according to Zulqarnain (2014). The well is located at 3,000 ft below mean sea level and wellbore configuration is described in Table 6. Since a WCD scenario assumes no restrictions in the wellbore, a drill string (or production tubing) was removed from Figure 62, accommodating the BOEM's recommendation for WCD estimation. Also, for simplicity, 7.725 in ID casing is assumed for wellbore instead of three different casing sizes. Zulqarnain (2014) modeled the variations in the reservoir properties by a series of probability distribution functions for a wide range of reservoir parameters (such as porosity, permeability, depth), rather than using deterministic properties. Monte Carlo simulations were performed to find the most probable values and the results are presented in Table 7.

Table 6. Wellbore configuration (Zulqarnain, 2014)

Casing	Depth (ft)	Length (ft)	Pipe roughness (in)	Inner diameter (in)
Upper casing	8800	5,800	0.001	12.125
Middle casing	11450	2,650	0.001	9.76
Lower casing	16726	5,276	0.001	7.725

T

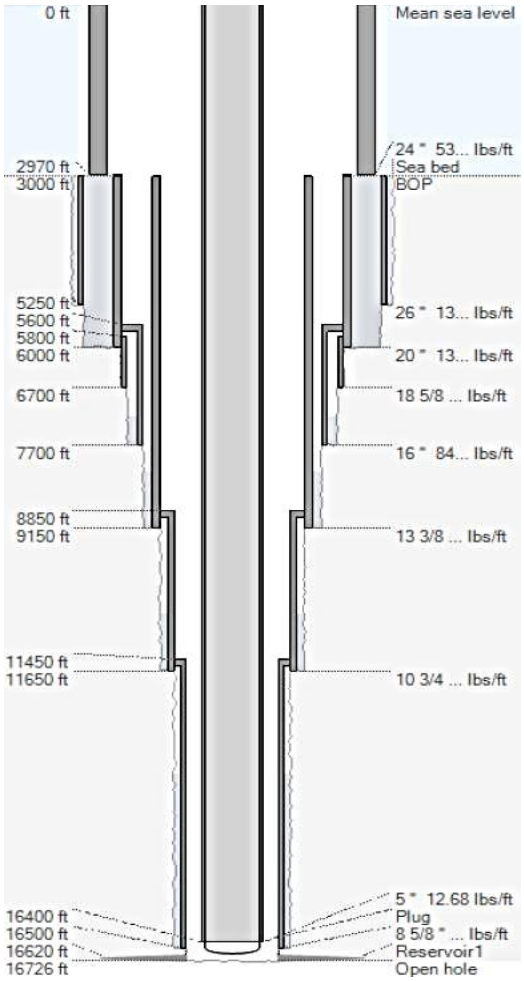

Figure 62. Well configuration adopted for WCD estimation (Zulqarnain, 2014).

Table 7. Reservoir and fluid properties (Zulqarnain, 2014)

Reservoir Properties	**Value**	**Unit**
Reservoir pressure	11,305	psia
Wellhead pressure	1,395	psia
Reservoir Temperature	210	°F
Thickness	106	ft
Permeability	246	md
Gas-oil-ratio	3400	scf/stb
Bubble point pressure	6,306	psi
Oil gravity	42	°API
Oil formation volume factor	1.39	res. bbl/stb
Oil viscosity	0.8	cP
Productivity Index (PI)	19.05	stb/day/psi

Figure 63 shows pressure profile for fluid in tubing. Estimated BHP by Bhagwat and Hasan are the lowest (4012 psig) and the highest (7104 psig) among the tested models, respectively, while the average is about 6110 psig. According to SPE Technical Report (2015), Duns and Ross Modified (1963) or Beggs and Brill (1973) should be used to obtain an upper limit on pressure drop in oil wells. Fancher and Brown (1963) was recommended to obtain a lower limit on pressure drop since it considers no-slippage between gas and liquid phases. Among the tested existing models, Beggs and Brill model estimates the upper limit on BHP and confirms the SPE recommendation. It is important to point out that PIPESIM showed warning messages for Ansari flow model, stating that this model exceeded the flow limit for this correlation. Such warnings are an additional indication that some models were not developed for the extreme conditions required for WCD calculations.

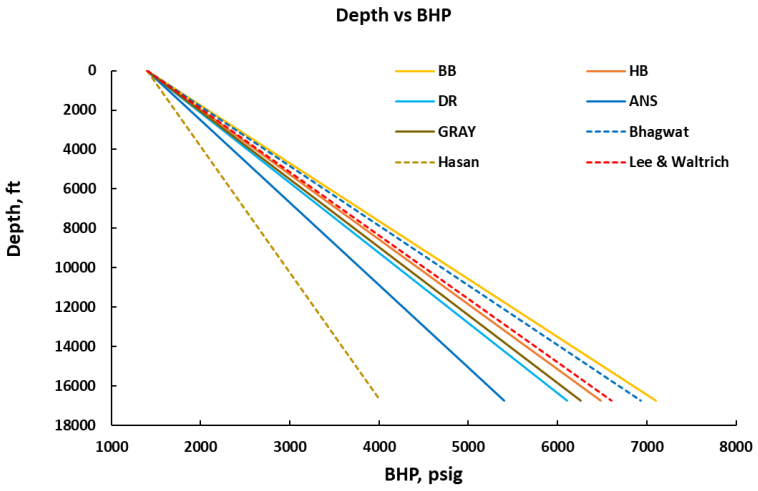

Figure 63. Pressure profile of tested models

TPR (Tubing performance relation) curves for tested flow models are plotted with IPR (Inflow performance relation) in Figure 64. The point where IPR and TPR intersect is an operating condition. Hasan and Beggs and Brill show the highest and the lowest flow rate at given wellhead pressure, respectively. As explained, Ansari shows unstable TPR curve between 20 and 40 Mstbd.

Hasan shows almost constant FBHP with increasing flow rates. BHP estimation by Lee and Waltrich is located between BHP estimated by Bhagwat and Hasan. This is consistent with the results of model validation with laboratory experiments in Figure 43–49. The result of Lee and Waltrich is somewhat close to the oil estimation by Hagedorn and Brown at the given reservoir properties. However, the estimated rates of the two correlations would be different at different IPR. The result of Hasan shows almost constant flowing BHP and the highest rate due to annular flow prediction for the most of oil rates and the corresponding C_O and u_d.

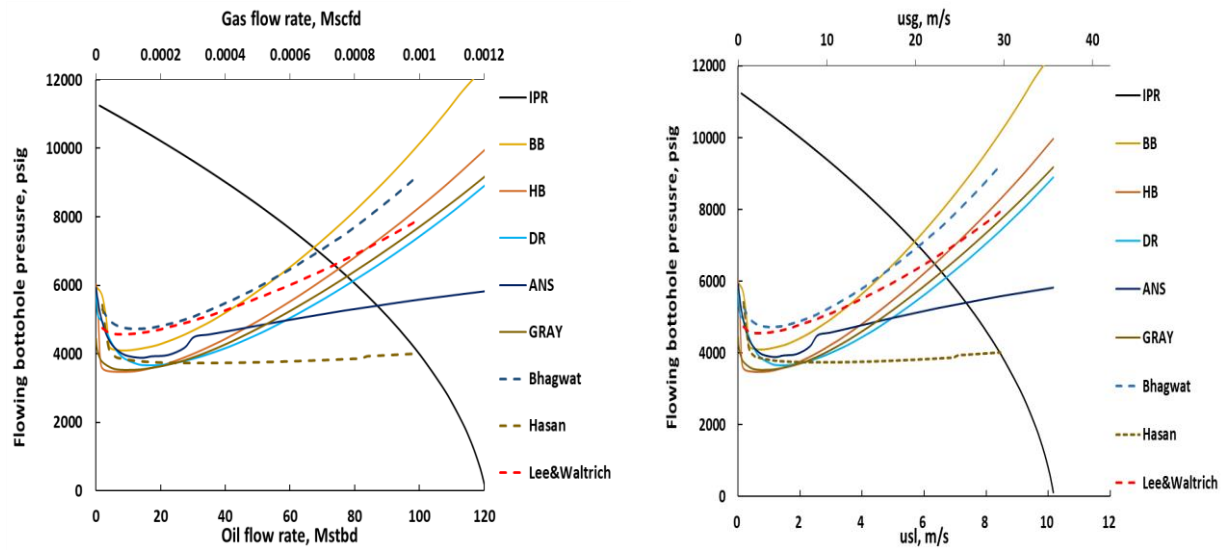

Figure 64. IPR & TPR with (left) oil rate and (right) with liquid superficial velocity

The estimated rate difference among the tested models is shown Table 9. At an average of 62,820 Stbd oil production, the lowest and highest has 32,600 Stbd difference. The big difference in rate and pressure indicates the importance of flow model selection. The impact of flow model selection would be less significant if pressure in wellbore is higher than bubble point pressure, which makes single phase flow. In other words, higher gas oil ratio, higher API, low pressure, and high bubble point pressure that creates more two-phase flow would cause a higher difference in rate estimation.

Table 8. Estimated rate and pressure

Flow model	Qo, Stbd	BHP, psig
BB	67,293	7,104
HB	74,995	6,482
DR	79,343	6,108
ANS	87,008	5,399
GRAY	77,581	6,262
Bhagwat	68,300	6,932
Hasan	99,895	4,012
Lee & Waltrich	74,100	6,601
Average	62,820	6,112

6. CONCLUSION AND RECOMMENDATIONS

The proposed model was evaluated for a wide range of operating conditions that include variations in pipe diameter, flow rate, fluid properties, pipe inclination, and operation pressure from laboratory and field data. The model was also compared with other drift-flux, mechanistic, and empirical two-phase flow models. The conclusions of this study are as follows:

- Models tested in this study demonstrated different performance on pressure estimations, which is related to the flow regime map and model development conditions of each model.
- It has been proven again that for low gas/liquid rates ($u_{sg}/u_{sl}<1$), all tested models are applicable for pressure estimation. However, at higher gas/liquid rates, where non-bubbly flow or churn flow is anticipated, pressure estimated by each model varies significantly.
- The model proposed in this study showed the lowest pressure estimation errors and standard deviations for the tested laboratory and field data, overall. The average absolute error and standard deviation for all the tested field data is about 10% and 18%, respectively. It also follows the pressure trends of measured data well, as proved with the results using laboratory data and Fancher and Brown (1963).
- Besides the proposed model, Hagedorn and Brown (1963) and Gray (1974) showed the second most reliable pressure estimations among all the tested models. The major reason for this would be that Hagedorn and Brown (1963) use no flow regime and hence perform better on field data, where churn flow is anticipated. Relatively low errors of Gray (1974) against Reinicke et al. (1987) led Gray (1974) to have low average errors, overall. However, average absolute errors and standard deviations for all tested field data are about 25%, and the average absolute errors and standard deviations for individual field data are as high as 55% for both models.

- Drift-flux models using different C_o estimation approach are compared in this study as well. Hasan et al (2010) assigns one value of C_o for each flow regime. Bhagwat and Ghajar (2014) is flow-regime independent for its void fraction model and C_o is dependent of gas/liquid density ratio and Reynolds number. Abrupt pressure changes are demonstrated in the results of Hasan et al., (2010) due to $C_o$conversion from 1.15 to 1.0 as flow regime prediction changes from slug/churn to annular flow. In general, over-estimated pressures are observed in the results of Bhagwat and Ghajar (2014), because their estimates $of\ C_o$is close to 1.2 for high gas rate data, although C_o= 1.2 is generally considered appropriate for bubbly flow, which has low void fraction. Meanwhile, the proposed model estimates pressure somewhere between Hasan et al. (2010) and Bhagwat and Ghajar (2014), which is attributable to the uniqueness of the proposed model related to the minimum pressure gradient method deployed. Bubbly/non-bubbly flow transition is defined using the minimum pressure estimated by a bubbly flow correlation in the proposed model. This makes flow transition vary by flow rates, pipe diameter, fluid density, and pressure, unlike other flow models using flow regime map, which has fixed flow regime boundaries. C_o calculated by iteration for each rate gradually changes along with flow rates within and across flow regime transitions. These results show no sudden pressure change or erroneous C_o estimations, as seen from the results of Hasan et al. (2010) and Bhagwat et al. (2014), specifically where churn/annular flow is anticipated.
- Friction factor correlations for smooth and rough pipes were compared with Almabrok's (2013) lab data and all of them had negligible difference in pressure gradient estimation at u_{SG} less than 20 m/s in 4 in diameter pipe. Between the two approximations of Colebrook correlation, Fang et al.'s (2010) estimated the pressure to be closer to Colebrook at higher gas velocity than Zigrang and Sylvester (1982).

- Bubbly – dispersed bubbly flow transition correlations were compared with the lab data. None of the tested correlations predicted dispersed bubbly flow. Since tested dispersed bubbly flow transition correlations were built and validated with pipe diameter less than 2 in, more study with large diameter pipes is needed. For dispersed bubbly flow, using drift-flux parameters for bubbly flow should give better pressure estimation than using the parameters for ideal-annular flow.
- The proposed model underestimated the pressure gradient when it was tested in Almabrok's (2013) flow experiment in 4 in diameter pipes at u_{SL} = 1 m/s, as u_{SG} gets larger than 10 m/s. When the proposed model applied drift-flux parameters for bubbly flow by assuming the tested condition as dispersed-bubbly flow regime, improved pressure estimation was observed.
- The flow rate and bottomhole flowing pressure was estimated for a hypothetical WCD scenario. At the given reservoir condition and properties, the difference between the lowest and the highest oil rates is 32,600 stbd, while the average is 62,820 stbd. In addition, BHP difference was about 3,000 psig while the average is 6,100 psig. As expected, proposed model estimated the flow rates to be higher than Bhagwat and Ghajar (2014) and lower than Hasan et al. (2010). The result indicates the importance of selecting a model for flow in pipes.

Since the proposed model had less reliability on pressure estimation at u_{SL} = 1 m/s and u_{SG} > 10 m/s in 4 in lab data where might be dispersed bubbly flow regime, the following studies are recommended to develop more robust models:

- Laboratory study on dispersed-bubbly flow in large diameter pipes
- Determine critical pipe diameter at which flow regime transits from bubbly to dispersed bubbly flow
- Drift-flux parameter calculation for dispersed-bubbly flow

LIST OF REFERENCES

Ali, S.F., 2009. Two-phase flow in a large diameter vertical riser.

Alves, I.M., Caetano, E.F., Minami, K. and Shoham, O., 1991. Modeling annular flow behavior for gas wells. SPE production engineering, 6(04), pp.435-440.

Ansari, A.M., Sylvester, N.D., Shoham, O. and Brill, J.P., 1990, January. A comprehensive mechanistic model for upward two-phase flow in wellbores. In SPE annual technical conference and exhibition. Society of Petroleum Engineers.

Ansari, M.R. and Azadi, R., 2016. Effect of diameter and axial location on upward gas–liquid two-phase flow patterns in intermediate-scale vertical tubes. Annals of Nuclear Energy, 94, pp.530-540.

Asheim, H., 1986. MONA, an accurate two-phase well flow model based on phase slippage. SPE Production Engineering, 1(03), pp.221-230.

Aziz, K. and Govier, G.W., 1972. Pressure drop in wells producing oil and gas. Journal of Canadian Petroleum Technology, 11(03).

Barnea, D. and Brauner, N., 1985. Holdup of the liquid slug in two phase intermittent flow. International Journal of Multiphase Flow, 11(1), pp.43-49.

Baxendell, P.B. and Thomas, R., 1961. The calculation of pressure gradients in high-rate flowing wells. Journal of Petroleum Technology, 13(10), pp.1-023.

Beggs, D.H. and Brill, J.P., 1973. A study of two-phase flow in inclined pipes. Journal of Petroleum technology, 25(05), pp.607-617.

Beggs, H.D. and Robinson, J., 1975. Estimating the viscosity of crude oil systems. Journal of Petroleum technology, 27(09), pp.1-140.

Bendiksen, K.H., 1984. An experimental investigation of the motion of long bubbles in inclined tubes. International journal of multiphase flow, 10(4), pp.467-483.

Bhagwat, S.M. and Ghajar, A.J., 2014. A flow pattern independent drift flux model based void fraction correlation for a wide range of gas–liquid two phase flow. International Journal of Multiphase Flow, 59, pp.186-205.

Brill, J.P. and Beggs, H.D., 1991. Two-phase flow in pipes.

Blasius, P. R. H. 1913. Das Aehnlichkeitsgesetz bei Reibungsvorgangen in Flüssigkeiten. Forschungsheft 131, 1-41

Camacho, Z., Brown, J.R. and Kitto, G.B., 1970. Purification and properties of trypsin-like proteases from the starfish Dermasterias imbricata. Journal of Biological Chemistry, 245(15), pp.3964-3972.

Choi, J., Pereyra, E., Sarica, C., Park, C. and Kang, J.M., 2012. An efficient drift-flux closure relationship to estimate liquid holdups of gas-liquid two-phase flow in pipes. Energies, 5(12), pp.5294-5306.

Chokshi, R.N., Schmidt, Z. and Doty, D.R., 1996, January. Experimental study and the development of a mechanistic model for two-phase flow through vertical tubing. In SPE western regional meeting. Society of Petroleum Engineers.

Chierici, G.L., Ciucci, G.M. and Sclocchi, G., 1974, Two-phase vertical flow in oil wells-prediction of pressure drop. Journal of Petroleum Technology, 26(08), pp.927-938.

Chen, N.H., 1979, An explicit equation for friction factor in pipe. Industrial Engineering, Chem. Fundam. 18 (3), 296-297

Colebrook, C. F., Blench, T., Chatley, H., Essex, E. H., Finniecome, J. R., Lacey, G., and Macdonald, G. G., 1939, Correspondence. turbulent flow in pipes, with particular reference to the transition region between the smooth and rough pipe laws (includes plates). Journal of the Institution of Civil engineers, 12(8), 393-422.

Duns Jr, H. and Ros, N.C.J., 1963, January. Vertical flow of gas and liquid mixtures in wells. In 6th world petroleum congress. World Petroleum Congress.

Dukler, A.E., Wicks III, M. and Cleveland, R.G., 1964. Frictional pressure drop in two-phase flow: B. An approach through similarity analysis. AIChE Journal, 10(1), pp.44-51.

Eaton, B.A., Andrews, D.E. and Knowles, C.R., 1967. Silberberg, H., and Brown, KE:" The Prediction of Flow Patterns, Liquid Holdup, and Pressure Losses Occurring During Continuous Two-Phase Flow in Horizontal Pipelines,". J. Pet. Tech, pp.815-828.

Espanol, J.H., Holmes, C.S. and Brown, K.E., 1969, January. A comparison of existing multiphase flow methods for the calculation of pressure drop in vertical wells. In Fall Meeting of the Society of Petroleum Engineers of AIME. Society of Petroleum Engineers.

Fang, X., Xu, Y., & Zhou, Z., 2011. New correlations of single-phase friction factor for turbulent pipe flow and evaluation of existing single-phase friction factor correlations. Nuclear Engineering and Design, 241(3), 897-902.

Fancher Jr, G.H. and Brown, K.E., 1962, January. Prediction of pressure gradients for multiphase flow in tubing. In Fall Meeting of the Society of Petroleum Engineers of AIME. Society of Petroleum Engineers.

Fevang, O., Fossmark, M.G., Nordaas Kulkarni, K., Lauritsen, H.T. and Skjaeveland, S.M., 2012, January. Vertical Lift Models Substantiated by Statfjord Field Data. In SPE Europec/EAGE Annual Conference. Society of Petroleum Engineers.

Flanigan, O., 1958. Effect of uphill flow on pressure drop in design of two-phase gathering systems. Oil and gas journal, 56(10), p.132.

Gray, H.E., 1974. Vertical Flow Correlation in Gas Wells, User Manual for API 14B, Subsurface Controlled Safety Valve Sizing Computer Program, App. B. EPR Report.

Gomez, L.E., Shoham, O., Schmidt, Z., Chokshi, R.N. and Northug, T., 2000. Unified mechanistic model for steady-state two-phase flow: horizontal to vertical upward flow. SPE journal, 5(03), pp.339-350.

Govier, G.W. and Aziz, K., 1972. The flow of complex mixtures in pipes (Vol. 469). New York: Van Nostrand Reinhold Company.

Govier, G.W. and Fogarasi, M., 1975. Pressure drop in wells producing gas and condensate. Journal of Canadian Petroleum Technology, 14(04).

Hagedorn, A.R. and Brown, K.E., 1964. The effect of liquid viscosity in vertical two-phase flow. J. Pet. Technol, 16, p.203.

Harmathy, T.Z., 1960. Velocity of large drops and bubbles in media of infinite or restricted extent. AIChE Journal, 6(2), pp.281-288.

Hasan, A.R. and Kabir, C.S., 1988. A study of multiphase flow behavior in vertical wells. SPE Production Engineering, 3(02), pp.263-272.

Hasan, A.R., Kabir, C.S. and Sayarpour, M., 2010. Simplified two-phase flow modeling in wellbores. Journal of Petroleum Science and Engineering, 72(1-2), pp.42-49.

Hewakandamby, B.N., Kanu, A.U., Azzopardi, B.J. and Kouba, G., 2014, August. Parametric study of churn flow in large diameter pipes. In Fluids Engineering Division Summer Meeting (Vol. 46247, p. V01DT38A004). American Society of Mechanical Engineers.

Hibiki, T. and Ishii, M., 2003. One-dimensional drift–flux model for two-phase flow in a large diameter pipe. International Journal of Heat and Mass Transfer, 46(10), pp.1773-1790.

Holmes, J.A., 1977. Description of the drift flux model in the LOCA-Code RELAP-UK, heat and fluid flow in water reactor safety.

Ishii, M., 1977. One-dimensional drift-flux model and constitutive equations for relative motion between phases in various two-phase flow regimes (No. ANL-77-47). Argonne National Lab., Ill.(USA).

Jayanti, S. and Brauner, N., 1994. Churn flow. Multiphase Science and Technology, 8(1-4).

Kataoka, Y., Suzuki, H. and Murase, M., 1987. Drift-flux parameters for upward gas flow in stagnant liquid. Journal of Nuclear Science and Technology, 24(7), pp.580-586.

McNutt, M.K., Camilli, R., Crone, T.J., Guthrie, G.D., Hsieh, P.A., Ryerson, T.B., Savas, O. and Shaffer, F., 2012. Review of flow rate estimates of the Deepwater Horizon oil spill. Proceedings of the National Academy of Sciences, 109(50), pp.20260-20267.

Mishima, K. and Ishii, M., 1984. Flow regime transition criteria for upward two-phase flow in vertical tubes. International Journal of Heat and Mass Transfer, 27(5), pp.723-737.

Mukherjee, H. and Brill, J.P., 1985. Pressure drop correlations for inclined two-phase flow.

Nicklin, D.J., 1962. Two-phase bubble flow. Chemical engineering science, 17(9), pp.693-702.

Nikuradse, J., 1933. Strömungsgesetze in rauhen Rohren. VDI-Verlag.

Ohnuki, A. and Akimoto, H., 2000. Experimental study on transition of flow pattern and phase distribution in upward air–water two-phase flow along a large vertical pipe. International journal of multiphase flow, 26(3), pp.367-386.

Omebere-Iyari, N.K., Azzopardi, B.J. and Ladam, Y., 2007. Two-phase flow patterns in large diameter vertical pipes at high pressures. AIChE journal, 53(10), pp.2493-2504.

Omebere-Iyari, N.K., Azzopardi, B.J., Lucas, D., Beyer, M. and Prasser, H.M., 2008. The characteristics of gas/liquid flow in large risers at high pressures. International Journal of Multiphase Flow, 34(5), pp.461-476.

Orkiszewski, J., 1967. Predicting two-phase pressure drops in vertical pipe. Journal of Petroleum technology, 19(06), pp.829-838.

Oudeman, P., 2010. Validation of blowout-rate calculations for subsea wells. SPE Drilling & Completion, 25(03), pp.282-289.

Pagan, E., Williams, W.C., Kam, S. and Waltrich, P.J., 2016, December. Modeling vertical flows in churn and annular flow regimes in small-and large-diameter pipes. In 10th North American Conference on Multiphase Technology. BHR Group.

Petalas, N. and Aziz, K., 1996. Development and testing of a new mechanistic model for multiphase flow in pipes. In The 1996 ASME Fluids Engineering Division Summer Meeting. Part 1(of 2), San Diego, CA, USA, 07/07-11/96 (pp. 153-159).

Poettman, F.H. and Carpenter, P.G., 1952, January. The multiphase flow of gas, oil, and water through vertical flow strings with application to the design of gas-lift installations. In Drilling and production practice. American Petroleum Institute.

Prasser, H.M., Beyer, M., Carl, H., Gregor, S., Lucas, D., Pietruske, H., Schütz, P. and Weiss, F.P., 2007. Evolution of the structure of a gas–liquid two-phase flow in a large vertical pipe. Nuclear Engineering and Design, 237(15-17), pp.1848-1861.

Pushkina, O.I., 1969. Breakdown of liquid film motion in vertical tubes. Heat Transfer-Sov. Res., 1(5), p.56.

Ros, N.C.J., 1961. Simultaneous flow of gas and liquid as encountered in well tubing. Journal of Petroleum Technology, 13(10), pp.1-037.

Schlegel, J.P., Sawant, P., Paranjape, S., Ozar, B., Hibiki, T. and Ishii, M., 2009. Void fraction and flow regime in adiabatic upward two-phase flow in large diameter vertical pipes. Nuclear Engineering and Design, 239(12), pp.2864-2874.

Standing, M.B., 1981. Volumetric and Phase Behavior of Oil Hydrocarbon System. Society of Petroleum Engineers of AIME, Dallas.

Schlegel, J., Hibiki, T. and Ishii, M., 2010. Development of a comprehensive set of drift-flux constitutive models for pipes of various hydraulic diameters. Progress in Nuclear Energy, 52(7), pp.666-677.

Schlegel, J.P., Macke, C.J., Hibiki, T. and Ishii, M., 2013. Modified distribution parameter for churn-turbulent flows in large diameter channels. Nuclear Engineering and Design, 263, pp.138-150.

Shen, X., Matsui, R., Mishima, K. and Nakamura, H., 2010. Distribution parameter and drift velocity for two-phase flow in a large diameter pipe. Nuclear Engineering and Design, 240(12), pp.3991-4000.

Shen, X., Hibiki, T. and Nakamura, H., 2015. Bubbly-to-cap bubbly flow transition in a long-26 m vertical large diameter pipe at low liquid flow rate. International Journal of Heat and Fluid Flow, 52, pp.140-155.

Shoham, O., 2005. Mechanistic Modeling Of Gas/Liquid Two-Phase Flow In Pipes (pp. 240-250). Spe.

Skopich, A., Pereyra, E., Sarica, C. and Kelkar, M., 2015. Pipe-diameter effect on liquid loading in vertical gas wells. SPE Production & Operations, 30(02), pp.164-176.

SPE Committee, Technical Reports. 2015. Calculation of Worst-Case Discharge (WCD). Society of Petroleum Engineers.

Takacs, G., 2001, January. Considerations on the selection of an optimum vertical multiphase pressure drop prediction model for oil wells. In SPE/ICoTA Coiled Tubing Roundtable. Society of Petroleum Engineers.

Taitel, Y. and Dukler, A.E., 1976. A model for predicting flow regime transitions in horizontal and near horizontal gas-liquid flow. AIChE journal, 22(1), pp.47-55.

Taitel, Y., Bornea, D. and Dukler, A.E., 1980. Modelling flow pattern transitions for steady upward gas-liquid flow in vertical tubes. AIChE Journal, 26(3), pp.345-354.

Tang, H., Bailey, W.J., Stone, T. and Killough, J., 2019. A Unified Gas/Liquid Drift-Flux Model for All Wellbore Inclinations. SPE Journal.

Thome, J.R., 2006. State-of-the-art overview of boiling and two-phase flows in microchannels. Heat Transfer Engineering, 27(9), pp.4-19.

Vazquez, M. and Beggs, H.D., 1980. Correlations for fluid physical property prediction. JPT 32 (6): 968–970. SPE-6719-PA. DOI: 10.2118/6719-PA.

Van der Meulen, G.P., 2012. Churn-annular gas-liquid flows in large diameter vertical pipes (Doctoral dissertation, University of Nottingham).

Wallis, G.B., 1969. One-dimensional two-phase flow.

Waltrich, P.J., Capovilla, M.S., Lee, W., Zulqarnain, M., Hughes, R., Tyagi, M., Williams, W., Kam, S., Archer, A., Singh, J. and Nguyen, H., 2017, April. Experimental evaluation of wellbore flow models applied to worst-case-discharge calculations. In SPE Health, Safety, Security, Environment, & Social Responsibility Conference-North America. Society of Petroleum Engineers.

Weisman, J. and Kang, S.Y., 1981. Flow pattern transitions in vertical and upwardly inclined lines. International Journal of Multiphase Flow, 7(3), pp.271-291.

Yuan, G., Pereyra, E., Sarica, C. and Sutton, R.P., 2013. An Experimental Study on Liquid Loading of Vertical and Deviated Gas Wells.

Zabaras, G., Menon, R., Schoppa, W. and Wicks III, M., 2013, May. Large diameter riser laboratory gas-lift tests. In Offshore Technology Conference, Houston, TX (pp. 6-9).

Zuber, N. and Findlay, J., 1965. Average volumetric concentration in two-phase flow systems.

Zuber, N. and Hench, J., 1962. Steady State and Transient Void Fraction of Bubbling Systems and Their Operating Limits: Steady State Operation. General Electric.

Zigrang, D. J., and Sylvester, N. D., 1985. A review of explicit friction factor equations.

VITA

Woochan Lee, born in Republic of Korea, worked as a reservoir engineer for several years in Korea after receiving his bachelor's degree in Petroleum Engineering from the University of Texas at Austin. As his academic interest grew, he decided to enter master and doctoral degree in Petroleum Engineering at Louisiana State University. After completion of his master's degree and doctoral qualifying exam, he went back to Korea to continue his doctoral degree as a part time student and a full time worker. He is working as a reservoir engineer with an oil company in United Arab Emirates, currently.